FUNDAMENTALS OF FAILURE IN TOPOLOGICALLY INTERLOCKED STRUCTURES
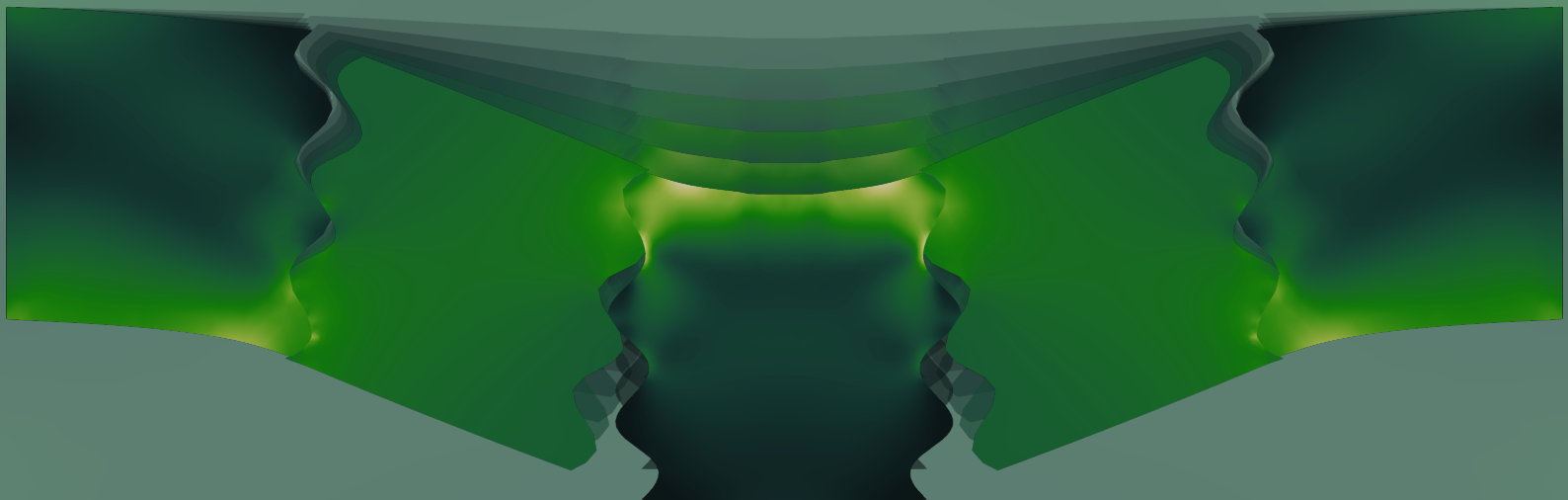
IOANNIS KOUREAS
DISS. ETH NO. 29731

DISS. ETH NO. 29731

Fundamentals of failure in topologically interlocked structures

A thesis submitted to attain the degree of

DOCTOR OF SCIENCES
(Dr. sc. ETH Zurich)

presented by

Ioannis Koureas

MSc Computational Engineering Design
University of Southampton, UK

born on 27 February 1993

accepted on the recommendation of

Prof. Dr. David S. Kammer, examiner
Prof. Dr. Francois Barthelat, co-examiner
Dr. Vladislav A. Yastrebov, co-examiner

2023

To my family

Acknowledgements

This thesis represents the culmination of a four and a half years research odyssey conducted within the Computational Mechanics of Building Materials (CMBM) group at Eidgenössische Technische Hochschule Zürich (ETH). The guidance and support of many individuals who have provided their skills, knowledge and unwavering help along the journey has been a major milestone in the achievement of this work. This appreciation is a testament to their invaluable contributions to shaping and expanding my scientific expertise and personal character.

My decision in pursuing this particular doctoral degree, is mainly attributed to my advisor, Professor David Kammer and the friendly environment he had created since our first meeting. I am grateful for having the opportunity to work on a very interesting subject as one of the first doctoral scientists in CMBM together with Julia Kamml. Being part of the group at such an early stage was definitely a unique opportunity, as I was able to gain knowledge on a plethora of topics outside my research field and learn how a successful research group is born. Moreover, Dave gave me the flexibility to explore and implement my own ideas on my research topic. I was really lucky to have an advisor who recognized my talents and helped me strengthen my weaknesses. His guidance extends beyond this thesis and will undoubtedly be invaluable to me for years to come.

I would like to thank Professor Francois Barthelat, my thesis committee member, for his time in reviewing this dissertation and his valuable comments. Furthermore, I would like to thank Doctor Vladislav Yastrebov, my co-supervisor and thesis committee member, for the stimulating scientific discussions and recommendations for refining my work.

I would like to thank all my colleagues at the CMBM. Particularly I express my sincere gratitude to Doctor Mohit Pundir and Doctor Shai Feldfogel with whom this work would have not been accomplished. Their guidance, thorough discussions and improvements on the numerical framework helped me to work effectively and professionally. Their mentoring approach also taught me how to think as a scientist, but also provided me with skills beyond science and the academic environment. I would like to thank Philip Muller, whom I consider as one of the most brilliant minds. Philip was my office mate for the majority of my time at the CMBM, where we had many enjoyable scientific and computational discussions. I would also like to thank Doctor Michal Hlobil, Doctor Stefanie Heyden, Doctor Alessandra Lingua, Doctor Antoine Sanner, Doctor Yuan Tian, Doctor Wang Xiaoyu, Julia Kamml, Yaqi Zhao, Miguel Castellano Merino, Zhichao Han, Luca Michel, Flavio Lorez, and You Wang for all the wonderful experiences and enjoyable discussions we had during coffee breaks and group activities. Moreover, I thank my friends both in Zurich and abroad for the unforgettable memories during these years.

Finally, an unparalleled thank you to my parents Niki and Michalis and my siblings Christiana and Antreas for their unconditional love and constant encouragement during these years. This thesis has been made possible thanks to their support.

Abstract

Topologically Interlocked Structures (TIS) are a new class of high performance structures that possess a remarkable combination of mechanical properties, specifically high toughness, strength, and stiffness. The combination of these properties is desirable in many engineering applications to resist failure and crack initiation and propagation. TIS are formed by using specially shaped unit blocks that come in contact at their interfaces. When an external load is applied, it triggers load transfer across the structure, activating local stick and slip mechanisms at the interfaces between the blocks. These interface mechanisms along with the geometry and surface morphology of the blocks are decisive for the mechanical response and failure of TIS. However, the fundamental link between the interface mechanisms, block geometry, and block surface morphology to the mechanical response and failure modes is not fully understood and requires further investigation.

This thesis, aims to examine the influence of these parameters on the overall performance of TIS. As a first step, we focus on simple geometric designs in the 2D space, forming beam-like structures with both planar- and non-planar-faced blocks. The suggested geometries, allow disregarding complex surface morphologies and focus solely on the interface mechanisms. This enables us to better understand the fundamental principles of TIS and provide a link between the interface mechanisms and the response capacities. We demonstrate that the geometry of the blocks together with the frictional resistance defines the nature of the failure mechanism as slip-governed or stick-governed. Furthermore, we show that independent of geometric and material properties, rotation of the blocks along with sticking mechanism across all interfaces determine a theoretical upper limit to the response capacities.

Achieving the theoretical limit requires an unrealistically high coefficient of friction, which calls into question whether this upper limit can be obtained in practice. Drawing inspiration from biological systems, we modify the surface geometry of the blocks by applying hierarchical patterns. This approach aims to increase the effective frictional strength of beam-like TIS with non-planar-faced blocks. Furthermore, it allows reaching the theoretical limit to the mechanical response with realistic friction coefficient, highlighting the importance of block surface morphology in optimizing the performance of interlocked structural systems.

Similarly, it is not clear if slab-like TIS with non-planar-faced blocks can achieve a saturated response with realistic friction coefficient. In addition, the exact characteristics of a non-planar surface morphology that can potentially contribute to improved mechanical response have yet to be addressed. Consequently, by implementing wave-like patterns on the block's surfaces, we show that it is possible to reach saturation to the response capacities with a realistic friction coefficient. Furthermore, we show that the key parameter responsible for the enhanced performance is the local angle of inclination at the structure's hinging points, which leads to improved work-to-failure and ultimate deflection.

The outcomes of this thesis provide insights and a fundamental understanding of the working principles of TIS. Their unique nature could allow for innovative applications in the near future. This could range from vibration absorption structures and outer-space applications to soundproofing and heat insulating devices, and even aesthetically pleasing buildings.

Zusammenfassung

Topologically Interlocked Structures (TIS) stellen eine neue Klasse von Hochleistungsstrukturen dar, die eine bemerkenswerte Kombination mechanischer Eigenschaften aufweisen, insbesondere hohe Zähigkeit, Festigkeit und Steifigkeit. Die Kombination dieser Eigenschaften ist in vielen ingenieurtechnischen Anwendungen wünschenswert, um Versagen sowie den Beginn und die Ausbreitung von Rissen zu widerstehen. TIS werden durch die Verwendung speziell geformter Bausteine gebildet, die an ihren Schnittstellen in Kontakt kommen. Wenn eine externe Belastung aufgebracht wird, löst sie die Lastübertragung über die Struktur aus und aktiviert lokale Haft- und Gleitmechanismen an den Schnittstellen zwischen den Blöcken. Diese Schnittstellenmechanismen zusammen mit der Geometrie und Oberflächenmorphologie der Blöcke sind entscheidend für das mechanische Verhalten und das Versagensverhalten von TIS. Es ist jedoch nicht vollständig verstanden, wie der grundlegende Zusammenhang zwischen den Schnittstellenmechanismen, der Blockgeometrie und der Blockoberflächenmorphologie auf das mechanische Verhalten und die Versagensmodi wirkt und erfordert weitere Untersuchungen.

Diese Dissertation zielt darauf ab, den Einfluss dieser Parameter auf die Gesamtleistung von TIS zu untersuchen. Als ersten Schritt konzentrieren wir uns auf einfache geometrische Designs im zweidimensionalen Raum, um balkenähnliche Strukturen mit sowohl planaren als auch nicht-planaren Blockoberflächen zu bilden. Die vorgeschlagenen Geometrien ermöglichen es, komplexe Oberflächenmorphologien zu vernachlässigen und sich ausschließlich auf die Schnittstellenmechanismen zu konzentrieren. Dies ermöglicht es uns, die grundlegenden Prinzipien von TIS besser zu verstehen und eine Verbindung zwischen den Schnittstellenmechanismen und den Reaktionskapazitäten herzustellen. Wir zeigen, dass die Geometrie der Blöcke zusammen mit dem Reibungswiderstand die Art des Versagensmechanismus als gleitgesteuert oder haftgesteuert definiert. Darüber hinaus zeigen wir, dass unabhängig von geometrischen und materiellen Eigenschaften die Rotation der Blöcke zusammen mit dem Haftmechanismus an allen Schnittstellen eine theoretische Obergrenze für die Reaktionskapazitäten bestimmt.

Das Erreichen der theoretischen Grenze erfordert einen unrealistisch hohen Reibungskoeffizienten, was die Frage aufwirft, ob diese Obergrenze in der Praxis erreicht werden kann. Inspiriert von biologischen Systemen, modifizieren wir die Oberflächengeometrie der Blöcke, indem wir hierarchische Muster anwenden. Dieser Ansatz zielt darauf ab, die effektive Reibungsfestigkeit von balkenähnlichen TIS mit nicht-planaren Blockoberflächen zu erhöhen. Darüber hinaus ermöglicht er das Erreichen der theoretischen Obergrenze für die mechanische Reaktion mit realistischem Reibungskoeffizienten und unterstreicht die Bedeutung der Blockoberflächenmorphologie bei der Optimierung der Leistung von ineinandergreifenden Struktursystemen.

Ebenso ist nicht klar, ob plattenähnliche TIS mit nicht-planaren Blockoberflächen eine gesättigte Reaktion mit realistischem Reibungskoeffizienten erreichen können. Darüber hinaus wurden die genauen Merkmale einer nicht-planaren Oberflächenmorphologie, die potenziell zu einer verbesserten mechanischen Reaktion beitragen kann, noch nicht behandelt. Folglich zeigen wir durch die Implementierung wellenartiger Muster auf den Blockoberflächen, dass

es möglich ist, eine Sättigung der Reaktionskapazitäten mit einem realistischen Reibungsko-effizienten zu erreichen. Darüber hinaus zeigen wir, dass der Schlüsselparameter für die verbesserte Leistung der lokale Neigungswinkel an den Scharnierpunkten der Struktur ist, was zu einer verbesserten Arbeit bis zum Versagen und zur ultimativen Durchbiegung führt.

Die Ergebnisse dieser Arbeit bieten Einblicke und ein grundlegendes Verständnis der Funktionsprinzipien von TIS. Ihr einzigartiger Charakter könnte in naher Zukunft innovative Anwendungen ermöglichen. Diese könnten von schwingungsabsorbierenden Strukturen und Anwendungen im Weltraum über schall- und wärmedämmende Vorrichtungen bis hin zu ästhetisch ansprechenden Gebäuden reichen.

Contents

List of Figures

1

Introduction

> Progress in design of new structures seems to be unlimited.
>
> Klaus-Jürgen Bathe

1.1 General Introduction

In the quest for innovative and resilient engineering structures, scientists and engineers seek inspiration from the elegance and wonder of natural systems, as well as historical architectural buildings. Among countless principles found in both nature and ancient architectural marvels, topologically interlocked structures (TIS) have emerged as a captivating paradigm [1]. The ingeniously intertwined and compactly arranged configurations of blocks (also referred to as elements), achieving both mechanical stability and robustness, have captured the attention of diverse disciplines, ranging from civil and mechanical engineering to materials science, architecture and mathematics.

In the realm of natural systems, biological materials such as mollusk shell, seashell, and bone are remarkable examples of inspiration [2]. Zooming into the micro world of these materials, we can spot distinct building elements arranged in an interlocked and hierarchical manner. The elements come in contact with their neighbors and therefore relative motion triggers disturbance of the structural system, the basic working principle of TIS.

Moving into the scope of historical architectural buildings, various cultures have utilized interlocking components to create stable and durable structures. Notable examples include ancient dry-stone construction methods in structures like the Pyramids of Egypt and Inca stone walls. These ancient architectural structures leveraged semi-interlocking techniques using stones, without the need for mortar to achieve stability.

As a first definition, we can say that TIS are assemblies of individual blocks, with distinct and specialized geometry, designed in a way that enables to achieve structural integrity through

interlocking connections at their interfaces. These structures rely solely on contact and coordination between the blocks to maintain their overall stability. TIS exhibit remarkable characteristics, including high strength, energy dissipation, and crack arrest abilities [3–5]. They have the potential to offer numerous benefits in engineering structures including sustainability, cost-effectiveness, and broad design space that promotes aesthetics.

TIS enabled an interdisciplinary level of collaboration between scientists and engineers from various fields aiming to understand how to design and construct more sustainable and failure-tolerant systems. TIS offer a wide range of potential applications across various disciplines, including the design of robust, high strength and toughness structures, vibration absorption mechanisms, and efficient heat-insulating and soundproofing devices. Even though TIS can be promising in many fields and applications ranging from the micro- to the macro-scale, there are still many fundamental unaddressed questions. One of the main challenges is to understand and explain the interface mechanisms and consequently, the failure modes of TIS.

In this thesis, we explore the profound potential of TIS with special focus on beam-like and slab-like (also referred to as plate-like) models, unveiling their underlying mechanics and working principles. To answer these fundamental questions, we develop numerical models that explore various aspects of the mechanical response of TIS.

1.2 Objectives of the thesis

The aim of this study is to provide a fundamental understanding on the working principles of TIS and the effect of TIS's mechanisms (*i.e.*, stick and slip) along with rotation, detachment, deformation, and surface morphology of the blocks on the response capacities (*i.e.*, structural stiffness, peak load, work-to-failure[1], and ultimate deflection).

Initially, our objective is to explore and understand the influence of various parameters on the overall performance of beam-like TIS with planar-faced blocks. More specifically, we address the effects of height and length of the structure, Young's modulus, and friction coefficient on the response capacities. Through this parametric study we seek to unveil the conditions under which TIS's mechanisms are either promoted or suppressed and whether the failure mechanism is slip-governed or stick-governed. In addition, we extend our investigation using curved-faced and kinked-faced blocks in an effort to explore whether our approach can be generalized in the broader context of beam-like TIS.

It is often expected that some of the studied parametric values may not be feasible in practical applications due to limitations in achievable material, interfacial and geometrical values. As a result, inspired by design characteristics of biological materials, the subsequent stage of this study involves introducing hierarchical alterations to the surface geometry of TIS's blocks. Through this approach, we aim to investigate the effect of hierarchical modifications on the block's surfaces and whether such modifications can improve the response capacities of beam-like TIS. More specifically, we explore if it is possible to obtain the upper limit in the theoretical response capacities of beam-like TIS with wave-faced blocks, using realistic friction coefficient values.

Moving from simple TIS models, that is, from beam-like to slab-like configurations, does not guarantee the preservation of the mechanical response. Therefore, as a next step, we explore slab-like TIS models with non-planar-faced blocks, in an effort to understand the role of surface morphology in influencing the response capacities. As a result, we address if it is possible to reach the theoretical saturation obtained with planar-faced blocks and high friction coefficients by using non-planar morphologies and realistic friction coefficient. Additionally, we aim to identify the key geometrical parameters of non-planar-faced blocks, in relation to the response capacities of slab-like TIS.

---

[1]In some cases, the terms "peak load" and "work-to-failure" are also refereed as "maximum load-carrying capacity" and "loading energy", respectively.

1.3   Modeling TIS response

To address the objectives of this study and model TIS, we employ the finite element method (FEM) incorporating frictional contact mechanics and geometrical non-linearities to accurately capture the continuum nature of solid bodies. The research code FiNICAS (**F**inite **N**umerical **I**ntegrator for **C**omputational **A**nalysi**S**), an in-house finite element tool, is utilized for this purpose. The numerical tool has been developed to accommodate for frictional sliding and sticking mechanisms across multi-block interactions, as well as large deformations that occur during various loading conditions. The proposed models are solved using an implicit static integration scheme.

In addition to the numerical simulations, this research employs theoretical approaches to analyze the observed phenomena. To validate and enhance the understanding of the numerical results, comparisons are made with analytical models and experimental findings from the literature. This comparative analysis reinforces the validity of the numerical outcomes, and contributes to a deeper comprehension of the mechanics governing the observed behavior. Furthermore, it sheds light on the influence of different material, interfacial and geometrical properties on TIS behavior.

1.4   Structure of the thesis

This thesis is structured in a cumulative format, and is organized in several chapters, which are summarized as follows:

Chapter 2 – State of the Art provides a comprehensive introduction to TIS. This is followed by an extensive literature review covering the main findings in the field, both experimentally and numerically. Additionally, this chapter highlights the wide range of inspiration drawn by scientists and the design foundations of TIS from a geometrical perspective. Furthermore, a brief overview of the main fabrication and assembling techniques is presented. Finally, a glimpse of the current challenges and limitations that engineers are facing in the broader context of TIS are discussed.

Chapter 3 – Numerical Framework briefly describes the numerical techniques utilized to carry out the simulations, addressing the objectives outlined in Sec. 1.2. As a result, a description of the fundamental principles behind FEM is provided. Additionally, the integration of FEM with frictional contact mechanics, and geometrical non-linearities is summarized. This approach is essential for modeling TIS as deformable bodies, while considering large frictional sliding at the interfaces.

Chapter 4 – On the failure of beam-like topologically interlocked structures provides a parametric study that is employed on beam-like TIS in an effort to understand the fundamentals of TIS's mechanical response. The relation between structural stiffness, peak load, work-to-failure, and ultimate structural deflection is investigated as well as the underlying failure modes. The goal is to provide an insight on the working principles and the effect of TIS's mechanisms on peak load and work-to-failure, and identify the parameters that maximize their performance. The study concluded that the sticking mechanism in combination with rotation of the blocks provides an upper bound to the structural stiffness, peak load, work-to-failure, and ultimate deflection of beam-like TIS.

Chapter 5 – Beam-like topologically interlocked structures with hierarchical interlocking focuses on investigating the effect of beam-like TIS with wave-faced blocks on the structural response capacities. This is achieved by implementing hierarchical modifications on the block surfaces in the form of wave-like patterns. Through this approach, we introduce the presence of a geometrical frictional resistance characteristic resulting from the non-planar block morphologies. Our findings demonstrate that we can reach the upper bound to the peak-load and work-to-failure with lower, realistic friction coefficient values.

Chapter 6 – The key to the enhanced performance of slab-like topologically interlocked structures with non-planar blocks explores the effect of non-planar-faced block morphologies on the mechanical performance of slab-like TIS. Particularly, we implement non-planar block morphologies in the form of wave-like patterns, both with and without initial inclination. Our findings show that we can reach the theoretical upper bound to the peak load using realistic friction coefficient. In addition, we show that the local angle of inclination at the hinging points is a key parameter for improving the work-to-failure of the structure and for enhancing a pseudo-ductile response. These properties cannot be obtained without non-planar morphologies.

Chapter 7 – Summary and Conclusion offers a comprehensive summary of the main findings, outcomes, and contributions arising from the current study. Furthermore, this chapter points out the main conclusions that contribute to our understanding of the mechanical response and performance of TIS. Finally, it focuses on critically evaluating the conducted research and assessing the key findings, contextualizing their significance.

Chapter 8 – Outlook provides a broader perspective of TIS and offers insights into the implications of the findings. Furthermore, it explores potential applications within the field and proposes recommendations for future research, based on the new findings and the current knowledge gaps.

2

State of the Art

The vision of designing high-performance structures is a long-term goal for scientists. A high-performance structure can be defined as one that exhibits exceptional resistance to a wide range of external stimuli, effectively mitigating the risk of premature failure or catastrophic structural collapse. The external stimuli encompass mechanical, electrical, chemical, thermal, acoustical or any combination thereof. This thesis primarily focuses on implementing fundamental research to improve structural efficiency, aiming to design high-performance structures, that exhibit exceptional levels of stiffness, strength, and toughness. The examined structures adopt advanced engineering principles, emphasizing the significance of interlocking features to enhance their mechanical response. This design approach is termed "topologically interlocked structures" (TIS). An example of such a structure is shown in Fig. 2.1.
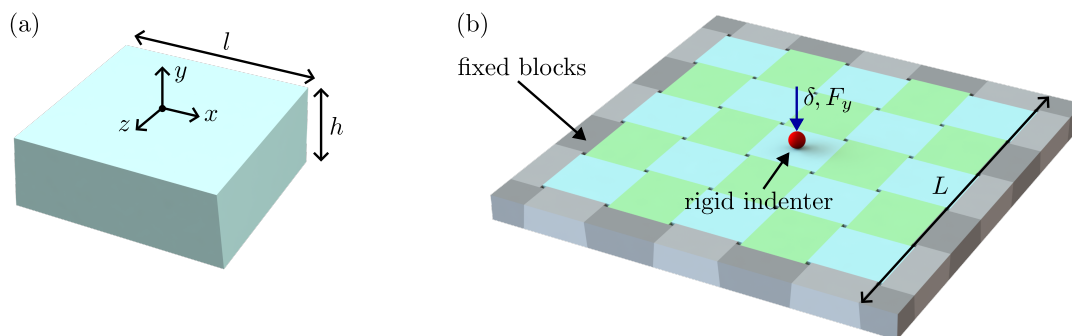
Figure 2.1: Schematic of (a) a planar-faced block with height h and length l. (b) A slab-like topologically interlocked structure with planar-faced blocks and structural length L. The peripheral blocks support the structure. A prescribed displacement δ is applied on the rigid indenter along y direction.

In TIS, load-carrying unit elements remain unbonded but fit together with geometric precision and interact through contact (see Fig. 2.1). Topological interlocking and frictional contact become the fundamental basis that govern the response of these structures. While the inter-elemental interactions ensure structural stability, they also exhibit slight movements relative to each other due to the geometric packing with neighboring blocks. When the structure is not subjected to an external load, the block interfaces can exhibit either full or partial contact with each other (see Fig. 2.2). Once the structure is loaded, the interface mechanisms (*i.e.*, stick and slip) along with rotation of the blocks are activated. Upon further increase of the applied load, separation between the blocks is promoted, decreasing the contact area. As a result, stress is localized at the contact interfaces of the blocks, triggering frictional sliding or fracture initiation. The objective is to design the interfaces in a way to reduce tensile forces and stress concentration, thereby delaying fracture initiation and propagation. The blocks' unbonded nature, allows the structure to absorb or dissipate the energy generated by block movements, due to interfacial interactions. This highly non-linear response gives rise to structures that exhibit high strength and toughness [3, 4, 6].
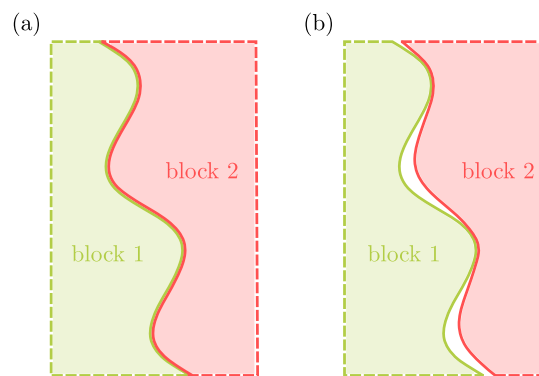
Figure 2.2: Schematic illustration of the interface contact area between two blocks in a topologically interlocked structure at the reference configuration. (a) Scenario where the blocks are in full contact at the interface and (b) with the blocks being partially in contact at the interface.

2.1 Foundations of TIS: Tracing the Roots

Starting from primitive structures and interlocked patterns, to emerging the concept of topological interlocking, scientists and engineers have drawn inspiration from diverse sources to explore the principles and characteristics of TIS. An influence that origins from nature, architecture, and mathematics leading to varied terminology. Some refer to these designs as topologically interlocked structures, while others call them topologically interlocked materials or assemblies or systems, highlighting the origin of their ideas from the various fields and the interdisciplinary approach.

Lessons from nature

Nature offers an unlimited source of inspiration [7]. Observing natural structures, such as beehives, bird nests, coral reefs, bone enamel [8], abalone shell [2], spider net, mollusc shell, ammonites shell [9], nutshells [10], turtle shell [11–13], wood sutures [14], and human skull [15, 16], has inspired scientists and engineers to develop topologically interlocked models that often exhibit high strength, toughness, and robustness.

In conventional engineering, achieving high strength and toughness simultaneously has been considered challenging and often mutually exclusive [17, 18]. Previous studies [17, 19], focusing on the nano- and micro-scales, have provided valuable insights into the design and behavior of materials, and opened up new possibilities for structural engineering. The knowledge gained from the micro-structure of these materials, motivated the field of topological interlocking for developing cohesive and robust structures that combine high strength and toughness. To overcome the trade-off between strength and toughness, several mechanisms

from natural materials have been observed, including hybrid design, controlled frictional motion, crack bridging, pull-out, cellular microstructure, suture joints, and hierarchical architecture (see Fig. 2.3). The principle of these mechanisms is to improve toughness and reduce local stress concentration thereby preventing material failure.
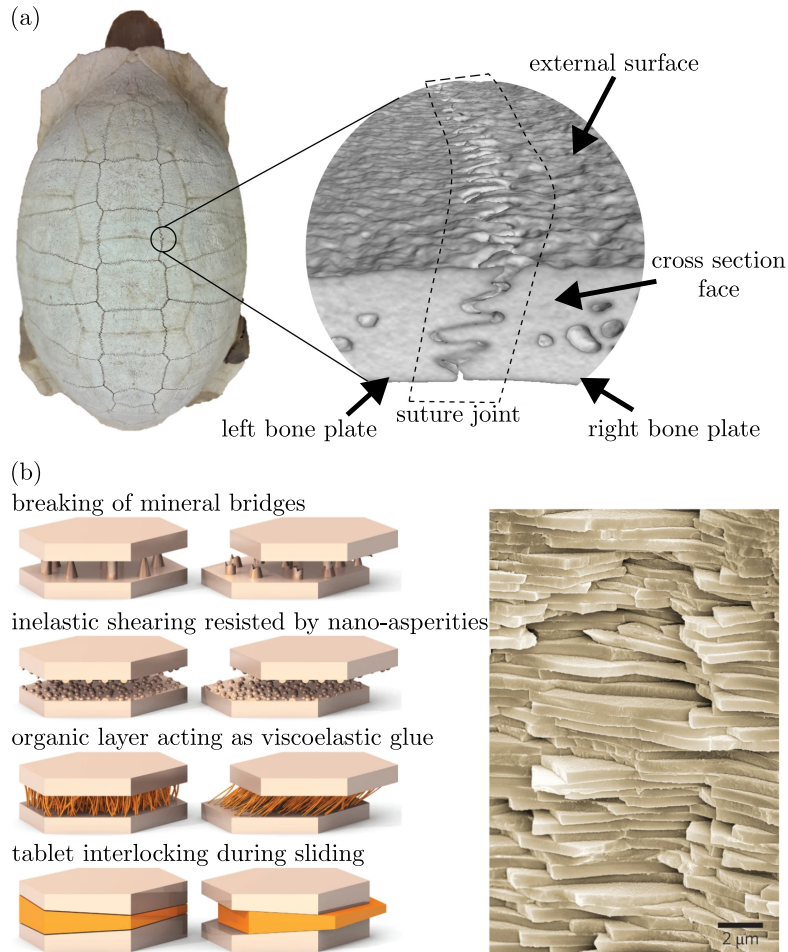
Figure 2.3: (a) Schematic of suture joint in a dehydrated turtle shell skeleton. Reprinted from [13] Journal of the Mechanics and Physics of Solids, 157, B. Alheit, S. Bargmann, and B. D. Reddy, Dynamic mechanical behavior of suture interfaces as inspiration for architectured hierarchical interlocking composites, Copyright © (2021), with permission from Elsevier. (b) Hierarchical brick-and-mortar micro-structure of nacre showing the hybrid design, controlled frictional motion, crack bridging, and pull-out mechanisms. Adapted by permission from SNCSC: Bioinspired structural materials, Ulrike G.K. Wegst, Hao Bai, Eduardo Saiz, Antoni P. Tomsia, and Robert O. Ritchie, Nature Materials, 14(1), 2015, [8], Copyright © (2015).

Natural material micro-structure is often characterized by hybrid bonding, in which a rigid and dominant material is combined with a much softer counterpart [20]. An indisputable example of such a material is nacre (see Fig. 2.3b), renowned for its mechanical properties, specifically the high stiffness, strength, fracture toughness and energy absorption [21, 22]. These unique characteristics arise from nacre's micro-structure, particularly from the presence of soft viscoelastic organic protein (5 wt%) and the brick-and-mortar micro-architecture of polygonal aragonite platelets [22]. This combination results in a high toughness, high strength structure compared to its main component (aragonite) which possess high strength but low toughness. The enhanced toughness in natural materials, is achieved through controlled frictional motion at the interface between mineral platelets (see Fig. 2.3b). This, in turn, facilitates controlled initiation and propagation of shear slip, relieving local stresses and promoting structural toughness.

Biological materials like seashell and bone, use crack bridging and pull-out mechanisms to enhance toughness [8]. This mechanism, allows natural materials to bridge across crack surfaces, distributing stress and enhancing the carrying load. In addition, the discrete microstructure of natural materials inhibits further crack propagation, as fracture is constraint within the boundaries of a single platelet or element. Moreover, the interlocking features of the discrete elements, contribute to resisting pull-out forces[1]. Furthermore, materials in nature, often incorporate hierarchical architectures with characteristic features on multiple length scales [21–24]. The hierarchical design allows for enhanced toughening mechanisms leading to materials with unique combinations of strength and fracture resistance.

These concepts, traditionally studied in material science, can be adopted and implemented to develop TIS with enhanced mechanical response. Utilizing these strategies, scientists can develop new structures with unprecedented levels of strength, toughness, failure tolerance, and damage resistance, making them suitable for safety-critical applications in structural engineering, architecture, and beyond.

Learning from architecture

The architectural and historical discoveries of ancient civilizations offer another source of inspiration. The Inca, Sumerians, Egyptians and Greeks, for instance, used assembly techniques in their masonry to build durable and stable structures without the need for mortar or adhesives. Most of these ancient techniques involve fitting stones together in specific patterns to create stable and durable walls. The Machu Pitchu (with a building technique called "ldquo ashlar"), the Anu Ziggurat, the Ziggurat of Ur, the pyramids and the Parthenon stand as prominent examples of such remarkable achievements.

Later, Leonardo da Vinci (1452 - 1519) proposed a design of a self-supporting bridge (known as the "Da Vinci Bridge"). The unique and innovative design was based on a structure of self-supporting arches. The interlocking sections form an arch-shaped structure, with no need for external supports or fasteners. His motivation was most probably the design of a bridge that could be assembled and disassembled easily without additional equipment.

A step closer to interlocked structures was made by Joseph Abeille in 1699 who invented the Abeille Vault [25], a novel system for the construction of flat vaults that uses short stone elements to cover a space with a flat ceiling. Sébastien Truchet further improved Abeille's model, by developing interlocking shapes increasing the bending resistance of the vault while allowing it to discharge loads during compression. The interfaces between the stones where in full contact, ensuring there are no gaps on the vault.

Later on towards the end of the 20th century, the engineer Michael Glickman reported the design of truncated tetrahedral blocks forming vertically interlocked paving structures [26]. TIS, as a research field, emerged at the very beginning of the 21st century [1] and has flourished during the last decade. Inspired by the key block theory [27], Dyskin et al. [1] introduced the concept of interlocking truncated tetrahedral blocks as potentially flexible structures with high strength, toughness and impact resistance abilities.

The mathematical beauty of TIS

Geometry and mathematics stand as a key elements in designing high-performance structures. Geometric shapes have played a significant role in designing TIS. Akpanya, Goertzen, and Wiesenhuetter [28] for instance introduces a construction kit centered around the "Versatile Block", a geometrically designed unit that allows for a diverse range of topological interlocked assemblies. The model is linked and inspired from Truchet tiles [29] aiming to aid the design of new interlocking patterns.

---

[1]These are forces occurring when one element tries to detach or slide out from a neighboring one due to external applied loads.

A famous, well established class of shapes adopted in TIS is Platonic shapes. These shapes are considered special because all their faces are regular polygons of the same shape and size, and the same number of faces meet at each vertex. They have fascinated mathematicians, artists, and scientists for centuries due to their unique and symmetrical properties. The five Platonic shapes are tetrahedron (pyramid with four triangular faces), hexahedron (cube with six square faces), octahedron (double pyramid with eight triangular faces), dodecahedron (polyhedron with twelve regular pentagon faces), and icosahedron (polyhedron with twenty equilateral triangular faces). The incorporation of Platonic shapes in topologically interlocked designs as shown in Fig. 2.4 is used thoroughly, highlighting their significance in creating stable and aesthetically pleasing structures [30–32]. Overall, the integration of geometric and mathematical concepts has been instrumental in inspiring and advancing the field of TIS.
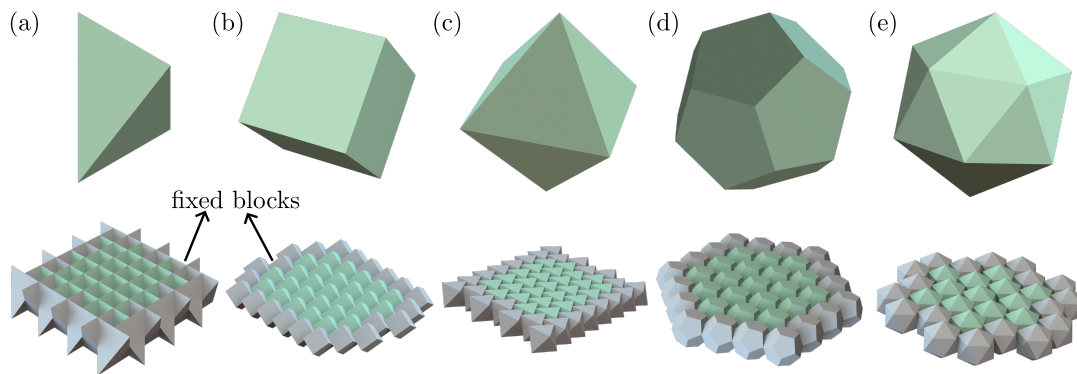
Figure 2.4: Schematic of all platonic shapes (top) and their topologically interlocked structure equivalent (bottom) for (a) tetrahedron, (b) hexahedron, (c) octahedron, (d) dodecahedron, and (e) icosahedron. The gray blocks serve as fixed supports constraining the structure in all directions.

2.2   Literature Review

The geometrical design of TIS's blocks

The tetrahedral block and its truncated equivalent, has emerged as the preferred case study scheme in the field of TIS [1, 33–35], both numerically and experimentally, due to the simplicity in designing and developing it. The popularity of truncated tetrahedral blocks, enabled their adoption as reference models for comparative analysis, validation, and further development of the field [4, 36]. The use of tetrahedral blocks was merely the predecessor; later, all Platonic shapes have been reported [3, 30, 37–40].

More advance and aesthetically pleasing shapes and designs have also been reported in the literature, such as tiling patterns [41]. Weizmann, Amir, and Grobman [42] focused on the use of TIS for constructing floors. The study presents various systems based on regular, semi-regular, and non-regular surface tessellations. The various challenges accompanied with implementing complex geometries are discussed as well as different assembly methods of such systems. The study is further extended by presenting a computational tool that automates the generation of new geometric patterns and designs with particular focus in architecture [43]. The proposed method by Weizmann, Amir, and Grobman [43] can be split in two stages: the generation of 2D patterns and the transformation of the patterns into 3D blocks. Further geometric designs have been proposed in the literature, including interlocked bricks [44], advanced geometric patterns [45], lego-inspired blocks [46, 47], and corbel dwellings with interlocking blocks [48]. These studies demonstrate a variety of geometric design concepts using interlocking blocks and serve as inspiration for further research in the geometric design of TIS.

Drawn from Joseph Abeille's novel design for vaults, Brocato and Mondardini [49] showcased a new design model of spherical vaults. These novel designs could fall in the category of
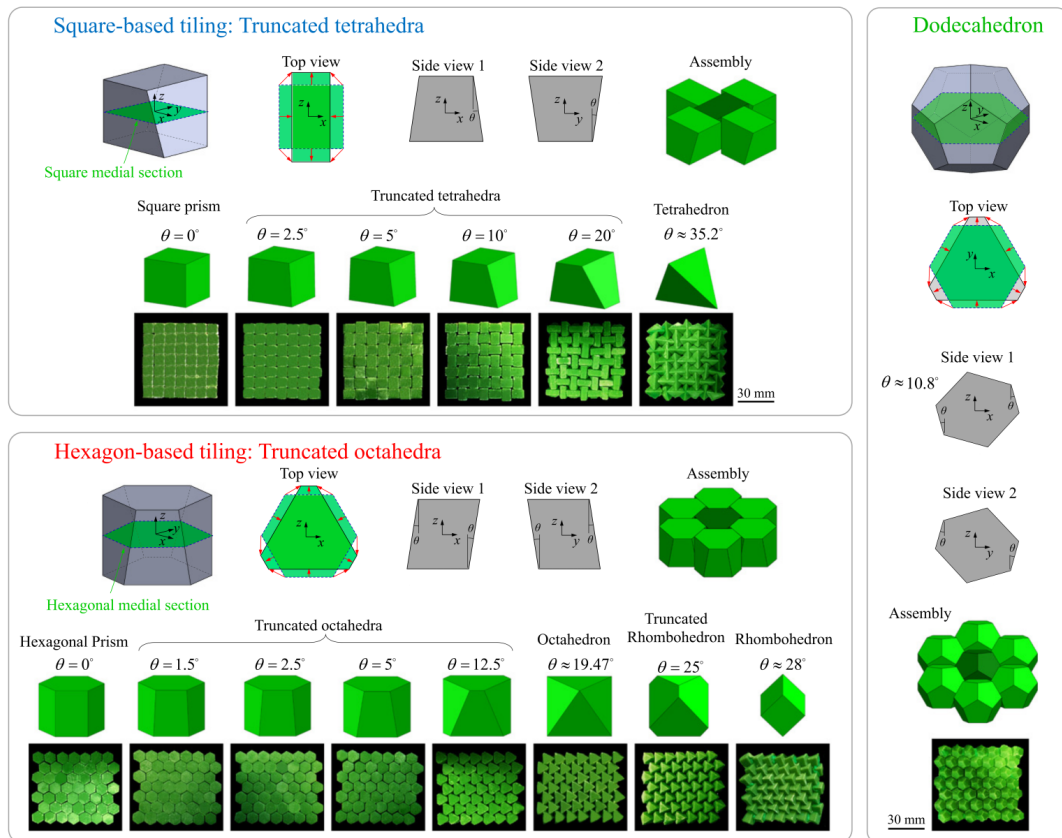
Figure 2.5: Illustration of TIS based on Platonic shapes and their truncated equivalents found in the literature. Adapted by permission: Simultaneous improvements of strength and toughness in topologically interlocked ceramics, Mohammad Mirkhalaf, Tao Zhou, and Francois Barthelat, PNAS, 115 (37), 2018, [3], Copyright © (2018).

curved-like TIS. Several curved-like interlocked structures have been proposed over the years both in the form of arches [50–52] as well as folded configurations [53–56]

The influence of nature in TIS

Nature is an incredible source of ideas for many novel structures [57–59], including TIS [60]. The exceptional mechanical properties of natural materials, such as strength, stiffness, and toughness, are a consequence of millions of years of evolution and adaptation to the environment. Several factors contribute to the remarkable mechanical properties of biological materials such as hybrid composition that allows to absorb and dissipate energy when subjected to external forces, suture joints at the interface and hierarchical structures that allow to distribute stress effectively, and cellular micro-structures.

Consequently, hybrid structures have also been proposed in the realm of TIS [61–63]. Such hybrid designs incorporate controlled interface behavior promoting frictional motion. Molotnikov et al. [61] introduced a method for designing lightweight sandwich structures where the core part of the assembly is composed using topologically interlocked building blocks. This design offers enhanced mechanical properties, flexibility, durability, crack propagation resistance, and energy absorption compared to sandwich panels with monolithic core. Djumas et al. [62] using additive manufacturing produced wave-faced blocks that have been examined under tensile test. The study demonstrated improvements both in maximum stress and elongation before failure compared to the traditional brick-and-mortar structure.

Suture joint structures and hierarchical surfaces share a strong connection by utilizing geomet-

ric patterns. Both techniques are used to optimize interface geometry, resulting in significant improvements in the mechanical response of the structure. Particularly, Li, Ortiz, and Boyce [23, 64] and Lin et al. [24] showed that suture joints offer improvements in various mechanical aspects such as load transmission, stiffness, strength, energy absorption, and fatigue resistance. In addition, using higher order of hierarchy in the design pattern, adds to the degree of geometrical interlocking and increases the contact area which significantly enhances the stiffness and toughness of these structures [65, 66]. Malik and Barthelat [67, 68] and Malik, Mirkhalaf, and Barthelat [69] focused on patterns and interfaces that arise from jigsaw shapes forming puzzle-like sutures. These designs were tested under tensile response using brittle-like materials resulting in a combination of non-linear large deformations, toughness, damping, and frictional pullout. Low friction and high interlocking angles were the key for achieving optimal performance.

Implementing hierarchical features (*i.e.*, non-planar-faced blocks with hierarchical surface morphology) in TIS can increase the contact area and improve local interlocking. These arrangements could potentially delay crack initiation, distribute stress, and enhance structural stability and toughness. Similarly to natural materials, the hierarchical design creates geometric arrangements at the surface of the blocks at multiple length scales, allowing for multiples levels of hierarchy (see Fig. 2.6). The impact of surface morphology and suture joints is particularly important for TIS, as it directly influences the degree of interlocking and promotes either sliding or sticking mechanisms. While research on this particular application remains somewhat limited, Djumas et al. [6] have already showcased exceedingly promising results. Particularly, the concept of hierarchical interlocking was applied by introducing modified osteomorphic blocks with secondary surface features. The results of the study, both experimental and computational, show that surface morphology patterns delay or even entirely suppress the onset of slip and lead to increased peak load and no softening in the load-displacement curve.
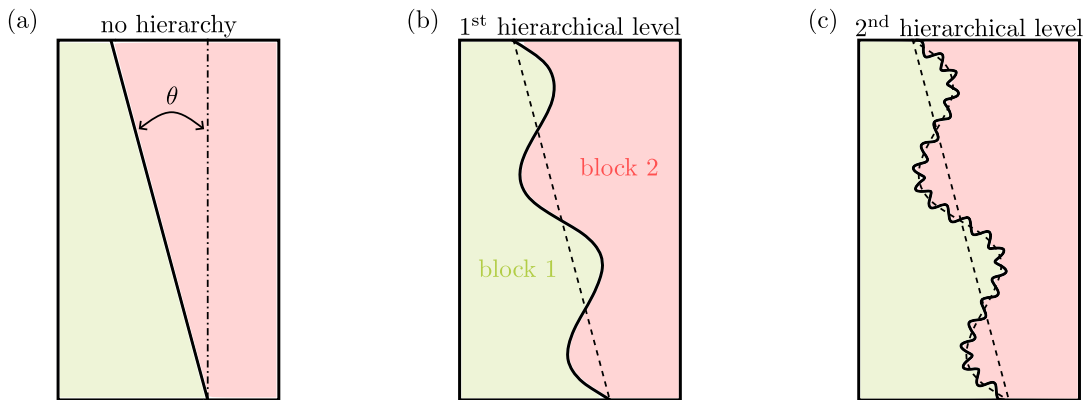
Figure 2.6: Schematic illustration of the level of hierarchy between two blocks in a topologically interlocked structure. (a) Scenario where no hierarchy is applied. (b) Scenario with one hierarchical level and (c) with two hierarchical levels.

Cellular and hollow TIS models have also been introduced in the literature. For instance, Khandelwal et al. [33] have shown that such structures can exhibit softening regardless of the relative density of the cellular units. Laudage, Guenther, and Siegmund [70] examined how material removal strategies affect the structural mechanical response under transverse loads. Despite material removal, the structure keeps its load-deflection characteristics, while the use of hollow building blocks can reduce the weight without compromising stability. Additionally, the material removal strategy and relative density allows customizing the stiffness, strength, and toughness of the structure.

Diving into the mechanical response of TIS

In addition to the wide range of design possibilities, TIS demonstrated a promising and unique mechanical response, showcasing remarkable stiffness, strength, and toughness

combination [3]. Structures composed of ceramic blocks demonstrated ten times higher ultimate deflection compared to monolithic equivalent [71]. In multiple occasions, scientists demonstrated the possibility to achieve high toughness structures without loss in strength while in some cases the strength also increases [3, 18]. In addition, in the event of failure, the already segmented structure permits crack initiation and propagation only within the boundaries of individual blocks and not throughout the whole structure [5]. Furthermore, if some blocks are pushed-out from the assembly, the integrity of the structure can be maintained. Remarkably, in some cases, the structure has the potential to recover and regain its original stiffness [72]. This property promotes sustainability and reusability because damaged blocks may be easily replaced without jeopardizing the overall structural integrity.

TIS have been studied under both static and dynamic loading conditions demonstrating high energy absorption abilities [4, 62, 73]. Mirkhalaf et al. [4] showed through experimental and numerical studies that interlocked structures exhibit higher energy absorption compared to monolithic equivalent structures both under quasi-static and impact conditions. Furthermore, Ali, Briet, and Chouw [74] analyzed mortar-free TIS columns and walls with and without rope reinforcement, to determine their dynamic and seismic response. Columns with ropes exhibited higher bending stiffness whereas those without ropes showed higher damping due to larger relative movements of the blocks. Overall, the study highlighted the potential of developing cost-effective, mortar-free columns and walls for earthquake-prone regions.

When considering loading-unloading scenarios, Estrin et al. [75] demonstrated a negative stiffness effect during unloading, in a cube-shaped TIS (hexahedra elements) under point-loading conditions. The behavior of the mechanical response is attributed to the interface mechanisms namely the contact and rotation of the blocks during loading and unloading. Similar configuration was examined by Schaare et al. [73] both experimentally and numerically. The study identifies many interesting non-linear responses, including post-peak softening, loading/unloading hysteresis, negative stiffness during unloading, and localization of irreversible rotations.

The effect of friction coefficient has been explored by Autruffe et al. [76] using interlocked structures made of ice. Specifically, the friction coefficient, was affected by temperature and sliding velocity, and has shown to influence the stiffness and energy dissipation of the interlocked structure. Later on, in a study conducted by Dalaq and Barthelat [77], it was demonstrated that the failure mode of architectured beams depends on the number of blocks, friction coefficient and the shape of interlocking interfaces. Specifically, the use of curved interfaces favors block sliding and delays hinging, leading to improved performance and stability. Building upon these findings, Dalaq and Barthelat [78] employed a family of curved and wavy surfaces combined with fillets at the corners, for further promoting sliding mechanism. The experiments let to 370-fold increase in toughness compared to the monolithic equivalent.

A combination of theory, experiments, and numerical analysis has been contacted by Khandelwal et al. [34] who developed a model based on the thrust-line analysis. The obtained scaling laws of the study, relate the mechanical stiffness to geometric and material properties of the structure. The structural stiffness scales with the product of Young's modulus, the area of the truss element, and the total number of blocks in the structure. In the case where slip mechanism is observed, the structural stiffness decreases. Furthermore, when adaptive external constraints are used, the stiffness and energy absorption can be tuned [35].

2.3   Fabrication and Assembling Techniques

TIS can range from micro-scale [79] to the macro-scale, providing a unique technique for designing novel structures that combine high strength and toughness. The manufacturing process of TIS can be distinguished in two main categories; bottom-up and top-down methods. The conventional technique (*i.e.*, bottom-up) consists of assembling methods like additive

manufacturing (*i.e.*, 3d printing), casting, and injection molding, where the discrete blocks are fabricated and then assembled to the final structure. Top-down assemblies include techniques like laser engraving and segmentation. The advantage of top-down techniques is that the TIS can be developed directly by engraving a monolithic panel in the final interlocked structure with the individual blocks being placed in their final position, therefore the assembling process is automatically taken care of. On the contrary, bottom-up methods can deal with multi-layer structures and structures having blocks with more complex shapes and geometries. However, the assembling process could be more intricate and time-consuming. When these factors are taken into consideration, they justify the difficulty in commercialization and mass production.

A notable example of bottom-up technique was presented by Zhou et al. [79] for assembling micro-scale TIS. The study presented a two-step microfluidic method for assembling octahedral blocks to form the interlocked structure. Initially, the blocks are aligned in 1D chains in the microfluidic channel and then compacted to form interlocked panels. The pattern of the interlocked panel influences its strength and toughness.

A recent fabrication technique involves vibration-assisted assembly of discrete building blocks [80, 81]. These studies demonstrate that vibration amplitude and frequency, along with block rotation and bouncing, are critical factors for improving the assembling process. The combination of vibration and gravity offer a relatively easy approach for fast, scalable, and low-energy fabrication method of TIS.

For ensuring structural integrity, TIS are constrained through external frames adjusted to hold the blocks together. Alternatively, TIS can be constrained internally through advanced geometrical interlocking designs, creating self-interlocked mechanisms. Another method includes incorporating secondary materials, such as tensioned wires passing through the blocks, to create a connection mechanism [35, 72, 74, 82]. However, the use of secondary materials, binders and advance geometrical shapes make the fabrication process more difficult, costly and time-consuming. Moreover, stress localization due to the use of binders and internal connectors could leave their advantages untapped.

2.4 Current Challenges

Currently, TIS constitute an interesting research topic mainly in academia. They hold the promise of being a fascinating method of converting stone-cutting pieces into art, applied to the engineering industry. However, they are rarely used in real-life applications due to the somewhat limited fundamental understanding, the non-existent laws and regulations governing the field as well as the lack of proper documentation and training for safely constructing such structures. At the moment applications of TIS can be found scarcely by research groups [45, 83], the Sugarcrete project and the gurus in architecture (*i.e.*, Kengo Kuma's interlocked designs) in an effort to promote aesthetics, sustainability and innovation.

3

Numerical Framework

This chapter, describes the approach used to numerically model topologically interlocked structures (TIS). The structure of the chapter is based on the three main components of the numerical solver: the Finite Element Method (FEM), geometrical non-linearity formulation, and frictional contact mechanics integration. Each of these components is essential to accurately study and analyze the complex mechanical response of TIS.

3.1   Fundamentals of the Finite Element Method

FEM is a numerical approach to solve physical problems (*e.g.*, solid mechanics, heat transfer, and fluid dynamics) which are described by partial differential equations (PDEs) or by the minimization of a functional. FEM involves breaking down the problem domain (see Fig. 3.1a) into smaller elements using a mesh, as shown in Fig. 3.1b. In 2D formulations, these elements are usually triangles or quadrilaterals while in 3D formulations tetrahedral or hexahedra. Within each element, an approximation function (interpolation function) is used to represent the solution. These functions are piece-wise defined within each element. Even with relatively simple approximation functions, FEM can provide accurate solutions to complex problems. The approximation function can capture the local behavior of the solution at each element and, when combined over the entire domain, approximate the actual solution reasonably well.

It is important to note that the accuracy of the solution is determined by the choice of the approximation functions, the element type, correct incorporation of the boundary conditions, the convergence strategies, and the proper assembly and solution of the global system of equations. Depending on the nature of the problem, static or dynamic, explicit or implicit, direct or iterative, linear or non-linear methods can be employed for solving the physical

problem.

Strong Formulation

The governing equation used for the current problem is the balance of linear momentum, a second-order PDE. This equation describes the behavior of the system in terms of stresses, strains, forces, and displacements. The balance of linear momentum in a given domain, Ω as shown in Fig. 3.1, can be expressed as:

$$\nabla \bullet \sigma + \rho b = \rho \ddot{u} \tag{3.1.1}$$

where $\rho(x, t)$ is the mass density, $\ddot{u}(x, t)$ is the acceleration, $\sigma(x, t)$ is the Cauchy stress tensor, and b is the body force.
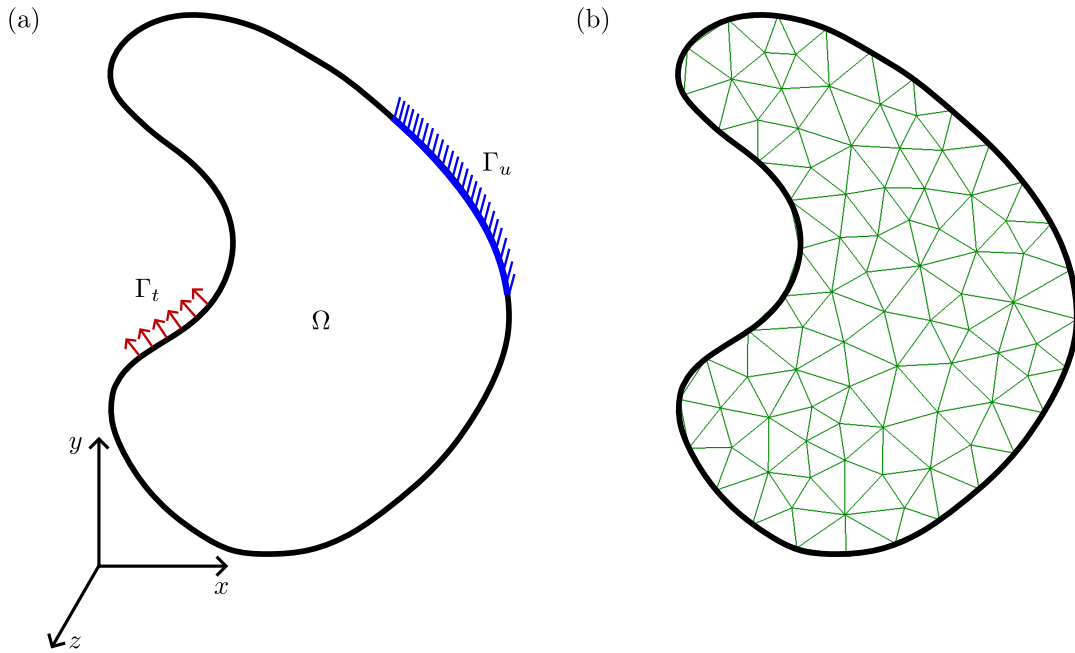
Figure 3.1: (a) Schematic of a domain Ω with Dirichlet and Neumann boundary condition Γ_u and Γ_t respectively. (b) Illustration of the discretized domain using triangular elements.

Weak Formulation

The governing PDE is then converted into a weak formulation (variational form), which is essentially a minimization problem of a functional. The functional represents a measure of the system's energy. To transform the governing equation into a weak formulation, we introduce a virtual displacement field that satisfies the boundary conditions (see Fig. 3.1a). The goal is to find the actual displacement field that minimizes the total potential energy of the system. This is done by minimizing the potential energy, which can be expressed as a functional, often called the potential energy functional:

$$\Pi = \int_\Omega \left(\nabla \bullet \sigma + \rho b - \rho \ddot{u} \right) d\Omega \tag{3.1.2}$$

Minimizing this functional leads to the equilibrium configuration of the structure.

The principle of virtual work states that the work done by internal forces is equal to the work done by the external forces when the domain is subjected to virtual displacements. Applying the principle of virtual work, we derive the variational equation:

$$\delta\Pi(u) = 0 \tag{3.1.3}$$

This equation represents the weak formulation and constitutes the foundation for FEM. The variation δ denotes a small perturbation in the displacement field. Integrating by parts the weak form of Eq. 3.1.2 over, Ω we can obtain the virtual work in matrix form as:

$$\delta\Pi(\boldsymbol{u}) = \underbrace{\int_{\Omega} \delta\boldsymbol{u}^T \rho\ddot{\boldsymbol{u}}\, d\Omega}_{\substack{\text{virtual work of internal} \\ \text{inertial forces}}} + \underbrace{\int_{\Omega} \delta(\boldsymbol{B}\boldsymbol{u})^T \boldsymbol{\sigma}\, d\Omega}_{\substack{\text{virtual work of the} \\ \text{internal stress}}} - \underbrace{\int_{\Omega} \delta\boldsymbol{u}^T \boldsymbol{b}\, d\Omega}_{\substack{\text{virtual work of} \\ \text{body forces}}} - \underbrace{\int_{\Gamma_t} \delta\boldsymbol{u}^T \boldsymbol{t}\, d\Gamma}_{\substack{\text{virtual work of} \\ \text{traction forces}}} = 0 \quad (3.1.4)$$

where $\boldsymbol{B}$ is the matrix strain operator and $\boldsymbol{t}$ the traction force vector.

Material Law

In this study, we assume that the blocks of a TIS follow a linear elastic constitutive law. This means that there is a linear relationship between the stress and strain of the material under elastic deformation. The linear elastic constitutive law can be expressed using Hooke's Law in 1D cases, described as $\sigma = E\varepsilon$, where E is Young's modulus and ε the strain. In the general form, Hooke's law can be expressed in Voigt notation as:

$$\sigma = \boldsymbol{C} \bullet \boldsymbol{\varepsilon} \tag{3.1.5}$$

where $\boldsymbol{C}$ is the stiffness tensor and $\boldsymbol{\varepsilon}$ the strain tensor. $\boldsymbol{C}$ can be expressed in 2D cases as:

$$\boldsymbol{C} = \underbrace{\frac{E}{1-\nu^2}\begin{bmatrix} 1 & \nu & 0 \\ \nu & 1 & 0 \\ 0 & 0 & \frac{1-\nu}{2} \end{bmatrix}}_{\text{plane stress}} \quad\text{or}\quad \boldsymbol{C} = \underbrace{\begin{bmatrix} \frac{\lambda(1-\nu)}{\nu} & \lambda & 0 \\ \lambda & \frac{\lambda(1-\nu)}{\nu} & 0 \\ 0 & 0 & \frac{\lambda}{\nu}\left(\frac{1}{2}-\nu\right) \end{bmatrix}}_{\text{plane strain}} \tag{3.1.6}$$

and in 3D cases as:

$$\boldsymbol{C} = \begin{bmatrix} \lambda+2\mu & \lambda & \lambda & 0 & 0 & 0 \\ \lambda & \lambda+2\mu & \lambda & 0 & 0 & 0 \\ \lambda & \lambda & \lambda+2\mu & 0 & 0 & 0 \\ 0 & 0 & 0 & \mu & 0 & 0 \\ 0 & 0 & 0 & 0 & \mu & 0 \\ 0 & 0 & 0 & 0 & 0 & \mu \end{bmatrix} \tag{3.1.7}$$

where λ and μ are as follows:

$$\lambda = \frac{\nu E}{(1+\nu)(1-2\nu)}$$
$$\mu = \frac{E}{2(1+\nu)} \tag{3.1.8}$$

and ν is Poisson's ratio.

3.2 Geometrically non-linear formulation

In many engineering problems, the considered domain undergoes infinitesimally small displacements and rotations. In that case, small strain theory will provide reliable results. As a result, the linear approximation of the Green-Lagrange strain tensor can be used as:

$$\boldsymbol{\varepsilon} = \frac{1}{2}\left(\nabla\boldsymbol{u} + (\nabla\boldsymbol{u})^T\right) \tag{3.2.1}$$

In the case where the domain of a problem undergoes large displacements and rotations (like in TIS), then this assumption does not hold anymore, and the analysis becomes non-linear. In such a scenario, total Lagrangian or updated Lagrangian formulation is used [84, 85]. The

strain components have to consider terms that account for changes in shape, volume, and orientation. As a result, the full Green-Lagrange strain tensor is used:

$$\varepsilon = \frac{1}{2}\left(\nabla u + (\nabla u)^T + \nabla u \bullet (\nabla u)^T\right) \tag{3.2.2}$$

Assuming a static model (*i.e.*, inertial and body forces are 0), the weak form presented in Eq. 3.1.4 over Ω can be updated to consider the full Green-Lagrange strain tensor as:

$$\delta\Pi(u) = \underbrace{\int_\Omega \delta(B_l u)^T S \, d\Omega}_{\substack{\text{virtual work of the} \\ \text{linear internal stress}}} + \underbrace{\int_\Omega \delta(B_{nl}u)^T S \, d\Omega}_{\substack{\text{virtual work of the} \\ \text{non-linear internal stress}}} - \underbrace{\int_\Omega \delta(B_l u)^T S \, d\Omega}_{\substack{\text{virtual work of} \\ \text{residual forces}}} - \underbrace{\int_{\Gamma_t} \delta u^T t \, d\Gamma}_{\substack{\text{virtual work of} \\ \text{traction forces}}} = 0$$

$$\tag{3.2.3}$$

where B_l is the linear strain operator matrix, B_{nl} is the non-linear strain operator matrix and S the second Piola-Kirchhoff stress tensor.

3.3 Computational frictional contact mechanics

Computational frictional contact mechanics is the field that studies and simulates the deformations and interactions of solid bodies when they come into contact. It is a highly non-linear problem, with the whole formulation taking place at the interface between the contacting bodies. These bodies experience both normal forces (forces acting perpendicular to the contact surface) and frictional forces (forces acting tangentially to the contact surface).

The relation between the normal and tangential (frictional) forces was established by Charles-Augustin de Coulomb (1736-1806) while conducting experimental investigations. His observations, today known as "Coulomb's friction law", state that the magnitude of the tangential component of the surface traction, will not exceed the product of the normal component of the surface traction and a constant called the friction coefficient. Later, Heinrich Hertz's (1882) [86] research "On the Contact of Elastic Solids" laid the groundwork for the theoretical analysis of contact mechanics. The theoretical and numerical study of contact mechanics involves the contribution of various scientists over time and does not have a single definitive attribution. A good overview in the field was established by Johnson [87] and Timoshenko and Goodier [88]. The need for solving complex problems involving frictional contact mechanics has led to the advancement of computational contact mechanics.

FEM is one of the first numerical tools used for tackling contact problems. At an early stage, several studies [89–93] demonstrated that numerical methods signal the beginning of an exciting era in the field. Wilson and Parsons [94] and Chan and Tuba [95] formulated contact mechanics using geometrical theory, a theory that has been further extended in recent years [96–98] and is also implemented in the current study.

Numerical approach

The numerical approach, in the current study, is based on differential geometry to accurately represent large rotations and deformations of the interacting bodies. This is combined with a fully covariant description, as it ensures consistent handling of contact interactions regardless of changes in the coordinate system. This approach ensures that the tangent matrix is symmetric in the case of sticking, which improves numerical stability and convergence [99].

Various algorithms exist for describing contact between two surfaces, amongst them the Node-To-Node (NTN), Node-To-Surface (NTS) and Surface-To-Surface (STS). In this study, a NTS algorithm is implemented regularized by the penalty method combined with Coulomb friction law for computing frictional forces between contacting surfaces.

To initially find any potential contact pairs between two bodies, a contact search algorithm is implemented on the updated configuration. This has its basis on the closest point projection

which helps identify if two surfaces are in contact and, if so, determines the closest points on each surface. As a result, two bodies are said to be in contact if a "slave" node penetrates at the closest distance into the "master" surface (or master segment for 2D configurations). The closest distance is defined as the minimum orthogonal distance (or gap) g between a slave node and a master surface as shown in Fig. 3.2 and is calculated as:

$$g = (r_s - \rho_m) \bullet n \tag{3.3.1}$$

where r_s is the slave node coordinate vector, ρ_m the projection vector of the master vector, and n the outward unit vector orthogonal to the master segment computed as:

$$n = \frac{\rho_1 \times \rho_2}{|\rho_1 \times \rho_2|} \tag{3.3.2}$$

where ρ_1 and ρ_2 are the base surface vectors tangent to the master surface. An in-depth explanation of the closest point projection can be found in Laursen [96] and Wriggers [97].
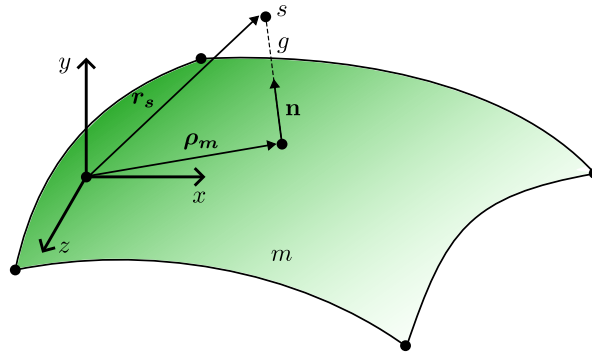
Figure 3.2: Illustration of the closest point projection used for computing the contact gap g between slave point s and master surface, m taken from the local surface coordinate system on master surface.

The final contact element consists of n nodes that describe the master surface, and one slave node. The solution of this optimization problem is systematically achieved by incorporating the contact elements into the FEM solver. The contact elements are subject to certain constraints (*i.e.*, non-penetration constraint, friction constraint, kinematic constraint) for minimizing the interpenetration and approximating the correct solution. The nodal vector for the NTS contact element can be expressed as follows:

$$\mathbf{X} = \left[\underbrace{X_m^{(1)}, X_m^{(2)}, ..., X_m^{(n)}}_{\text{master surface}}, \underbrace{X_s}_{\text{slave node}} \right] \tag{3.3.3}$$

where $X_m^{(i)} = (x, y)_m^{(i)}$ and $i = 1, 2, ...n$ represents the ith master node and X_s the slave node. The surface vector can be described as:

$$\rho = \sum_k N_k(\xi^j) \mathbf{X}^{(k)}, \; j = 1, 2 \tag{3.3.4}$$

where $N_k(\xi^j)$ are the shape functions described by the surface coordinate ξ^j at the local coordinate system and $\mathbf{X}^{(k)}$ the set of master and slave nodal coordinates that compose the contact element k. The base surface vectors are given by:

$$\rho_j = \frac{\partial \rho}{\partial \xi^j}, \; j = 1, 2 \tag{3.3.5}$$

Weak formulation

The virtual work $\delta \Pi_c(u)$ of the contact tractions at the current configuration between deformable bodies Ω_1 and Ω_2 that come in contact at surfaces Γ_1 and Γ_2 (as shown in Fig. 3.3)

can be expressed as:

$$\delta \Pi_c(u) = \int_{\Gamma_1} (T_n \boldsymbol{n} + \boldsymbol{T_t}) \bullet (\delta \boldsymbol{u}_1 - \delta \boldsymbol{u}_2) \, d\Gamma_1 \tag{3.3.6}$$

where T_n is the normal traction, $\boldsymbol{T_t}$ is the frictional traction tangential to $\boldsymbol{n}$ and $\delta \boldsymbol{u}_i$ the variation of the displacement on the surface Γ_i. Using the penalty method, allowing for a small penetration, the normal traction can be computed as $T_n = \varepsilon_n \langle g \rangle$ and the frictional tangential traction as $\boldsymbol{T_t} = \varepsilon_t(\boldsymbol{\Delta u})$. In this case, $(\boldsymbol{\Delta u})$ represents the tangential slip distance between a slave node and the master surface, computed based on the covariant derivative approach [99, 100]. The Macaulay brackets $\langle \rangle$ are used in the form:

$$\langle g \rangle = \begin{cases} 0, & \text{if } g > 0, \\ g, & \text{if } g \leq 0. \end{cases} \tag{3.3.7}$$
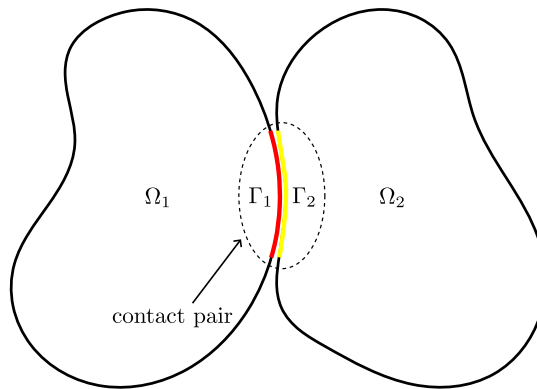
Figure 3.3: Schematic of domains Ω_1 and Ω_2 that come in contact at surfaces Γ_1 and Γ_2.

The proposed contact problem is approached by treading T_n and $\boldsymbol{T_t}$ as dependent variables. Therefore, the contact tractions are penalty regularized similarly to [96, 97, 99, 101]. In addition, the penalty parameters ε_n and ε_t are area regularized, to maintain the stability and accuracy of the contact solver regardless of the underlying mesh resolution [102, 103]. Tuning the value of ε_n and ε_t is critical as they determine the stiffness of the contact forces and consequently minimize the penetration of the salve node to the master surface.

To address the dilemma in selecting master and slave surface, a two-pass algorithm is implemented [102, 103]. This approach includes calculating contact forces twice at each node. In the first pass, one surface is considered as the slave while, in the second pass, as a master. This technique increase the computational burden, but can improve stability and convergence, especially in scenarios with complicated surface geometries and large sliding.

Summary

In this chapter, we explored the numerical approach used for simulating TIS. The numerical solver incorporates FEM with geometrical non-linearities and frictional contact mechanics. Geometrical non-linearities, is an essential consideration for TIS as it involves large deformations and rotations. Moreover, the implementation of frictional contact mechanics is, an essential consideration in TIS where multiple surfaces interact. Integrating Coulomb's friction law into the computational framework, allows capturing tangential forces and stick-slip mechanisms effectively. In conclusion, this framework provides a robust toolkit to explore the fundamentals of TIS.

4

On the failure of beam-like topologically interlocked structures

No amount of experimentation can ever prove me right; a single experiment can prove me wrong.

Albert Einstein

Ioannis Koureas [a], Mohit Pundir [a], Shai Feldfogel [a], David S. Kammer [a,*]

[a] Institute for Building Materials, ETH Zurich, 8093 Zurich, Switzerland
[*] Corresponding author

Key findings:

- The response capacity for beam-like TIS saturates with high friction coefficient values
- The response parameters increase with the height of the structure
- The response parameters scale linearly with Young's modulus
- The study uncovers the conditions that control stick and slip mechanisms

Author contributions: Conceptualization, all authors; methodology, all authors; software, I.K.; validation, I.K.; formal analysis, I.K.; investigation, all authors; resources, D.S.K.; data analysis, I.K.; writing–original draft preparation, I.K.; writing–review and editing, all authors; visualization, I.K.; supervision, D.S.K., S.F., M.P.; project administration, D.S.K.

---

[1]This is a post-print of Koureas et al. [104], differing from the published paper only in terms of layout and formatting.

Abstract

Topologically interlocked structures are architectured by fitting together blocks that are constrained geometrically through contact and friction by their neighboring blocks. As long as the frictional strength is nowhere exceeded, the blocks stick against each other, allowing for large rotations. Once the interfacial stresses exceed the frictional strength, relative sliding between the blocks alters the structure's mechanical response. Improving the structural performance, precisely the strength and the toughness, has been one of the main focal points in the literature. However, many fundamental questions regarding the role and effect of the interface mechanisms (stick and slip) and rotation of the blocks have not been addressed yet. Here, we carry out a parametric analysis to understand the effect of Young's modulus, friction coefficient, and geometry of the blocks on the dominance of the stick or slip-governed mechanism. We combine analytical and computational tools to analyze the failure mechanisms and the response capacities of beam-like topologically interlocked structures. This is achieved using the finite element method coupled with a penalty-based approach for enforcing contact constraints along interfaces. We show that the combination of the structure's height and the friction coefficient controls whether the failure mechanism is slip-governed or stick-governed. Furthermore, we demonstrate that the sticking mechanism across all interfaces along with the rotation of the blocks dictates a saturation level to the mechanical performance of a given structure, irrespective of geometric and material properties. This provides a theoretical upper bound for the structural response of topologically interlocked structures and establishes a theoretical benchmark of achievable performance.

Keywords: Architectured Structures; Frictional Contact; Stick-Slip Governed Failure; Saturation Level

4.1   Introduction

Topologically interlocked structures (TIS) are assemblies of building blocks that hold together due to the blocks' unique interlocking shapes [1, 30, 62, 73, 105]. The unbonded nature of the blocks means that TIS rely on contact and frictional interactions between blocks for structural integrity (Fig. 4.1a). TIS enjoy unique structural properties, including high toughness against failure for structures made from brittle material [3, 19, 62] and structural integrity despite partial failure (*e.g.*, missing blocks in plate-like TIS) [5]. However, TIS have not yet found widespread application in engineering because their highly complex, non-linear behavior and failure are not yet fully understood, hindering the ability to design them safely. A better understanding of the behavior and failure of TIS is therefore required and is at the focus of this study.

The main mechanisms governing the behavior and failure of TIS are local slip and stick combined with large block rotations [3, 4, 35]. These mechanisms take more or less prominent roles in the structural response, depending on the TIS design and material properties. However, it remains unclear how these properties determine which mechanism will likely be the more dominant one in a given TIS configuration and how they affect the global structural response in terms of load-carrying capacity, loading energy, global stiffness and ultimate deflection.

In the relatively simple case where the response is entirely stick-governed, the behavior can be described by analytical models, as in [33–35]. Khandelwal *et al.* modeled TIS as a truss and derived analytical expressions for the horizontal and vertical reaction forces F_h and F_v at the local pivoting point A (Fig. 4.2a), which goes as follows:

$$F_v = F_h \left(\frac{h_{\text{eff}} - \delta}{l_{\text{eff}}} \right) = E \mathcal{A} \frac{l_{\text{eff}}}{\sqrt{l_{\text{eff}}^2 + h_{\text{eff}}^2}} \left(\frac{\sqrt{l_{\text{eff}}^2 + h_{\text{eff}}^2}}{\sqrt{l_{\text{eff}}^2 + (h_{\text{eff}} - \delta)^2}} - 1 \right) \left(\frac{h_{\text{eff}} - \delta}{l_{\text{eff}}} \right) \quad (4.1.1)$$

where E is Young's modulus of the material, h_{eff} and l_{eff} are the effective height and length
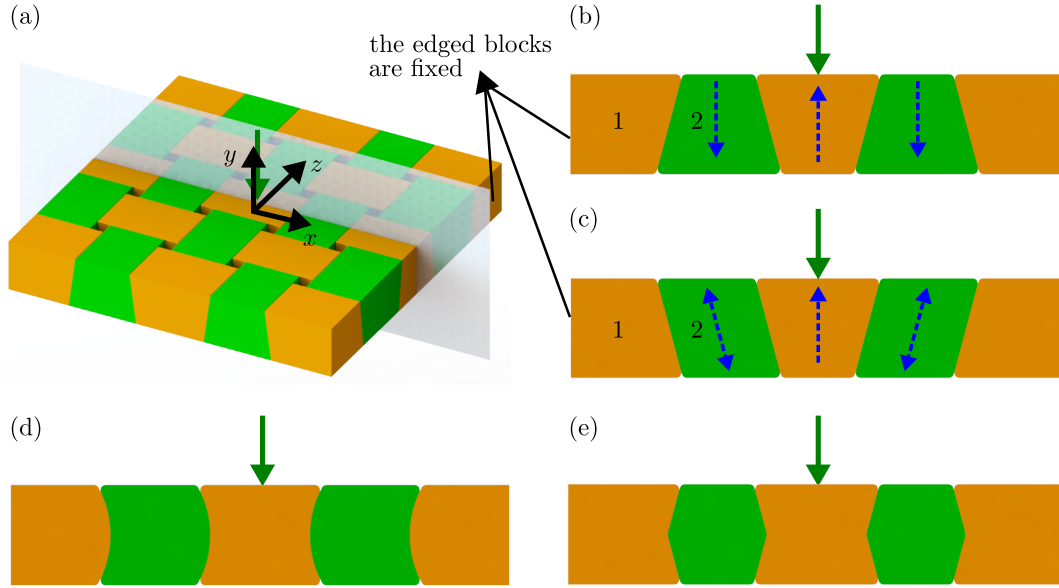
Figure 4.1: Rationale for the examined configuration: (a) A topologically interlocked structure (TIS) assembly with planar-faced blocks [4]. (b) Central cross-section in the x–y plane and (c) the basic configuration, which is used for the bulk of this study, is obtained from the original x–y cross-section with the inclination between blocks 1 and 2 flipped. The beam-like structures with (d) curved and (e) kinked surfaces are examined later in relation to Fig. 4.8 for generality and completeness of the study.

respectively (Fig. 4.2), $\mathcal{A}$ is the cross-sectional area of the truss model and δ the applied displacement if no slip occurred so far. Eq. 4.1.1 clearly demonstrates that in a sticking situation, the load-carrying capacity (*i.e.*, $2F_v$) scales linearly with E and is strongly dependent on h_{eff} and l_{eff}. Although Eq. 4.1.1 does not apply when slip occurs, we can still qualitatively explain how local slip reduces global stiffness by examining a specific slipped configuration. Specifically, when slip occurs, the initial pivoting point B moves to B' (Fig. 4.2b), reducing h_{eff}, F_h and hence, the load-carrying capacity $2F_v$. However, these observations remain qualitative, particularly regarding the possible co-existence of stick and slip. Specifically, they do not account for the occurrence of local slips and the consequent evolution of slip-governed failure mechanism. To capture a slip-governed response, which is the most common one in practice and the more challenging one to model, computational methods are required.

The finite element method (FEM) has been shown to capture and quantify the experimentally observed failure and the load-displacement curve in beam-like TIS [77, 106]. Dalaq *et al.* [77] showed that the failure mode depends on the number of blocks, friction coefficient and the shape of the interfaces, specifically that curved interfaces (a similar configuration is shown in Fig. 4.1d) promote sliding of the blocks and delay hinging (*i.e.*, stick and rotation) [78]. However, Dalaq *et al.* [78] focused on a specific material and did not investigate the effects of Young's modulus E on the failure mechanisms and the structural capacity. In addition, the effect of the assembly's height h, which governs the bending stiffness of TIS assemblies, see Zakeri *et al.* [107], was not considered [2].

In summary, the effects of h, E and μ on the type of failure, *i.e.*, a slip-governed or stick-governed one and on the associated structural capacities of TIS have hitherto not been addressed in the literature and remain only partially understood. Here, we aim to clarify and quantify these effects. Specifically, we aim to better understand how different combinations of h, E and μ tend to make the response more slip-, or stick-governed and how they affect the structural capacity in terms of maximal load, loading energy, global stiffness and ultimate deflection. Towards that aim, we perform a three-way $E - \mu - h$ parametric study using FEM, based on the latter's ability to capture and quantify experimentally observed failure

---

[2]The scaling of the response capacities has not been explicitly verified.
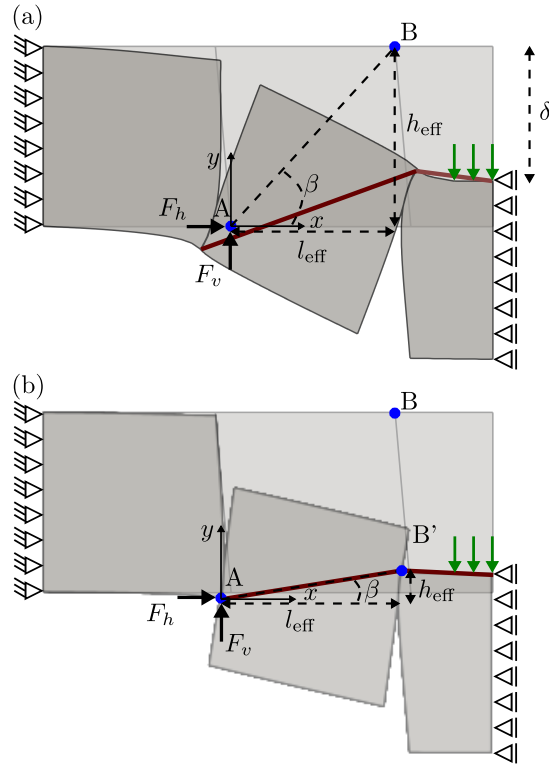
Figure 4.2: Equivalent truss model (dark red color) in a topologically interlocked structure (TIS) for (a) a stick and (b) a slip scenario. The effective height h_{eff} and length l_{eff}, as well as the displacement, δ are shown for the deformed structures.

mechanisms, in particular the slip-governed one, in beam-like TIS [77, 78]. In contrast with previous parametric studies that were limited to the stick-regime, the main strength of the present study is that it treats both the stick and the slip regimes within a unified FEM-based framework. This allows us not only to better understand the previously unaddressed effects of E, μ and h on the slip-governed failure, but also to better understand the conditions that control the two mechanisms.

In the following, we discuss the choice of examined configuration and the FEM formulation (Sec. 4.2). In Sec. 4.3 we present and discuss the results of the parametric study and give an outlook on how the gained knowledge can aid the design of TIS.

4.2 Numerical Model

4.2.1 Examined configuration

To address the effects of E, μ and h on the failure and response capacity of TIS, we choose a beam-like configuration inspired by the centrally loaded plate-like planar-faced TIS studied experimentally in [4]. The original configuration from [4] is presented in Fig. 4.1a. The central cross-section of the structure in the $x - y$ plane is depicted in Fig. 4.1b. The configuration we use for this study is modified compared to the cross-section of the actual 3D TIS such that the angle of inclination of the planar interface between blocks 1 and 2 is reversed, as shown in Fig. 4.1c.

The concept of simplifying 3D TIS to 2D beam-like structures with a representative cross-section of the 3D equivalent goes back to [33–35, 77, 78]. This approach, well-established in structural analysis of monolithic structures, is motivated in the present TIS context by computational and methodological considerations. The computational cost of modeling slip-governed failure in TIS with FEM is always very high and, in TIS with more than a few

Table 4.1: List of symbols and notations

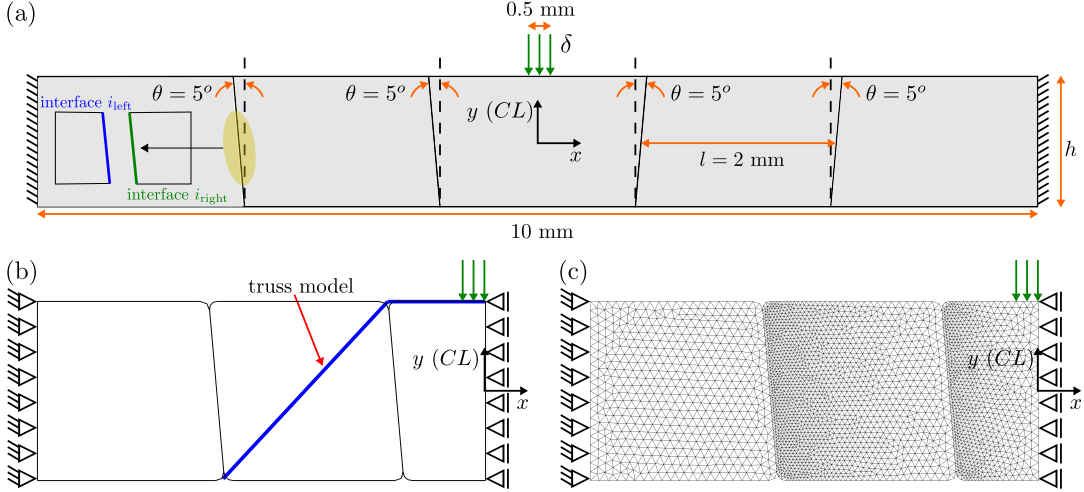| Symbol	Description	Unit
E	Young's modulus	N/m^2
F_a	Resultant force at a given pivoting point of the truss model	N
F_y	Load-carrying capacity of the structure	N
$F_{\max}$	Maximum load-carrying capacity of the structure	N
h	Height of a block (= structural depth)	m
h_{eff}	Effective height in a TIS	m
K	*Normalized* global stiffness of the structure	-
l	Length of a block	m
l_{eff}	Effective length in a TIS	m
N	Normal force along a TIS interface	N
t	Thickness of a TIS	m
T	Tangential force along a TIS interface	N
δ	Prescribed displacement at the top central surface of the middle block	m
U	Loading energy of the structure	Nm
β	Angle controlled by h_{eff} and l_{eff}	^{o}
ε_n	Normal penalty parameter	N/m^3
ε_t	Tangential penalty parameter	N/m^3
θ	Inclined angle	^{o}
μ	Friction coefficient	-
μ_{sat}	Saturated friction coefficient	-
ν	Poisson's ratio	-

blocks, may be prohibitive [78]. Methodologically, we assume that the effects of material properties (E and μ) and the structural height (h) on the structural response are qualitatively similar in 3D and 2D TIS, as they are in monolithic counterparts, therefore, we consider the latter. The structural action of beams is much simpler, and it allows studying these effects in pure form, in accordance with the objectives of the present study.

We note that our configuration is not fully interlocked because there are directions (indicated by blue arrows in Fig. 4.1b and c) in which the blocks are not kinematically constrained by the neighboring blocks. This scenario is due to the 3D nature of topological interlocking, and it is very typical of 2D cross-section representation, like the actual cross-section in Fig. 4.1b and other beam-like TIS configurations studied in the literature [33–35, 78]. To effectively constrain our configuration, we required that (a) the structure has structural integrity under its self-weight and (b) that it is interlocked under the examined loads. Requirement (a) motivated reversing the angle of inclination between blocks 1 and 2 compared to the actual cross-section of the TIS. Requirement (b) is met in our configuration, since we only examine a downward load on the central block. By avoiding loads in the few specific directions that are not kinematically constrained (the degrees of freedom in which our configuration deviates from a strictly defined TIS), our configuration may be considered to be effectively TIS under the examined loads. In order to examine the generality of the observation, we consider two additional cases with non-planar interfaces, a curved interface (Fig. 4.1d) and a kinked interface (Fig. 4.1e).

4.2.2 Numerical formulation

FEM is used for the numerical analyses in this study. We employ finite strain formulation to account for the large deformations and large rotations of the building blocks [84]. Thus, considering n deformable bodies Ω_n^i, the weak formulation at load increment i is described as:

$$\sum^n \int_{\Omega_n^i} \underline{\underline{\varepsilon}}^i : \mathbb{C} : \delta\underline{\underline{\varepsilon}}^i \, d\Omega_n^i \; + \; \sum^n \int_{\Omega_n^i} \underline{\underline{S}}^i : \delta\underline{\underline{\eta}} \, d\Omega_n^i \; = \; W_{\text{ext}}^{i+1} \; - \; \sum^n \int_{\Omega_n^i} \underline{\underline{S}}^i : \delta\underline{\underline{\varepsilon}} \, d\Omega_n^i \qquad (4.2.1)$$

Figure 4.3: Schematic representation of model set-up showing (a) the geometric parameters and boundary conditions in a five-block topologically interlocked structure (TIS). Every structure consists of i interfaces, where $i = 1, 2, ..., k$ with k being the total number of interfaces in a structure. Every interface consists of two sides, the left and the right. (b) Schematic illustration of the symmetric model with respect to the center line (CL). The blue line represents the truss model. (c) Mesh and boundary conditions as used in the simulation.

where, $\underline{\underline{S}}$ and $\underline{\underline{\varepsilon}}$ are the 2nd Piola-Kirchhoff stress tensor and the linear strain tensor, respectively. W_{ext}^{i+1} is the virtual work of the external forces, $\underline{\underline{\eta}}$ represents the nonlinear incremental strain tensor and $\mathbb{C}$ the 4th order constitutive tensor. A node-to-segment contact algorithm, with penalty-based constraints, is employed [96, 99, 108–111] to enforce contact and frictional constraints along the interfaces of n deformable bodies. We use the penalty method for its computational simplicity. The virtual work δW_c of the contact forces at the current configuration for n deformable bodies that come in contact at k interfaces S_k is expressed as:

$$\delta W_c = \sum^{k} \int_{S_{k_{\text{slave}}}} \left(T_n \boldsymbol{n} + \boldsymbol{T_t} \right) \bullet \left(\delta \boldsymbol{u}_{k_{\text{slave}}} - \delta \boldsymbol{u}_{k_{\text{master}}} \right) dS_{k_{\text{slave}}} \tag{4.2.2}$$

where T_n is the traction along the normal $\boldsymbol{n}$ to the interface and $\boldsymbol{T_t}$ is the frictional traction tangential to $\boldsymbol{n}$ integrated over one of the two contact surfaces termed as slave surface. Based on the penalty approach, $T_n = \varepsilon_n \langle g \rangle$ is approximated as a linear function of the orthonormal gap between a slave node and the master surface. Similarly, $\boldsymbol{T_t} = \varepsilon_t (\boldsymbol{\Delta u_t})$ is approximated as a linear function of the tangential slip distance $(\boldsymbol{\Delta u_t})$ between a slave node and the master surface, computed based on the covariant derivative approach [99, 100]. The penalty parameters $(\varepsilon_n, \varepsilon_t)$ are area regularized to ensure that the computed contact forces are mesh independent [102, 103]. In order to overcome the biases in choosing a slave and master surface at an interface (see Eq. 4.2.2), a two-pass algorithm [102, 103] is employed whereby at each load increment, the contact forces at a node are computed considering once a surface as a slave and then as a master. The FE code, with the finite strain formulation and the node-to-segment contact algorithm, is developed as in-house code and has been validated for frictional cases (more details provided in Sec. A.1.1).

The examined structure is depicted in Fig. 4.3a. We consider a five-block assembly with a span length of 10 mm and three different heights ($h = 1$ mm, $h = 1.5$ mm and $h = 2$ mm). It is fixed at its ends (i.e., $u_y(\pm 5, y) = u_x(\pm 5, y) = 0$) and it is loaded incrementally by prescribing the displacement $u_y (-0.25 \leq x \leq 0.25, h/2) = \delta = h/500$. The total force corresponding to δ is denoted by F_y. Using the symmetry about the y-axis, we model only the left half of the structure, where the symmetry boundary condition $u_x = 0$ is prescribed along $x = 0$.

Each block is characterized by its angle θ, height h and length l. The blocks are considered to be isotropic linear elastic material with Young's modulus E, Poisson's ratio ν and friction

coefficient μ. A description of the symbol notation we use is provided in Table 4.1. The material and geometrical values used for the parametric analyses are presented in Table 4.2. We chose values of E that cover an essential range of brittle materials and allow us to study the effect of material elasticity on the global stiffness of TIS. Furthermore, we explore a wide range of μ to understand the effect of interfacial friction of the blocks. The effects of fracture are not accounted.

For the numerical analysis, the topologically interlocked beam (Fig. 4.3b) is modeled as a 2D structure under plane-strain conditions. The structure is discretized using first-order triangular elements (Fig. 4.3c) and the corners are rounded to avoid non-physical stress singularities. All simulations are performed under static conditions. Therefore, dynamic effects of friction and inertial effects that may be associated with the structural response are not considered.

Table 4.2: Material and geometric parameters

Parameter	Value
E (GPa)	1, 2, 3, 10, 20, 30
h (mm)	1.0, 1.5, 2.0
l (mm)	2.0
t (mm)	1.0
θ (^{o})	5
μ	0.2, 0.4, 0.6, 0.8, 1.0, 1.2
ν	0.2

To validate our FE formulation in the context of TIS, we analyzed the five-block pre-compressed assembly studied in [77]. The results show that the model compares well, both qualitatively and quantitatively, with the analytical model and reasonably well with the experiments (Fig. 4.4), supporting the validity of our approach.
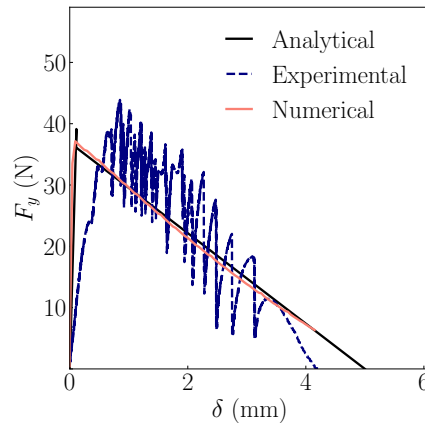
Figure 4.4: Load-carrying capacity F_y against the prescribed displacement δ for a five-block pre-compressed structure with angle $\theta = 0^o$. The experimental and analytical results have been taken from [77].

A sensitivity analysis based on the global load response and the local interface mechanism is performed (see Sec. A.1.2). We chose mesh refinement and the penalty parameters such that both converged.

4.3   Results and Discussion

4.3.1   Global response

In our analysis we explore the effects of h, E and μ on the slip and stick-governed failure mechanisms and on the global response. Specifically, the maximum load-carrying capacity ($F_{\max}$), loading energy (U), global normalized stiffness (K) and ultimate deflection. $F_{\max}$ is computed as the maximum value of F_y and the loading energy as $U = \int_0^{\delta_{\max}} F(\delta) d\delta$ with $\delta_{\max}$ such that $\mathbf{F}(\delta_{\max}) = 0$ and $\frac{\partial F}{\partial \delta}\Big|_{\delta_{\max}} < 0$. K is defined by the secant slope in the $F_y - \delta$ curves at $\delta/h = 0.05$ (Fig. 4.5a). Since fracture is neglected, the failure of the structure is characterized by the central block being completely pushed out of the structure. The relation between $F_{\max}$, U, K and ultimate deflection is investigated for the different structures with a focus on the underlying mechanisms causing these properties.

Fig. 4.5 depicts the normalized $F_y - \delta$ curves for all values of h, μ and E examined. F_y is normalized with respect to h, t and E while the deflection is normalized with respect to h to remove the scalability effect. In all cases, there is a non-monotonic behavior. The force initially increases linearly with the prescribed displacement. It gradually deviates from the linear behavior and eventually reaches a peak value $F_{\max}$. Beyond that point, the force decreases until it reaches zero similar to other studies [4, 33].
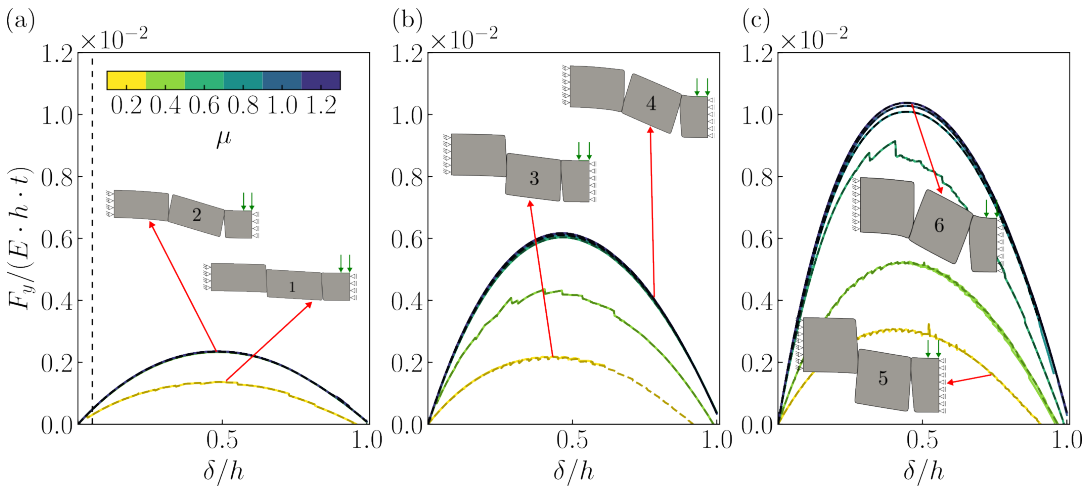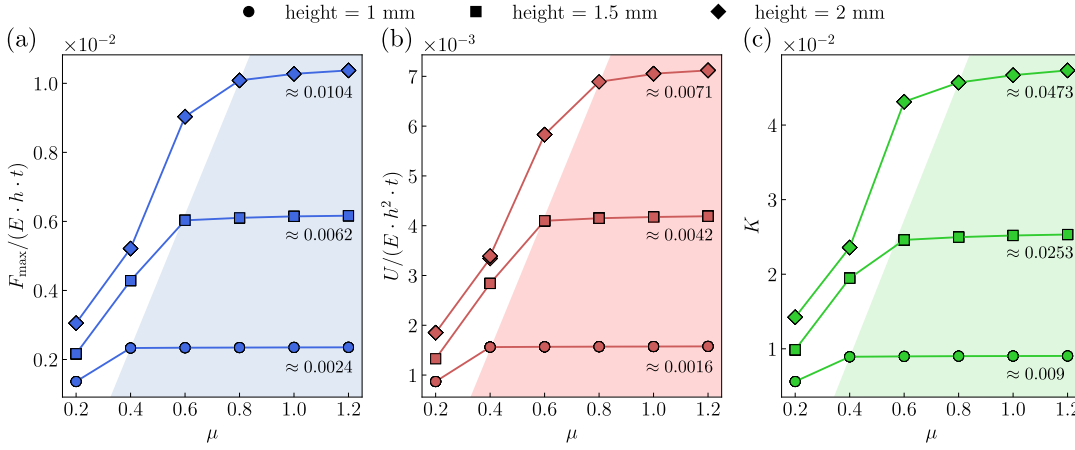

Figure 4.5: Load-carrying capacity F_y normalized with respect to Young's modulus E, the height h and thickness t of the structure against the prescribed displacement δ normalized with respect to h. The curves correspond to a structure with angle $\theta = 5^o$ with (a) $h = 1.0$ mm, (b) $h = 1.5$ mm and (c) $h = 2.0$ mm. The structures numbered 1, 3 and 5 show cases where the slip mechanism is observed while structures 2, 4 and 6 show cases where the stick mechanism is observed. The dashed lines on the normalized $F_y - \delta$ curves represent the lowest value of E (1 GPa). Each curve is an overlap of six curves that correspond to the different values of E. The dashed vertical black line represents $\delta/h = 0.05$ which is used to compute the global stiffness K.

Effect of μ

Fig. 4.5 shows that, for each of the examined h's, the curves with the lowest F_{max} are associated with the smallest μ's indicated by yellow lines. The associated mechanism in these cases, represented by snapshots 1, 3 and 5, involves slip along the interfaces. In contrast, the curves with the highest F_{max} are associated with the highest μ's and the associated mechanisms, represented by snapshots 2, 4 and 6, are entirely stick-governed. These observations mean that higher μ is conducive to increasing the structural capacity insofar as it promotes sticking mechanisms.

Fig. 4.6 depicts the direct dependence of F_{max}, as well as U and K, on μ, for all examined beam

heights (indicated by different markers). All three response parameters initially increase as a function of μ, but later saturate at higher values of μ (shown by the shaded regions in Fig. 4.6). The saturation of all three response parameters is reached at effectively the same μ, denoted by μ_{sat}. The μ_{sat} for $h = 1, 1.5$ and 2 mm are 0.4, 0.6 and 0.8, respectively, as indicated in Fig. 4.6.

Figure 4.6: Overview of the mechanical performance of beam-like TIS, showing the saturation for (a) the maximum load-carrying capacity $F_{\max}$, (b) the loading energy U normalized with respect to Young's modulus E, the height h and thickness t of the structure and (c) the normalized global stiffness K plotted against the friction coefficient μ for structures with $h = 1.0$ mm, $h = 1.5$ mm and $h = 2.0$ mm. By increasing μ the structure reaches a maximum value for all cases (see the approximated value). The lines have been added as a visual aid. The shaded areas signify the saturated regions.

To address the effects of spatial variability of μ along the interfaces, we consider the case where μ is randomly chosen from a normal distribution with mean 0.6 and a standard deviation of 0.4 (with $h = 2$ mm). Fig. 4.7 depicts $F_y - \delta$ from 50 random realizations, indicated in light yellow. While μ varied within 66% of the mean, F_{max} varied within only 20% of the average value, indicated by the green dashed line and it is close to the response without μ variability, indicated by the blue dashed line. This suggests that the effect of spatial variability of μ is relatively mild. Also, even the realizations with the highest F_{max} do not exceed the saturated response ($\mu_{sat} = 0.8$) corresponding the same geometry, shown by the black dashed line. This shows that having higher-than-saturated μ's along the interface can never lead to higher F_{max} than the saturated one.

Effect of h

$F_{\max}$, U and K increase as a function of h (Fig. 4.6). In addition, Fig. 4.5 shows that while h increase, more $F_y - \delta$ curves lie below the saturated curves. These curves are characterized by sliding mechanism. For example, for $h = 1$ mm sliding occurs only for $\mu = 0.2$ (Fig. 4.5a structure 1). For $h = 1.5$ mm sliding occurs when $\mu = 0.2$ (Fig. 4.5b structure 3) and $\mu = 0.4$. Finally, for $h = 2$ mm sliding occurs when $\mu = 0.2$ (Fig. 4.5c structure 5), 0.4 and 0.6. For a constant μ, as h increases, the magnitude and the direction of the thrust line changes, which alters the normal and tangential forces at the contact points. Based on Coulomb friction, a point is reached where the ratio between the tangential and normal forces exceeds the friction coefficient and the structure starts sliding. Based on the results, but also from analytical expressions derived in the literature [34, 77], we find $K \propto h$. The smaller the h, the smaller the compression experienced by TIS and, therefore, the smaller the $F_{\max}$, U and K. We therefore conclude that the increase of h promotes sliding.

The ultimate deflection in a beam-like TIS in our study never exceeds the structure's height (h). This is in agreement with the analytical expression from Eq. 4.1.1. When the applied displacement becomes equal to the structure's height, the reaction force becomes zero, showing that the maximum deflection is equal to h. Therefore, μ, h and E are the main parameters that
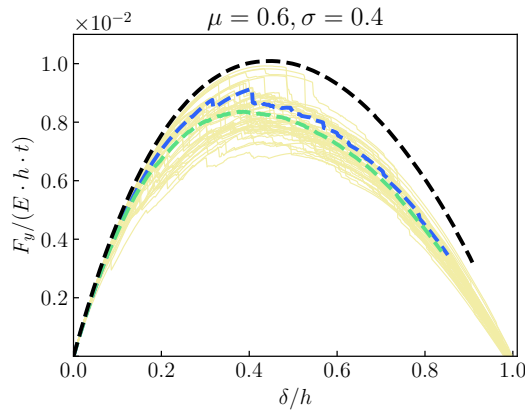
Figure 4.7: Effect of μ variation along an interface. Load-carrying capacity F_y normalized with respect to Young's modulus E, the height h and thickness t of the structure against the prescribed displacement δ normalized with respect to h for $\mu = 0.6, \sigma = 0.4$. 50 simulations were run for each case, shown by the light yellow curves. The average load response of 50 simulations is shown by the green dashed curve. For comparison, we also show the load responses for the cases where $\mu = 0.6$ is constant along the interface, (shown in dashed blue curve) and where $\mu = \mu_{sat} = 0.8$ is constant along the interface (shown in black dashed curve).

affect the global response of TIS and ultimately F_{max}, U, K and ultimate deflection.

Effect of E

In Fig. 4.5, the $F_y - \delta$ curves are normalized by E. We found that, for each h and μ (*e.g.,* the yellow curve in (Fig. 4.5a) corresponding to $h = 1$ mm and $\mu = 0.2$), the normalized curves to the six examined E are identical. This exact linear scaling with E suggests that the response is qualitatively identical in the six cases and that E only affects the magnitude of the response parameters (irrespective of μ and h), but not the mechanisms (as we indeed show later in Sec. 4.3.2). The presence of a linear relationship between E and mechanical response for such a wide range of friction coefficients is a new observation. Such a linear dependency can be predicted for high values of μ, assuming that slipping is suppressed along the interfaces (see Eq. 4.1.1 and [34]). However, for lower values of friction coefficient ($\mu = 0.2, 0.4$), where the slipping occurs, such a linear dependency has not been shown.

Effect of interface geometry

Our work shows that the described beam-like structures reach theoretical maximum response capacities with μ_{sat} independently on the material properties (E) and geometrical parameters (h, l). This observation was obtained based on the behavior of blocks with planar interfaces. To further generalize our observation, we consider two additional structures (with $h = 2$ mm). The first one is a five-block structure with curved interfaces and curvature ratio $c = l/R = 1$. Here R is the radius of the curvature. The second is a five-block structure with kinked interfaces and inclined angle $\theta = 5^o$. The capacity saturation curves and a snapshot of the failure mechanism are shown for the two cases in Fig. 4.8c and Fig. 4.8d. Like the blocks with planar interfaces, the load-carrying capacity attains saturation. However, for structures with curved interfaces, the saturation level required a greater μ (*i.e.,* $\mu_{sat} = 2$) compared to the cases with straight interfaces (*i.e.,* $\mu_{sat} = 0.8$ and $h = 2$ mm). This observation is in agreement with Dalaq *et al.* [77], who showed that curved surfaces can promote sliding mechanism and delay sticking. Finally, we note that the use of curved surfaces reduces the value of the saturation level (*i.e.,* $F_{max}/(E \cdot h \cdot t) \approx 0.008$) compared to ($F_{max}/(E \cdot h \cdot t) \approx 0.01$) for the planar interfaces. In addition, sliding does not allow the structure to reach the maximum theoretical deflection.
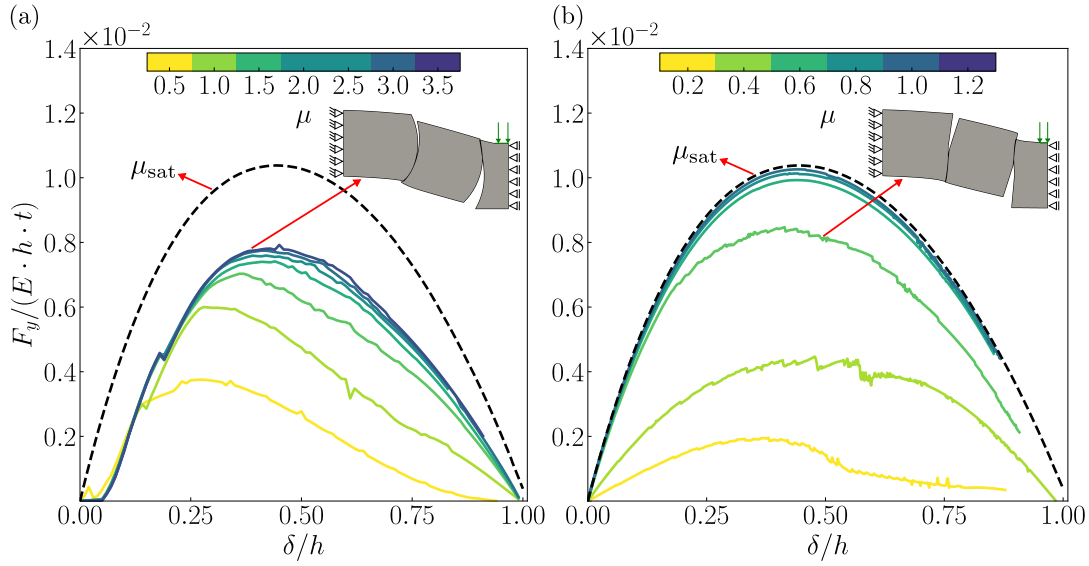
Figure 4.8: Load-carrying capacity F_y normalized with respect to Young's modulus E, the height h and thickness t of the structure against the prescribed displacement δ/h. The curves correspond to (a) a five-block structure with curved interfaces and curvature ratio $c = l/R = 1$ with R being the radius of the curvature and (b) a five-block structure with kinked interfaces and angle $\theta = 5^o$. The black dashed line corresponds to the equivalent saturated curve for five-block structure with planar interfaces and $\mu = 1.2$.

## 4.3.2 The type of failure mechanism

The nature of TIS suggests that their mechanical performance is the direct result of interfacial mechanisms. To better understand the effect of TIS mechanisms on the mechanical behavior of the structure, we deemed necessary to take a closer look at the interface between the blocks. We now consider which combinations of h and μ lead to a stick-governed failure and which lead to a slip-governed one. We also verify that E does not affect the interface mechanism, as discussed in the previous section.

Stick and slip can be defined per a given load increment and per the entire response, the latter being the definitive one for our discussion. Per a given increment, we distinguish between the node level, the interface level and the structure level. The node level is binary - a node sticks when the tangential traction is smaller than the tangential capacity and slips otherwise. At the interface level, we define the slipping percentage to be the percentage of nodes that slip, and we consider an interface to stick when at least one node sticks, that is when the slipping percentage is less than 100%. The structural level is also binary - a structure is sticking if and only if all the interfaces are sticking and sliding otherwise.

At the level of the entire response, we also consider the distinction between stick and slip to be binary — the response is stick-governed if and only if the structure sticks in all load increments and slip-governed otherwise.

Fig. 4.9 illustrates these definitions for $h = 2$ mm, $\mu = 0.6$ and all examined E. Fig. 4.9a shows the evolution of sliding percentage in both interfaces throughout the response. The overall mechanism does not change by changing E. Fig. 4.9b indicates interfaces 1 and 2 and shows snapshots of the deformed structure at $\delta/h = 0.15$ and at 0.35. Fig. 4.9a shows that interface 1 is slipping up to about $\delta/h = 0.25$ (sliding percentage = 100%) and alternately sticks and slips thereafter. Interface 2 is sticking throughout (sliding percentage < 100%). From the fact that there are load increments with 100% sliding, we conclude that the response in this case is slip-governed.

Based on the above definitions, Fig. 4.10 depicts the type of failure as a function of μ and
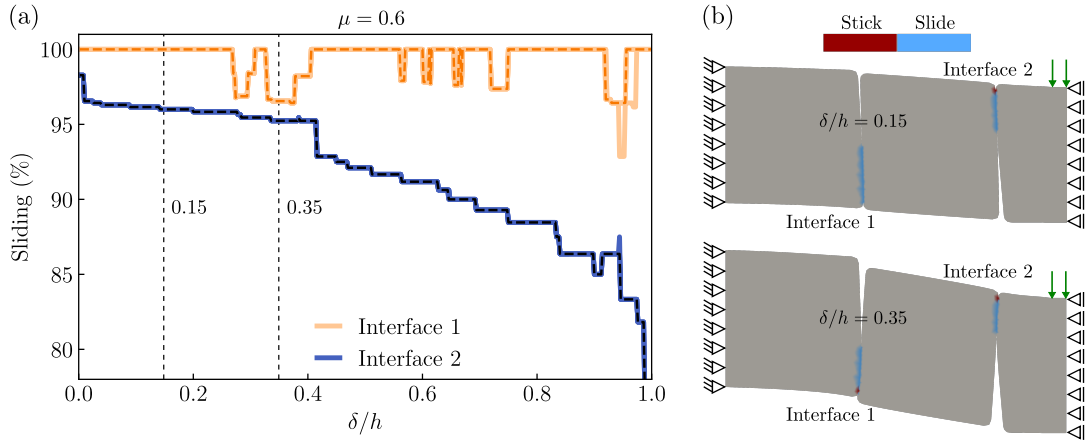
Figure 4.9: Interface mechanism. (a) Percentage of sliding against the prescribed displacement δ/h at every interface of a structure with height $h = 2$ mm and $\mu = 0.6$. (b) Snapshots capturing the sliding and sticking mechanisms at the interfaces of the structure at $\delta/h = 0.15$ and $\delta/h = 0.35$. The colored dashed lines represent the sliding percentage for $E = 1\ GPa$.

h with red and blue circles indicating slip- and stick-governed responses, respectively. In addition to the results of our analyses, Fig. 4.10 also includes an analytically derived line based on [34] which parses the parameter space to stick- and slip-governed regions (see Sec. A.1.3 for the derivation of the analytical line). Fig. 4.10 shows that the higher the h is, the response is slip-governed for higher μ. This quantitatively supports the previous observation that higher h promote sliding. The fact that the response is slip-governed for most of the realistic range of μ between 0.2-0.4 reflects the larger prevalence of this mechanism observed in experiments, which designates this regime as the one of more practical relevance. This underlines the importance and relevance of accounting for the effects of E, μ and h specifically in the slip-governed context, which is at the focus of the present research. Lastly, the fact that the analytically derived line is in close agreement with our results supports the validity of our modeling approach.
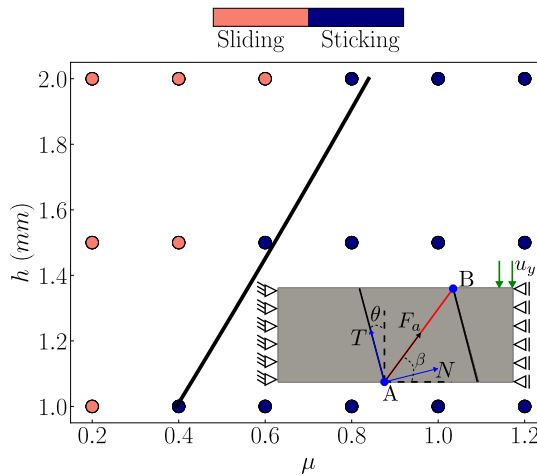
Figure 4.10: Global failure mechanism. Dark points correspond to setups that lead to failure governed by sticking, whereas light points correspond to setups that lead to slip-governed failure. The black line represents the boundary based on the analytical solution from the truss model (Eq. A.1.6).

4.3.3 Saturated friction coefficient from a design perspective

In all cases examined, the saturation level has been reached for high μ_{sat} for common building materials. This raises a question regarding the practical relevance of capacity saturation. Nevertheless, recalling that what defines capacity saturation is the condition of no-slip and

that high μ_{sat} is but one way of obtaining this condition, capacity saturation is actually relevant in systems where slips are suppressed by means other than high μ_{sat}. One example of increasing the effective surface resistance to sliding is through architectured surfaces, or surface-level-interlocking, see Djumas et al. [6]. In such systems, the high μ_{sat} can be viewed as an approximate measure of the (geometrically-induced) macroscopic surface resistance to sliding. Considering μ as a generalized measure of effective sliding resistance, the phenomenon of capacity saturation is realistic and relevant in all systems where this resistance can be increased to the point of suppressing sliding completely, regardless of the actual friction coefficient.

4.3.4 General comments

The sliding and rotation of the blocks are crucial for the mechanical behavior of TIS as it introduces a non-linear behavior in a structure made from a linear elastic material. When sticking occurs, applied work is stored in the form of elastic energy [6, 71]. In that case, K is controlled by E of the blocks, l_{eff} and h_{eff}. The structure can be described as elastic when the model is characterized by the stick and rotation mechanisms. As a result, the model is load-independent. When sliding occurs, however, the structure becomes load-path dependent. The advantage of such a structure is that the building blocks do not physically undergo plastic deformation but only the structure. Moreover, it is possible to have a structure that initially sticks (behaves elastically) within the service range. However, it can also behave inelastically (through sliding) once it exceeds a specific value. Design parameters alongside material properties are considered the main factors affecting the ultimate behavior of TIS. Therefore, we conclude that TIS made from linear elastic materials can express both elastic and inelastic behavior at the structural scale.

4.4 Conclusion

This study presented a parametric analysis of TIS to understand how the elastic modulus E, the friction coefficient μ and the structural height h affect the interfacial failure mechanisms and the response capacity of beam-like topologically interlocked structures. From this parametric analysis, we can conclude that as μ increases, the response is more stick-governed and the response parameters increase with h and (linearly) with E. For all examined block geometries and given E and h, there always exists a saturation level of the structural capacity as a function μ. In addition, for relatively small values of μ, sliding occurs at interfaces, decreasing the effective height of the structure, which in turn leads to a decrease in the load-carrying capacity. Finally, h and E of the blocks mainly control the structure's response capacity while μ and the interface geometry control the type of mechanism (stick or slip) that governs the failure. Specifically, the response parameters scale linearly with E not only in the stick mechanism (as observed previously) but also in the more commonly observed slip mechanism. Alongside the observation of capacity saturation with increasing μ, the two main and original, contributions of this study are: (a) that it addresses the effects of E, μ and h on the slip-governed failure of TIS; and (b) that it elucidates the conditions that govern the occurrence of the stick or the slip mechanisms. The insights and observations from this study, particularly the phenomenon of capacity saturation, are relevant from a design perspective and they will serve as the starting point for future work.

5

Beam-like topologically interlocked structures with hierarchical interlocking

> The important thing in science is not so much to obtain new facts as to discover new ways of thinking about them.
>
> Sir William Lawrence Bragg

Ioannis Koureas [a], Mohit Pundir [a], Shai Feldfogel [a], David S. Kammer [a,*]

[a] Institute for Building Materials, ETH Zurich, 8093 Zurich, Switzerland
[*] Corresponding author

Key findings:

- The response capacity of beam-like TIS with wave-faced blocks saturates at realistic friction coefficients
- The saturated response capacity of beam-like TIS with wave-faced blocks converges to that of beam-like TIS with planar-faced blocks and high friction coefficient.

Author contributions: Conceptualization, all authors; methodology, all authors; software, I.K.; validation, I.K.; formal analysis, I.K.; investigation, all authors; resources, D.S.K.; data analysis, I.K.; writing–original draft preparation, I.K.; writing–review and editing, all authors; visualization, I.K.; supervision, D.S.K., S.F., M.P.; project administration, D.S.K.

---

[1]This is a post-print of Koureas et al. [112], differing from the published paper only in terms of layout and formatting. A freely available version can be found on arXiv.

Abstract

Topologically interlocked materials and structures, which are assemblies of unbonded interlocking building blocks, are promising concepts for versatile structural applications. They have been shown to exhibit exceptional mechanical properties, including outstanding combinations of stiffness, strength, and toughness, beyond those achievable with common engineering materials. Recent work has established a theoretical upper limit for the strength and toughness of beam-like topologically interlocked structures. However, this theoretical limit is only achievable for structures with unrealistically high friction coefficients; therefore, it remains unknown whether it is achievable in actual structures. Here, we demonstrate that a hierarchical approach for topological interlocking, inspired by biological systems, overcomes these limitations and provides a path toward optimized mechanical performance. We consider beam-like topologically interlocked structures that present a sinusoidal surface morphology with controllable amplitude and wavelength and examine the properties of the structures using numerical simulations. The results show that the presence of surface morphologies increases the effective frictional strength of the interfaces and, if well-designed, enables us to reach the theoretical limit of the structural carrying capacity with realistic friction coefficients. Furthermore, we observe that the contribution of the surface morphology to the effective friction coefficient of the interface is well described by a criterion combining the surface curvature and surface gradient. Our study demonstrates the ability to architecture the surface morphology in beam-like topological interlocked structures to significantly enhance its structural performance.

Keywords: Architectured Structures; Surface Morphology; Frictional Contact

5.1   Introduction

Topologically interlocked structures (TIS) are assemblies developed from specially-shaped building blocks that hold together without adhesives. The interfacial contact and the blocks' geometry provide the structural integrity of TIS. Since the blocks are not bonded, they can stick, slip and rotate with respect to each other. Biological materials like nacre use the concept of topological interlocking on the micro-scale allowing them to have better properties compared to conventional engineering structures. For instance, mechanical properties of TIS, such as toughness and strength, are highly adjustable and can be controlled by modifying a given structure's geometrical and material properties [3, 4, 6, 59, 62, 73].

TIS were first introduced by Dyskin et al. [1, 105], who presented the concept of using segmented tetrahedral blocks to form a structure. Apart from high toughness and strength, TIS enjoy many advantages such as fracture tolerance [5], structural integrity even when a few blocks fail [5], and customizability, which comes due to the extensive design space of the TIS [40]. In terms of generalizing the geometric design space, TIS can be classified into three main categories; plate-like structures [3, 4, 35], beam-like structures [77, 78, 104, 113] and curvilinear-like structures [50]. Here, we focus on beam-like structures to take advantage of the simple geometric configuration, which can facilitate their modeling and analysis using both computational and theoretical methods [33–35]. This can be particularly useful for understanding the underlying physics of TIS and for developing predictive models of their behavior, which can then be transferred to the more complex plate- and curvilinear-like TIS.

The present work builds on a previous study [104] in which we showed that beam-like TIS have a maximum theoretical load-carrying capacity. We demonstrated that this theoretical capacity is achieved by increasing the friction coefficient between the blocks up to the point where slip suppression is maximized. Similar observations that suggest forming the working envelop of TIS have been observed by Khandelwal et al. [35] using fixed constraints and by Odessa and Shufrin [113] through geometric modifications. In addition, an equivalent maximum theoretical limit for the load-carrying capacity has been observed for plate-like TIS [36]. However, in all examined cases in [104], the friction coefficient that led to the

maximum theoretical limit was much higher than the friction coefficients of common pairs of engineering materials. Fig. 5.1a shows the theoretical limit for a planar-faced beam-like structure as shown in Fig. 5.1c with friction coefficient $\mu \geq 0.8$ and compares it with other beam-like TIS from the literature [77, 78]. We see at least one order of magnitude difference between the theoretical maximum load-carrying capacity obtained with $\mu \geq 0.8$ and the experimentally observed load-carrying capacities obtained with materials that have $\mu = 0.12$. This raises a question regarding the practical attainability of the theoretical maximum load-carrying capacity for beam-like TIS. Therefore, this study aims to show how the theoretical limit to the load-carrying capacity can be obtained with realistic friction coefficient values.
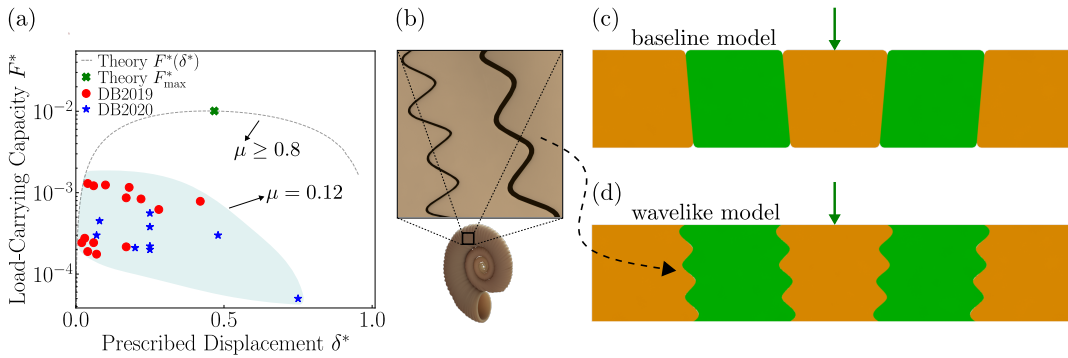
Figure 5.1: (a) Illustration of the normalized load-carrying capacity given by $F^* = F_y/(E \cdot h \cdot t)$ where E is Young's modulus, h the height and t the thickness of the structure, against the normalized prescribed displacement $\delta^* = \delta/h$. The dashed curve corresponds to the theoretical limit of planar-faced beam-like TIS with friction coefficient $\mu \geq 0.8$ [104]. Its maximum carrying capacity F^*_{max} (green cross) is compared to the maximum load-carrying capacity F^*_{max} of beam-like TIS from experiments by Dalaq and Barthelat [77] (marked as DB2019) and Dalaq and Barthelat [78] (DB2020). (b) Schematic of hierarchical suture interface in ammonite shell that inspired the current TIS design. (c-d) The rationale for the configurations: A beam-like topologically interlocked structure (TIS) with planar interfaces (c) as used in [104], and an updated configuration with hierarchical interfaces (d). The green arrows represent the loading direction.

It has shown in [23, 24, 64–69] that hierarchical interlocking, of which surface waviness is one type, is a major contributor to the strength and the stiffness of biological materials like mollusk shells, conch shells, purpuratus shells, and ammonites shells (see Fig. 5.1b). The concept of hierarchical interlocking by planar spikes over planar and non-planar interfaces was first introduced by Djumas et al. [6] in the context of plate-like TIS. Djumas et al. [6] demonstrated that the use of hierarchy provides an additional degree of interlocking and delays the onset of slip of the blocks. Inspired by these examples, we employ here a wave-based hierarchical interlocking to reach the theoretical capacities of TIS beams. Specifically, we introduce simple sinusoidal alterations to planar-faced surfaces (Fig. 5.1c and d) to increase the frictional resistance between the blocks in beam-like structures. We explore the effects of these altered surfaces on the mechanical response for realistic values of friction coefficients and show that such simple geometric surface alterations are sufficient to increase the overall frictional resistance and thereby reach the maximum theoretical load-carrying capacity of the TIS, presented in Koureas et al. [104].

In the following, we discuss the examined configuration and the surface alterations to increase the frictional resistance to reach the theoretical maximum load-carrying capacity in beam-like TIS (Sec. 5.2). In Sec. 5.3, we present and discuss the effect of hierarchical morphology on the load-carrying capacity of TIS and give an outlook on how the gained knowledge can aid the design of TIS.

5.2 Numerical Setup

5.2.1 Examined Configuration

To investigate the influence of surface morphology on the mechanical response of TIS, we focus on a centrally loaded beam-like structure with span length $L = 50$ mm, made of five blocks with height $h = 10$ mm and length $l = 10$ mm (see Fig. 5.2). The central loading configuration was chosen because it constitutes the most critically loaded scenario. On top of the planar surfaces defined by $\theta = 5^o$, which were used by [104] for obtaining the theoretical upper limit, we apply a hierarchical surface morphology. To generate surface morphology, we superimposed, a sinusoidal function defined by wavelength λ and amplitude $\mathcal{A}$ on top of the inclined angle θ.
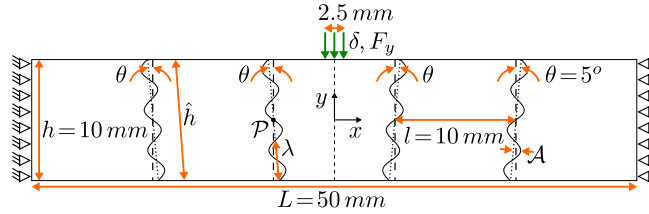
Figure 5.2: Schematic illustration of model set-up with the geometric parameters and boundary conditions in a beam-like TIS with hierarchical interfaces consisting of five blocks. The angle θ is computed between the vertical dashed lines and the inclined dotted lines.

The surface hierarchy of these beam-like TIS is modeled using a rotational (by angle θ) transformation of a sinusoidal curve about the local midpoint $\mathcal{P}$ of the interface (see Fig. 5.2) as

$$f(r) = \begin{bmatrix} \cos(\theta) & -\sin(\theta) \\ \sin(\theta) & \cos(\theta) \end{bmatrix} \begin{bmatrix} r \\ \mathcal{A}\sin\left(\left(r + \frac{h/2}{\cos(\theta)}\right)\frac{n\pi}{\frac{h/2}{\cos(\theta)}}\right) \end{bmatrix} + \begin{bmatrix} \mathcal{P}_x \\ \mathcal{P}_y \end{bmatrix}, \qquad (5.2.1)$$

where $n = \frac{\widehat{h}}{\lambda}$ is the number of oscillations across the interface (note that n does not need to be an integer number), $\mathcal{A}$ is the amplitude, $\widehat{h}$ is the total length of the interface without the hierarchical modification (Fig. 5.2), and r is bounded by

$$-\frac{h/2}{\cos(\theta)} \leq r \leq \frac{h/2}{cos(\theta)} . \qquad (5.2.2)$$

For our study, the blocks are modeled as isotropic and linear elastic materials with Young's modulus E, Poisson's ratio ν, and friction coefficient μ. Further, we note that our model does not account for possible fracture of blocks.

5.2.2 Parametric Study

To analyze the effect of surface morphology, we design a range of hierarchical interfaces by varying n and $\mathcal{A}$. The geometric parameters h and l, as well as the material properties $E = 30$ GPa and $\nu = 0.2$, are kept constant. Finally, μ ranges between $0.1 - 0.4$ covering a wide range of experimentally observed values for TIS [4, 6, 63, 77, 78].

To solve the proposed model, we use the Finite Element framework described in [104], which accounts for geometrical non-linearities [84] and uses a penalty-based node-to-segment frictional contact algorithm [96, 99, 103, 108–111] to resolve contact and frictional constraints along interfaces. We employ Coulomb's friction law ($T = \mu N$, where T and N are tangential and normal interface tractions, respectively) to describe frictional forces along an interface and the stick-slip transition. Using the structures' symmetry about the y-axis, we model only the left half of the TIS (see Fig. 5.2). The lateral surface of the TIS (*i.e.*, left side) is constrained in x and y directions.

Finally, the load is applied as displacement-controlled boundary conditions along a section of the top boundary of the central block as described by

$$u_y(-\frac{l}{4} \leq x \leq 0, \frac{h}{2}) = -\delta \, . \tag{5.2.3}$$

The 2D beam-like structures are modeled using first-order triangular elements under plane-strain conditions. The simulations are performed under static conditions. We note that we performed a mesh- and penalty-based sensitivity analysis to ensure that the load-displacement response and the interface behavior are converged.

5.3 Results and Discussion

We explore the effect of n and $\mathcal{A}$ on the global response using realistic values of μ. Since we neglect fracture, we assume failure of the structure when the load drops to zero.

5.3.1 Effect of surface morphology

We analyze the normalized load-deflection curves $F_y - \delta$ for beam-like TIS with different friction coefficients μ, number of oscillations n, and amplitude $\mathcal{A}$. To remove scalability effects, F_y is normalized with respect to h, t, and E. δ is normalized with respect to h. In all the considered cases, the load-carrying capacity increases as a function of μ, n, and $\mathcal{A}$ (see Fig. 5.3). The complete study for all values of μ, n, and $\mathcal{A}$ is presented in Sec. A.2. We can distinguish two different types of the $F_y - \delta$ curves. The first type (Fig. 5.3a and c) follows a bell-shape behavior similar to other TIS [4, 77, 104]. In the second one (Fig. 5.3b with $\mu = 0.2$), there are more than one local maxima. In all of our cases with more than one local maxima, the first maximum is always the global maximum.
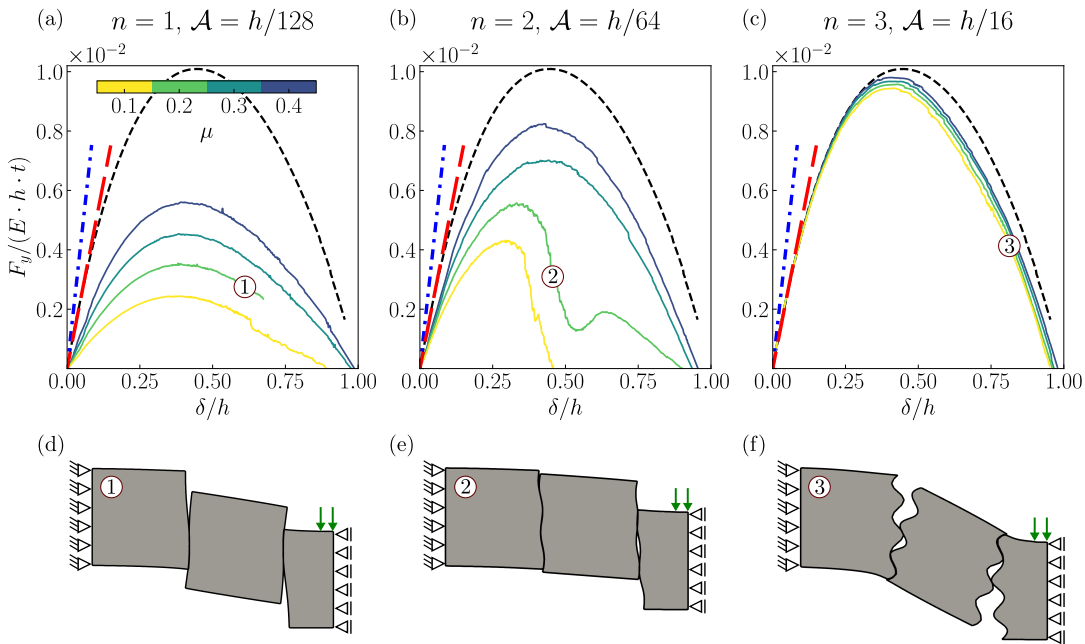
Figure 5.3: Normalized load-carrying capacity $F_y/(E \cdot h \cdot t)$ of the structure against the normalized prescribed displacement δ/h for various interface properties. (a-c) The curves correspond to structures with different friction coefficients μ, oscillations n, and amplitude $\mathcal{A}$. (d-f) The schematics numbered 1, 2, and 3 show snapshots of the structures at given δ/h. The curves are compared with the theoretical upper limit (dashed black curve) of planar-faced beam-like TIS with $\mu \geq 0.8$ [104]. The red dashed line represents the normalized structural stiffness K of the saturated curve (≈ 0.05) and the blue dashed line represents K of the monolithic equivalent (computed to be ≈ 0.089 with finite-element simulations).

The $F_y - \delta$ capacities are compared with the theoretical limit of the load-carrying capacity from

our previous study with planar-faced beam-like TIS (dashed black line in Fig. 5.3). We see that, by increasing n and $\mathcal{A}$, the structures approach the theoretical limit with much smaller, and realistic friction coefficients. Moreover, for high values of n and $\mathcal{A}$ (*i.e.*, $n = 3$ and $\mathcal{A} = h/16$), the effect of μ on the load-carrying capacity response becomes very small. This demonstrates that using hierarchical interlocking through architecting the surface morphology enables us to reach the theoretical capacities of TIS with realistic friction coefficients. In addition, Fig. 5.4a shows that the scaling of the structural load-carrying capacity with respect to the friction coefficient remains the same as observed in planar-faced TIS [36, 104]. At the same level of normalized $F_{\max}$, the slope is the same between planar-faced and hierarchical TIS, but the level of friction (*i.e.* μ) at which this occurs is different. In the following, we will use this observation to characterize the effect of surface morphology on the mechanics of the interfaces.
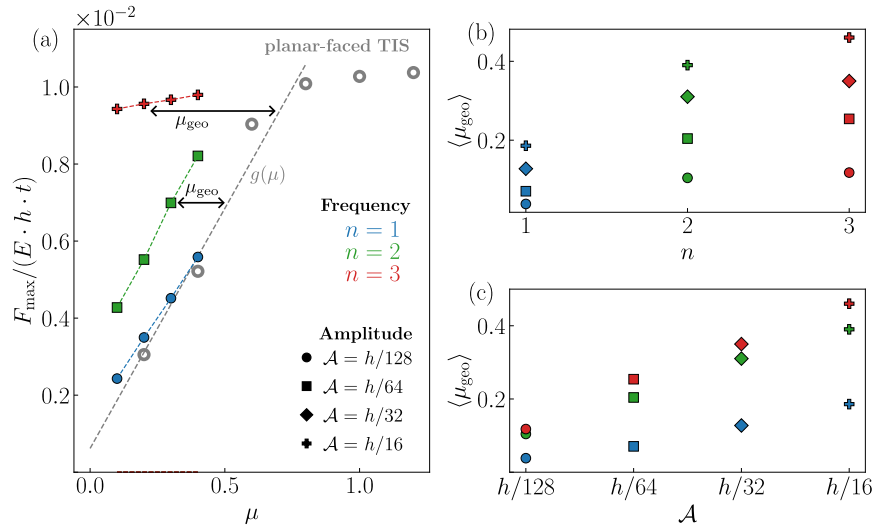
Figure 5.4: Geometric coefficient of friction. (a) Normalized maximum load-carrying capacity $F_{\max}/(E \cdot h \cdot t)$ against the friction coefficient μ. The same cases as in Fig. 5.3 are shown, with oscillation $n = 1$ and amplitude $\mathcal{A} = h/128$ (shown in blue), $n = 2$ and $\mathcal{A} = h/64$ (shown in green) and $n = 3$ and $\mathcal{A} = h/32$ (shown in red). The gray points represent the normalized maximum load-carrying capacity for planar-face beam-like TIS, reported in [104]. (b, c) Variation of average geometrical friction coefficient $\langle \mu_{\text{geo}} \rangle$ with respect to n and $\mathcal{A}$, respectively. Standard deviations are omitted here for clarity but shown in Fig. 5.5.

Fundamentally, we note that the introduction of surface morphology increased the effective frictional resistance without increasing material friction, *i.e.* for a given μ the normalized $F_{\max}$ is higher than in planar-faced TIS (see Fig. 5.4a). To describe this effect, we propose to distinguish between a material contribution μ and a geometrical contribution due to surface morphology μ_{geo} to the effective friction resistance of the interfaces μ_{eff} as experienced by the structure. Therefore, the effective friction coefficient can be defined as

$$\mu_{\text{eff}} = \mu + \mu_{\text{geo}} \,. \tag{5.3.1}$$

While in our previous work [104] with planar-faced surfaces (*i.e.*, $\mu_{\text{geo}} = 0$), the effective interface friction was given by $\mu_{\text{eff}} = \mu$, and hence material friction had to be increased to unrealistically high values to reach the theoretical limit, for hierarchical interfaces, $\mu_{\text{geo}} > 0$ provides new opportunities. In this case, μ remains in a range of realistic values for engineering materials, and by modifying the surface morphology of the structures, we can tailor μ_{eff} via μ_{geo}. In other words, a geometric modification of the surface morphology can lead to the theoretical limit with realistic μ (see red points in Fig. 5.4a).

To get a better understanding of μ_{geo} and its dependence on surface morphology (*i.e.*, n and $\mathcal{A}$) we compare the maximum load-carrying capacity $F_{\max}$ between the hierarchical TIS and the equivalent planar-faced beam-like TIS from Koureas *et al.* [104]. We describe $F_{\max}$

for planar-face beam-like TIS as a function of μ_{eff}, that is $F^P_{\max} = g(\mu_{\text{eff}})$ (as represented by gray line in Fig. 5.4, note that $\mu_{\text{eff}} = \mu$ for planar-faced TIS). We then compute μ_{eff} for hierarchical surfaces by projecting $F_{\max}$ for a given set of $(\mu, n, \mathcal{A})$ on to the function g, that is $\mu_{\text{eff}} = g^{-1}(F_{\max}(\mu, n, \mathcal{A}))$. Using Eq. 5.3.1, we calculate the corresponding μ_{geo} (as shown by arrows in Fig. 5.4a). We perform the same calculations to compute μ_{geo} for every combination of n, $\mathcal{A}$ and μ considered in the parametric study (see Sec. A.2). An average geometrical friction coefficient $\langle \mu_{\text{geo}} \rangle$ is then computed for a given set of values of n and $\mathcal{A}$ (*i.e.*, $\langle \mu_{\text{geo}} \rangle = \sum_{\mu_i} \mu_{\text{geo}}(\mu_i, n, \mathcal{A})/4$ where $\mu_i \in [0.1, 0.2, 0.3, 0.4]$). We observe $\langle \mu_{\text{geo}} \rangle$ increases with increasing n or $\mathcal{A}$ (see Fig. 5.4b and c). However, none of these two parameters is sufficient to describe the observed μ_{geo}.

The effects of n and $\mathcal{A}$ can be combined in a measure that is computed via the gradient of the surface morphology, as commonly done in tribology [114, 115]. For this purpose, we compute the root mean square of the surface gradient $\sqrt{\langle (\nabla f)^2 \rangle}$ and compare the variation of $\langle \mu_{\text{geo}} \rangle$ as a function of $\sqrt{\langle (\nabla f)^2 \rangle}$. We observe that the cases with $n = 2$, 3 collapse onto a single curve (see Fig. 5.5a), however, the behavior of μ_{geo} for $n = 1$ is different. This suggests that the surface gradient is a good measure for morphologies that are tending to rougher profiles (which approach conditions common in tribological systems). Alternatively, in the context of TIS, surface morphology has previously been described by the surface curvature [78]. Here, we describe the local surface curvature as $\kappa = \frac{|\nabla^2 f|}{(1 + \nabla f^2)^{3/2}}$ where f represents the surface profile function (see Eq. 5.2.1). We then compare $\langle \mu_{\text{geo}} \rangle$ with the normalized average curvature $\langle \kappa \rangle \cdot h$. The results show that $\langle \kappa \rangle \cdot h$ as a function of curvature collapses well for $n = 1, 2$ but leads to a different dependence for $n = 3$ (see Fig. 5.5b). This is consistent with observations by [78], where curvature was sufficient as the considered morphologies were relatively smooth.

Based on these observations, we propose a combined surface measure to characterize the geometrical friction coefficient of hierarchical interfaces, which is given by the product of surface curvature and surface gradient: $\langle \kappa \rangle \cdot h \cdot \sqrt{\langle (\nabla f)^2 \rangle}$. The results, shown in Fig. 5.5c, illustrate a unique dependence of μ_{geo} on this proposed surface measure. Therefore, the proposed surface measure appears to be able to account for the full spectrum of morphologies of hierarchical interfaces and can provide a better characterization of a surface's geometrical friction coefficient.
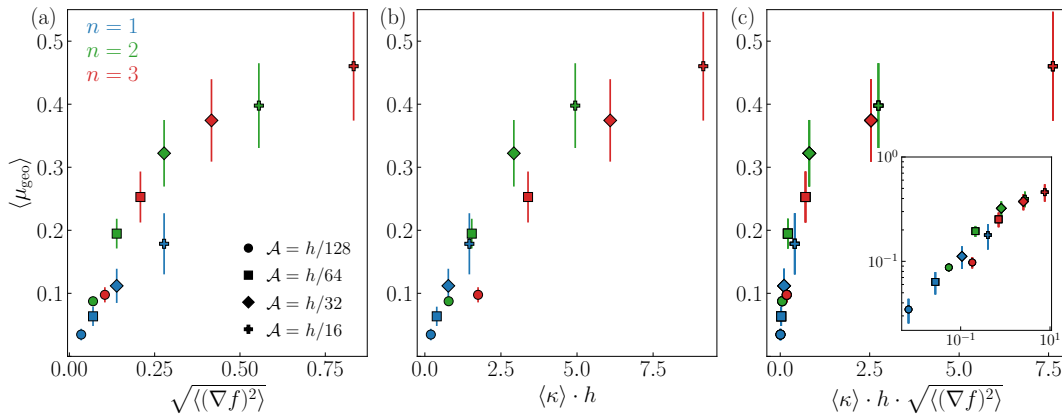

Figure 5.5: Variation of average geometrical friction coefficient $\langle \mu_{\text{geo}} \rangle$ with respect to (a) root mean square of the surface gradient $\sqrt{\langle (\nabla f)^2 \rangle}$, (b) normalized average curvature $\langle \kappa \rangle \cdot h$ and (c) product of $\langle \kappa \rangle \cdot h$ and $\sqrt{\langle (\nabla f)^2 \rangle}$. Error bars indicate computed standard deviations. (inset) Same plot on log-log axis.

5.3.2 Interface mechanisms in TIS with hierarchical interlocking

The origin of the observed saturation level can be understood as the result of a collective interface behavior. Therefore, to analyze the impact of local interface mechanisms on struc-

tural properties, we define the sliding fraction as the contact area that slides at a given interface. Fig. 5.6 shows that the structures can approach the theoretical limit of the load-carrying capacity (Fig. 5.6a) even when some interfaces are fully sliding (*i.e.*, sliding fraction ≈ 1) (Fig. 5.6b and c), compared to [104] where the saturation was reached only when all interfaces stick.
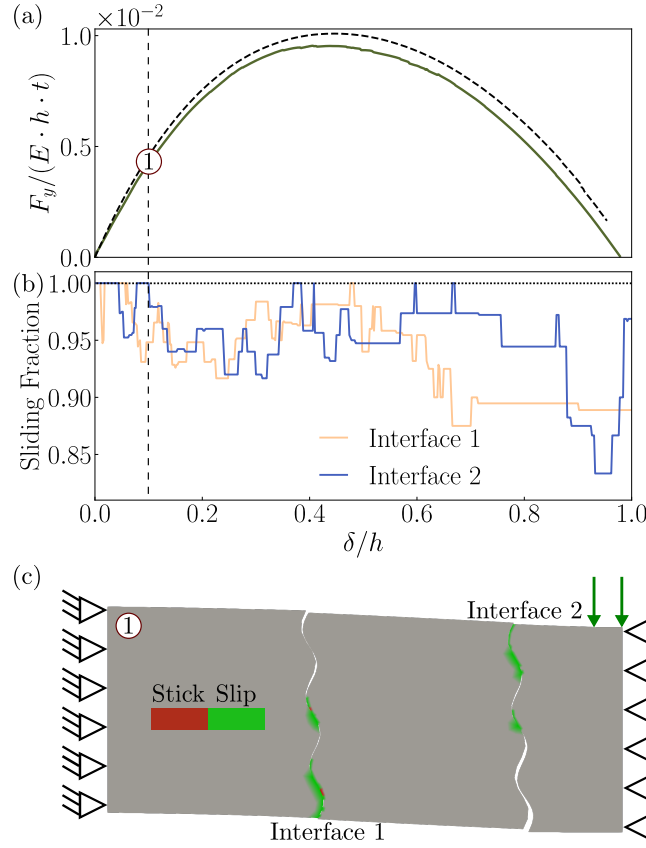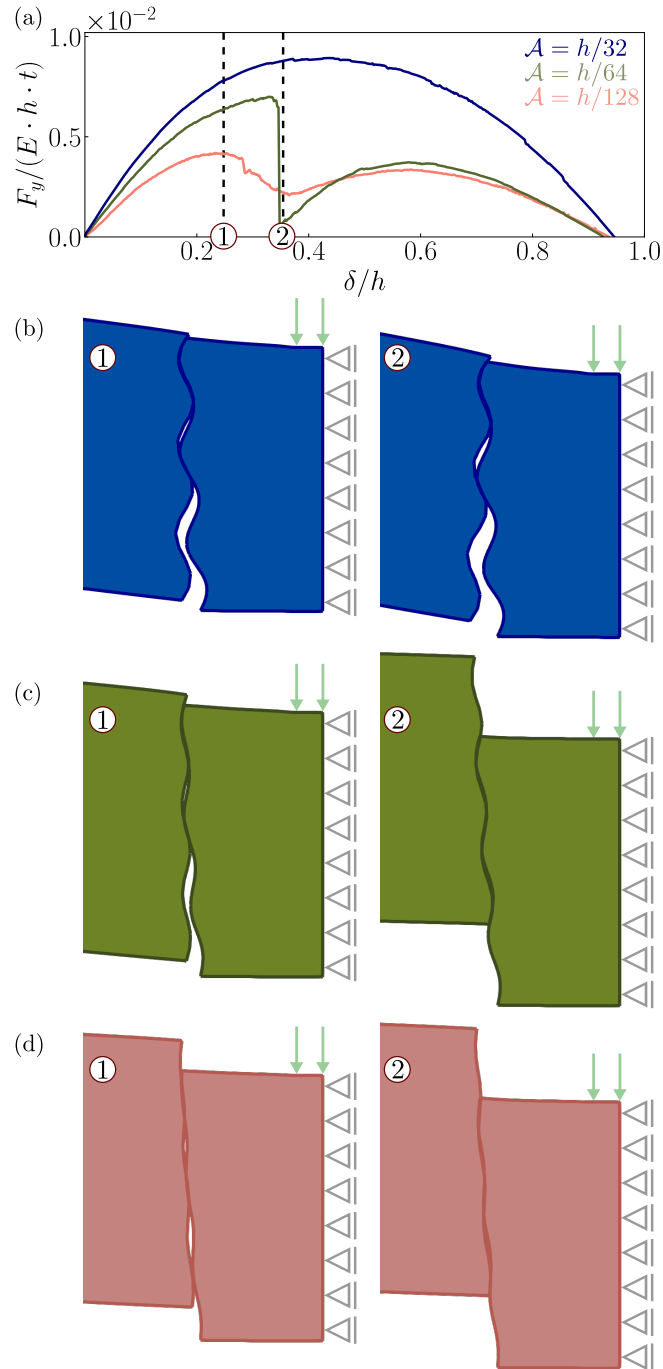

Figure 5.6: Interfacial behavior of representative case with friction coefficient $\mu = 0.4$, number of oscillations $n = 3$, and amplitude $\mathcal{A} = h/32$. (a) Normalized load-carrying capacity $F_y/(E \cdot h \cdot t)$. The curve is compared with the theoretical response (dashed curve) of planar-faced beam-like TIS with $\mu \geq 0.8$ [104]. (b) Sliding fraction against the prescribed displacement δ/h for each interface of the structure. (c) Snapshot capturing the sliding and sticking mechanisms at the interfaces of the structure at $\delta/h = 0.1$. The horizontal black dotted line instigates a fully sliding interface (sliding fraction = 1).

In hierarchical TIS, local sliding dominates the interface mechanisms, which has direct implications on the structural behavior. Our simulations show that we can distinguish three types of $F_y - \delta$ curves (see Fig. 5.7). The first type (with $\mathcal{A} = h/32$), is able to reach the theoretical limit (see Fig. 5.7a and Fig. 5.7b) thanks to an effective combination of μ and μ_{geo}. The second type (with $\mathcal{A} = h/64$), presents a sharp load drop that indicates structural instability. From Fig. 5.7a and Fig. 5.7c, it is clear that this drop is associated with an interfacial slip-jump across a full wave. This unstable type of response corresponds to an undesirable combination of μ and μ_{geo}. In the third type (with $\mathcal{A} = h/128$), the structure never reaches the theoretical limit. The low value of μ_{eff} makes the central block to smoothly slide across the interface (see Fig. 5.7a and Fig. 5.7d) providing a stable movement of the block. These results suggest that a hierarchical modification of a beam-like TIS can potentially present these three regimes, which need to be identified for a given structure to avoid falling into the unstable regime which might cause uncontrolled response behavior.

5.3.3 General Comments

In this work, we considered TIS as beam-like structures. To put the observed saturated response in perspective to a monolithic structure, we compare the initial normalized stiffness

Figure 5.7: (a) Normalized load-carrying capacity $F_y/(E \cdot h \cdot t)$ against the normalized prescribed displacement δ/h of beam-like TIS with friction coefficient $\mu = 0.2$, number of oscillations $n = 3$ and amplitudes $\mathcal{A} = h/32$, $h/64$, $h/128$. (b-d) Snapshots at $\delta/h = 0.25$ and $\delta/h = 0.35$ show the evolution of the central block for (b) a case where the structure reaches the theoretical limit, (c) a case where interfacial sliding presents an instability marked by a sharp load drop, and (d) a case with smooth and continuous sliding of the central block.

K of saturated TIS with that of a monolithic equivalent (see Fig. 5.3). We define K for TIS by the secant slope in the $F_y - \delta$ curves at $\delta/h = 0.05$. The initial stiffness of a monolithic structure represents an upper limit for the structural stiffness of TIS (see blue dashed line in Fig. 5.3). We observe that the saturated initial stiffness of the beam-like TIS is approximately 56% of the stiffness of the monolithic beam. We also note that the maximum carrying capacity and toughness of monolithic beams depend directly on the material failure criterion, which

is not defined in this study. Hence, strength and toughness comparisons between TIS and monolithic beams are left for future work.

Here, we focused on *centrally* loaded beam-like TIS as it is the most critical load configuration and, hence, most commonly studied in the literature. Other boundary conditions, where the load is asymmetrically applied on other blocks than the central one, will present the same mechanics but with quantitative differences. For instance, the initial stiffness and the maximum load-carrying capacity of the structure increase for asymmetric loading compared to the symmetric case, as can be expected from simple beam theory and the truss model by Khandelwal et al. [33]. However, structures with interface morphology and friction that lead to the sticking of all interfaces will reach a configuration-specific saturation of the maximum load-carrying capacity. Hence, the findings of our work are qualitatively applicable to asymmetric loading configurations of TIS.

Another important structural property of TIS is the loading energy which is computed by the integral of the load versus imposed displacement (*i.e.* the area under a $F_y - \delta$ curve). Maximizing the loading energy is a typical objective when designing TIS. For beam-like TIS, the maximum loading energy is directly related to the maximum load-carrying capacity, as has previously been demonstrated [33–35]. Since the displacement δ cannot exceed the height h in beam-like TIS, the saturated load-carrying capacity occurs for systems that reach $\delta = h$ (see Fig. 5.3). Therefore, a saturation of the load-carrying capacity implies saturation of the loading energy for beam-like TIS.

Finally, it is important to note that our model does not consider the possibility of block fracture, which could potentially impact the performance of the TIS. To obtain the full theoretical range of the $F_y - \delta$ curves, we assumed that the failure of the structure occurs when the central block is pushed out of the assembly. While this scenario is realistic for many configurations [66–69], it may not be applicable in all cases and leaves open questions regarding the exact point at which fracture initiation occurs, and how it will affect the structural response. Interestingly, local fracture in a block may not lead to structural failure, but it can introduce new smaller bodies that affect the overall response capacity.

5.4 Conclusion

This study focused on the effects of bio-inspired hierarchical interlocking on beam-like topologically interlocked structures (TIS). Specifically, we sought to test whether it was possible, by architecting the surface morphology of blocks, to reach the theoretical capacities of these structures with realistic friction coefficients, which cannot be achieved with planar-faced blocks. To this end, we tested a centrally loaded TIS, where different patterns of surface waviness were superimposed on the originally planar-faced blocks. We found that, with certain waviness patterns, it is possible to reach the theoretical limit at much lower and more realistic friction coefficients. Moreover, we found that the load-carrying capacity of structures with wavy block surfaces converges to that of a planar-faced beam-like TIS at high friction. Our observations demonstrate the usefulness of hierarchical interlocking in TIS and highlight its potential in the design of TIS.

6

The key to the enhanced performance of slab-like topologically interlocked structures with non-planar blocks

> There are 360 degrees, so why stick to one?
>
> Zaha Hadid

Ioannis Koureas [a], Mohit Pundir [a], Shai Feldfogel [a], David S. Kammer [a,*]

> [a] Institute for Building Materials, ETH Zurich, 8093 Zurich, Switzerland
> [*] Corresponding author

Key findings:

- The response capacity for slab-like TIS with non-planar blocks saturates with realistic friction coefficient
- A pseudo-ductile failure mode is observed in structures with non-planar blocks
- The key to the enhanced performance is the local angle of inclination at the hinging points of the structure

Author contributions: Conceptualization, all authors; methodology, all authors; software, I.K.; validation, I.K.; formal analysis, I.K.; investigation, all authors; resources, D.S.K.; data analysis, I.K.; writing–original draft preparation, I.K.; writing–review and editing, all authors; visualization, I.K.; supervision, D.S.K., S.F., M.P.; project administration, D.S.K.; funding acquisition, D.S.K.

---

[1]This is a post-print of Koureas et al. [116], differing from the published paper only in terms of layout and formatting.

Abstract

Topologically interlocked structures are assemblies of interlocking blocks that hold together solely through contact. Such structures have been shown to exhibit high strength, energy dissipation, and crack arrest properties. Recent studies on topologically interlocked structures have shown that both the peak strength and work-to-failure saturate with increasing friction coefficient. However, this saturated structural response is only achievable with nonphysically high values of the friction coefficient. For beam-like topologically interlocked structures, non-planar blocks provide an alternate approach to reach similar structural response with friction properties of commonly used materials. It remains unknown whether non-planar blocks have similar effects for slab-like assemblies, and what the achievable structural properties are. Here, we consider slab-like topologically interlocked structures and show, using numerical simulations, that non-planar blocks with wave-like surfaces allow for saturated response capacity of the structure with a realistic friction coefficient. We further demonstrate that non-planar morphologies cause a non-linear scaling of the work-to-failure with peak strength and result in significant improvements of the work-to-failure and ultimate deflection – values that cannot be attained with planar-faced blocks. Finally, we show that the key morphology parameter responsible for the enhanced performance of non-planar blocks with wave-like surfaces is the local angle of inclination at the hinging points of the loaded block. These findings shed new light on topologically interlocked structures with non-planar blocks, allowing for a better understanding of their strengths and energy absorption.

Keywords: Frictional Contact; Wave-faced Blocks; Topologically Interlocked Structures; Architected Surfaces

6.1   Introduction

Topologically interlocked structures (TIS) are assemblies of interlocking blocks that rely solely on contact along the interfaces to achieve structural integrity [1, 30]. Slab-like TIS panels (also referred to as plate-like [41, 117, 118]), a commonly used type of TIS (as shown in Fig. 6.1a), exhibit high strength, energy dissipation [119], crack arrest abilities [4, 5, 120], and work-to-failure (the area under the load-deflection curve, elsewhere referred to as toughness [3, 4] or loading energy [104, 112]).

High work-to-failure U results from the combination of a high peak load $F_{\max}$ and a high ultimate deflection δ. Regarding peak load, it has been shown in [36, 104, 121] that, in TIS with planar-faced blocks (henceforth referred to as planar blocks), the peak load saturates for high friction coefficients and cannot exceed a well-defined upper bound, see Fig. 6.1b. Regarding ultimate deflection, the 'envelope' saturated response is commonly capped at relatively small normalized deflection compared to the theoretical upper bound given as $(N+1)/2$ where N is the number of internal blocks at a given row [122]. For instance, the achieved deflection for a slab-like TIS with 5-by-5 internal blocks is $\delta/h \approx 1.3$ (see Fig. 6.1b), which is ≈ 2.3 times smaller than the theoretical upper bound $\delta/h = 3$. The limited ability to achieve a high deflection is a direct consequence of the fact that these TIS systems fail in a brittle-like manner as soon as the peak load is reached (see sharp load drop for saturated response in Fig. 6.1b), which results in a linear scaling between the work-to-failure and the peak load (see Fig. 6.1c). As a result, the work-to-failure cannot exceed the value associated to the saturated response (see theoretical envelope in Fig. 6.1b), which points to a large untapped potential for increased work-to-failure (see dark gray region in Fig. 6.1b).

In fact, the untapped potential for work-to-failure is practically even larger because reaching the theoretical envelope requires materials with unrealistically high friction coefficients μ. With realistic μ in common TIS (*i.e.*, $\mu = 0.23$ as used in [4]), the maximally achievable peak load $F_{\max}$ is considerably lower (indicated by the black dot on the black curve in Fig. 6.1b obtained with numerical simulations), and since there is a linear dependence between $F_{\max}$ and U, the realistically achievable work-to-failure U is also much lower (see arrows in

Possible avenues for increasing the work-to-failure in slab-like TIS made from common materials consist of 1) increasing the peak load to approach the theoretical envelope, and 2) increasing the ultimate deflection to go beyond this theoretical envelope into the untapped potential. As we will show here, this is achievable through the use of blocks with non-planar surface morphologies (henceforth referred to as non-planar blocks). Such non-planar morphologies include osteomorphic (double curvature) blocks [37, 52, 72, 123–126], double-face osteomorphic blocks [63, 118, 127, 128], and hierarchical morphologies [6].
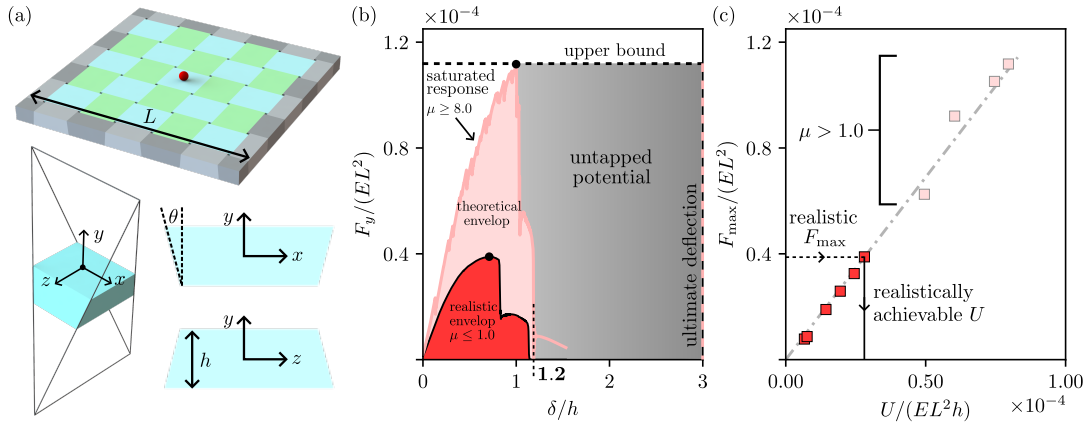
Figure 6.1: (a) Schematic illustration of slab-like TIS with planar-faced blocks along with a single planar block and its cross-sectional area showing the inclination angle θ. (b) Normalized load-deflection curve $F_y/(E \cdot h^4/L^2)$ vs δ/h, where E is Young's modulus, h the height and L the side length of the panel. The light red curve corresponds to the saturated response of the examined TIS with planar-faced blocks achieved with an (unrealistic) friction coefficient of $\mu = 7.0$. The black curve shows the load-deflection numerically obtained with $\mu = 0.23$, a value commonly used for TIS structures in experiments [4]. The light red shaded region corresponds to the established theoretical envelope, and the gray shaded region shows the untapped potential based on [122]. The black points correspond to the peak loads of each curve. (c) Normalized peak load versus work-to-failure. The linear relationship between the two measures shows that for planar blocks, saturation in one measure leads to saturation in the other, achieved with very high values of friction coefficients.

The reason non-planar blocks may outperform planar ones in terms of practically achievable work-to-failure is that they enable a saturated response with realistic μ, as has been shown for beam-like TIS in [112]. If this is also true for slab-like TIS (which are the most common TIS application and the one at the focus of the present study), this would mean an immediate major improvement in the practically achievable work-to-failure by extending the range of accessible values on the linear relation shown in Fig. 6.1c. In addition, if non-planar blocks allowed for less brittle failure, this would correspond to a different scaling between the peak load and the work-to-failure, which, in turn, could lead to further increases in the work-to-failure. Therefore, the degree to which non-planar blocks can help access the untapped work-to-failure potential of slab-like TIS depends on the following questions: Is it possible to reach the saturated response obtained of planar blocks with high μ by using non-planar morphologies and realistic μ? Is it possible to reach higher ultimate deflections with non-planar blocks than with planar ones? What do such potentially larger deflections mean in terms of achievable work-to-failure and the latter's scaling with the peak load?

While the many studies in the TIS literature that considered non-planar blocks [6, 37, 52, 63, 72, 118, 123–129], provide valuable data and insight, to our knowledge, they did not address the aforementioned questions in the context of slab-like TIS. The objective of the present study is, therefore, to address these questions with a focus on wave-like surface morphologies, and thereby shedding new light on TIS with non-planar blocks, and pointing to ways in which their hitherto untapped work-to-failure potential can be exploited.
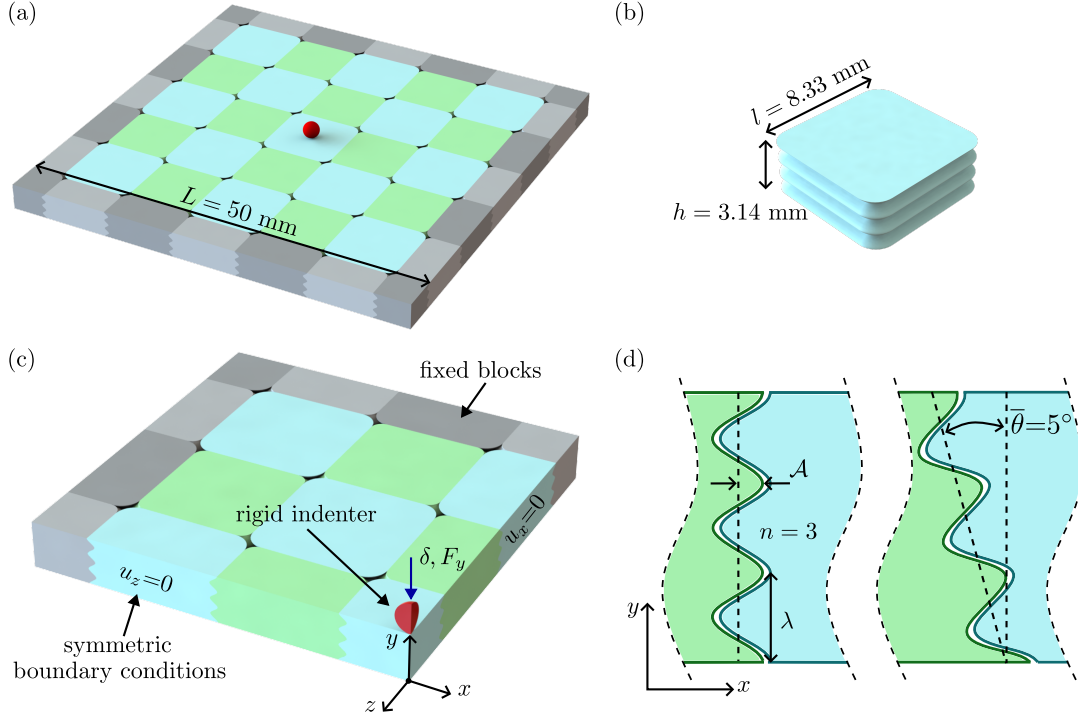
Figure 6.2: Schematic illustration of (a) a 5-by-5 slab-like topologically interlocked structure with non-planar blocks and structural length $L = 50$ mm. The immovable peripheral blocks (indicated by gray) support the structure. (b) A single non-planar block with number of oscillations $n = 3$, amplitude $\mathcal{A} = 0.25$ mm, height $h = 3.18$ mm and average $l = 8.33$ mm. (c) Schematic of a quarter of the structure used in the numerical analyses. The rigid indenter is pushed down on the central block by a prescribed displacement δ. (d) Cross-sectional representation of a block's non-planar surface with $\mathcal{A} = 0.25$ mm, $n = 3$, wavelength λ, and an average inclination $\bar{\theta} = 0°$ (left) and $\bar{\theta} = 5°$ (right).

6.2 Problem Statement

6.2.1 Physical problem

In this study, we consider the 5-by-5 slab-like TIS depicted in Fig. 6.2a. Each block has length $l = 8.33$ mm and height $h = 3.18$ mm (see Fig. 6.2b). The immovable peripheral blocks are halves and quarters (in the four corners) and are used to support the structure (see Fig. 6.2c). We consider an isotropic and linear elastic material with Young's modulus $E = 18.7$ GPa, and Poisson's ratio $\nu = 0.2$. A friction coefficient value of $\mu = 0.23$ is assumed at the blocks' interface. This configuration was chosen because it allows us to compare the effects of non-planar interfaces with those of planar interfaces [4, 36] with high friction coefficients [36], as available in the literature.

6.2.2 Planar-faced blocks

Slab-like TIS with planar-faced blocks as depicted in Fig. 6.1a have been widely used in the literature [4, 33–36, 60, 122]. Here, we use them as a reference for comparison with non-planar block morphologies.

6.2.3 Blocks with non-planar morphologies

Following [6, 23, 24, 64, 67, 77, 78, 112], we consider sinusoidal wave-like patterns at the interface of the TIS (see Fig. 6.2) as prototypes of general non-planar surface morphologies. They are defined by wavelength λ, number of oscillations n, and amplitude $\mathcal{A}$ (see Fig. 6.2d) with average inclination angle $\bar{\theta} = 0°$ (*i.e.*, simple rectangular block). To understand the effects of each of these variables and to find the governing non-dimensional parameters of

non-planar morphologies, we consider different combinations of $n = 2, 3, 4$ (note that n does not need to be an integer number) and $\mathcal{A} = 0.025, 0.05, 0.1, 0.15, 0.2, 0.25, 0.3$ mm.

6.2.4 Numerical model

The 5-by-5 assembly is loaded by applying displacement δ on a rigid spherical indenter. The peripheral blocks are fully fixed (in all their nodes). Using the structures' symmetry about the x- and z-axes, we model only a quarter of the TIS (see Fig. 6.2c). The sharp edges of the blocks are filleted to reduce stress concentrations. We note that our model does not account for block fracture. Therefore, we define the failure of a structure when the loaded central block loses contact with all its neighbors.

The presented model is solved using the Finite Element software Abaqus [130]. We use a static non-linear solver that accounts for geometrical non-linearities and uses a penalty-based surface-to-surface frictional contact algorithm for handling contact and frictional constraints at interfaces. For describing the frictional forces along an interface and the stick-slip transition, we apply Coulomb's friction law ($T = \mu N$, where T and N are tangential and normal interface tractions, respectively). The blocks are discretized using first-order tetrahedral elements. The element size was determined through a mesh convergence analysis, in which the effects of further mesh refinement on the mechanical response were found to be negligible.

6.3 Results and Discussion

### 6.3.1 Load-deflection response for planar-faced blocks

The load-deflection curves ($F_y - \delta$) with planar blocks, are shown in Fig. 6.3a. Our normalization approach is based on scaling factors derived in the literature for tetrahedral blocks [131]. Similarly to the Level-Set-Discrete-Element-Method (LS-DEM) [36], our FEM model captures the saturation to the peak load as observed for unrealistically high μ (*i.e.*, $\mu \geq 5.0$). In addition, for lower values of μ (*i.e.*, $\mu = 0.6$) the blocks initially stick leading to a peak load and then slip of the central block occurs causing a sharp load drop as shown in Fig. 6.3a. When μ is decreased even further to experimentally equivalent values [4], (*i.e.*, $\mu = 0.23$) the peak load is kept to minimum and failure occurs due to sliding mechanism.

6.3.2 The effects of non-planar surface morphologies on load-deflection response

Turning to TIS with non-planar blocks, we consider the $F_y - \delta$ response with the sinusoidal patterns depicted in Fig. 6.3b. Similarly to planar-faced block structures, we observe a saturation to $F_{\max}$. However, contrary to planar-faced blocks, where unrealistic μ are needed to reach saturation, with high values of $\mathcal{A}$, the peak load saturates at the relatively low value of $\mu = 0.23$. This means that a theoretical upper bound capacity of slab-like TIS can be obtained through non-planar block morphologies.

In terms of ultimate deflection and the associated work-to-failure, both are visibly larger with non-planar blocks compared with planar ones. Specifically, for cases with $\mathcal{A} \geq 0.05$ mm, the ultimate deflection approaches $\delta \approx 2.3h$, considerably larger than that with planar-faced blocks ($\delta \approx 1.3h$ as shown in Fig. 6.1b). These findings suggest that non-planar morphologies are inherently superior to planar-faced blocks in terms of (structural) ductility and energy absorption/dissipation.

We note that the results in Fig. 6.3 are theoretical since our model does not account for material non-linearity, damage, or fracture. It is likely that in practice, these effects will lead to reduced peak loads and work-to-failure, even for small interlocking angles.
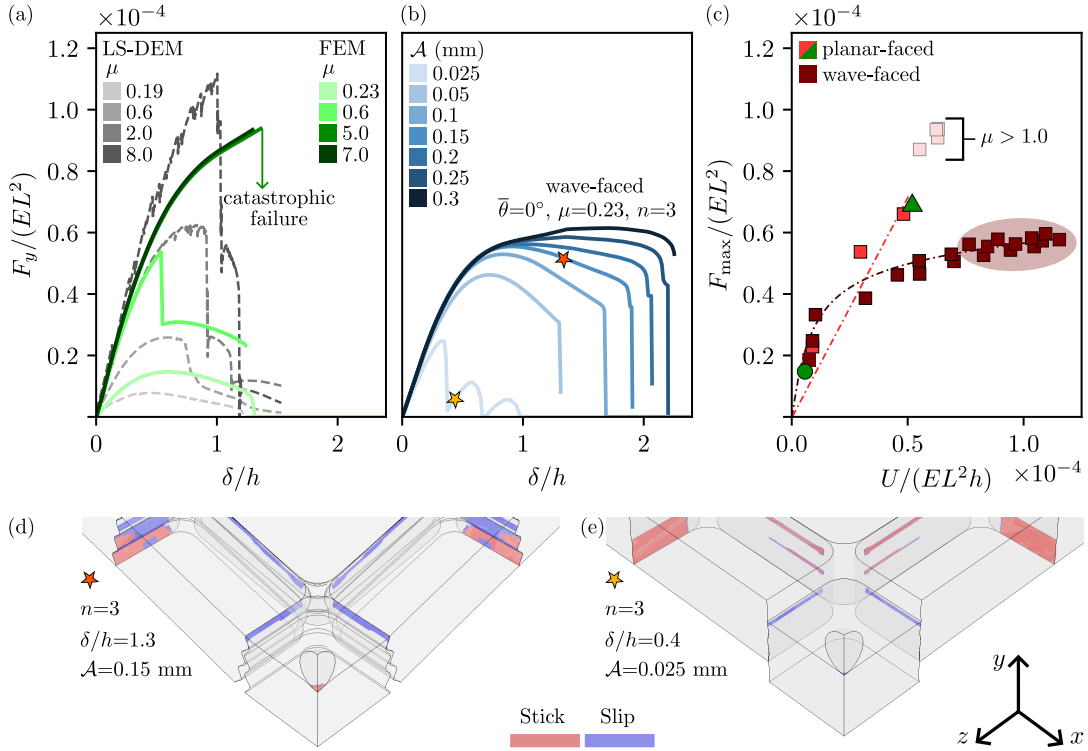
Figure 6.3: Normalized load $F_y/(E \cdot h^4/L^2)$ plotted against the normalized prescribed displacement δ/h for (a) structures with planar-faced blocks. (b) Structures with wave-faced blocks and average inclination angle $\bar{\theta} = 0°$, oscillation $n = 3$, and different amplitudes $\mathcal{A}$. (c) The normalized peak load $F_{max}/(E \cdot h^4/L^2)$ for each curve (for all n and $\mathcal{A}$) is plotted against the normalized work-to-failure $U/(E \cdot h^4/L)$ for TIS with planar-faced and wave-faced blocks. The dark-shaded cluster denotes the area where F_{max} saturates for wave-faced blocks. For the complete study of $F_y - \delta$ curves for slab-like TIS with wave-faced blocks examined (*i.e.*, $n = 2$ and $n = 4$), see A.3.1. (d, e) Stick-slip mechanism for structures with $n = 3$, $\mathcal{A} = 0.15$ mm, and $\mathcal{A} = 0.025$ mm.

6.3.3 Non-linear scaling of load and work-to-failure for TIS with non-planar blocks

Differently from the case of planar-faced blocks [4, 36, 60] where the work-to-failure U scales linearly with the peak load, see Fig. 6.3c, with non-planar blocks, it scales sub-linearly. This is due to the latter's ability to sustain F_{max} (or values close to it) for greater deflections (see Fig. 6.3b) compared to planar-faced blocks. In this case, U continues to increase even after F_{max} reaches saturation (see shaded cluster in Fig. 6.3c). The sub-linear scaling with wave-faced blocks is favorable compared to the linear scaling with planar blocks as it promotes increased work-to-failure. We refer to this ability as pseudo-ductility, since it does not involve actual ductile deformation of the bulk material. We attribute it to local enhanced interlocking, that is, the improvement of interlocking between blocks through local non-planar morphologies[2].

To put this result into context with regard to TIS with planar-faced blocks, we highlight two cases. First, we focus on TIS with the same μ (*i.e.*, 0.23) but with different block types, *i.e.* TIS with planar blocks (highlighted by a red square marker in Fig. 6.3c) with TIS with non-planar blocks (highlighted by a shaded cluster in Fig. 6.3c). TIS with non-planar blocks not only increase significantly the peak load (*i.e.* more than four times), as could have been expected from beam-like observations [112], but also the work-to-failure is increased by more than a factor of 19 compared to TIS with planar blocks. This clearly demonstrates the capacity of TIS with non-planar surface morphologies to significantly improve the work-to-failure – and this while simultaneously increasing the peak load. In addition, if the same peak load

---

[2]Based on this definition, planar-faced blocks, which lack such local features, have a smaller degree of overall interlocking.

needs to be achieved with planar blocks, one would need a friction coefficient as high as 1.0 (highlighted by a green square marker in Fig. 6.3c) and that would still cause a decrease in work-to-failure by more than a factor 2. Hence, these results suggest that when a material is given for a particular TIS application, introducing non-planar block surface morphology may improve TIS performance both in terms of peak load and work-to-failure.

While TIS with non-planar blocks have been explored previously, they do not exhibit the same improved performance we have identified. This stems from specific surface characteristics, particularly the way the local angle of the surface changes. If we consider osteomorphic blocks as an example, the curvature of the interface promotes smooth sliding along the surface, resulting in sustained work-to-failure, but lower peak loads. In contrast, a wavy pattern, as suggested here with multiple oscillations, introduces curvature that restricts neighboring blocks from sliding extensively across the whole interface. This localized sliding on the curved surface allows us to achieve both high peak loads and work-to-failure, and therefore to access the untapped potential.

6.3.4 The importance of the local angles of inclination at hinging contact regions

The design of non-planar surface pattern creates enhanced interlocking due to the high local inclination of the interface. While both unrealistically high μ and non-planar surface patterns can lead to F_{max} saturation, high μ alone cannot provide pseudo-ductile behavior and enhanced work-to-failure. This means that, regardless of how high the friction coefficient is, it cannot provide the high levels of work-to-failure provided by high local interlocking angles.

The effect of local enhanced interlocking is significant compared to increasing the angle of inclination (θ) in a planar-faced block because the angle of inclination is limited (design constraint). On the contrary, non-planar blocks with wave-like surfaces can locally introduce very high inclinations, which favor this behavior of promoted work-to-failure while maintaining blocks with attainable shapes. This raises a question regarding the underlying characteristic of the non-planar interfaces that causes the non-linear scaling response.

To quantify the effects of each of the parameters governing non-planar block morphologies, we consider U first as a function of $\lambda/4$ where λ is the wavelength of the surface pattern Fig. 6.4a, and next as a function of waviness amplitude $\mathcal{A}$ in Fig. 6.4b. While $\lambda/4$ does not seem to directly influence U as indicated by the large scatter of the data points, there appears to be some correlation with $\mathcal{A}$. Since, we expect the local interlocking to be the main factor, we consider U as a function of $\mathcal{A}/(\lambda/4)$, which represents the average slope at the top of the interface (see Fig. 6.4e) as a measure of the degree of interlocking, and observe that the data points collapse and saturate neatly (see Fig. 6.4c), as they also do for F_{max} in Fig. 6.4d. This characteristic promotes large rotations and constraints sliding to a specific local area of the overall interface (see Fig. 6.3d). This means that (a) the local angle at the top of the interface of the loaded block (where it is in contact with its neighbors, see θ^{top} in Fig. 6.4e), not the wavelength or the amplitude independently, is the governing non-dimensional parameter defining the effects of non-planar blocks on the structural response; (b) the local angle is the key to the enhanced work-to-failure and ultimate deflection obtainable with non-planar interfaces; and (c) there is a limit to θ^{top} beyond which its further increase does not affect the structural performance.

We note that high local angles are likely to be associated with high surface tractions and bulk stresses, which can lead to material damage and fracture. This means that the practical applicability of our findings might require technical solutions to address these phenomena.
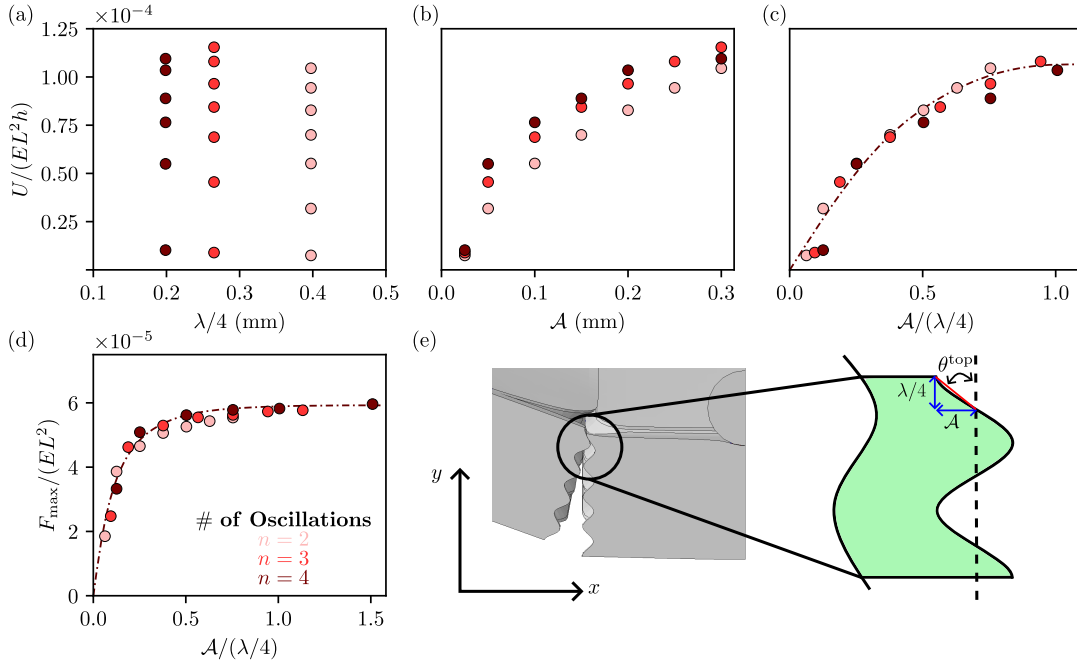
Figure 6.4: Normalized work-to-failure, plotted against (a) $\lambda/4$ where λ is the wavelength of the surface pattern, (b) the amplitude $\mathcal{A}$ and (c) the top inclination $\mathcal{A}/(\lambda/4)$. (d) The normalized peak load for each curve is plotted against the top inclination $\mathcal{A}/(\lambda/4)$. The dashed lines in (c) and (d) have been added as a visual aid to demonstrate the saturation of the work-to-failure and peak load, respectively. (e) Schematic illustration of the top inclination angle between the central and a neighboring block.

6.3.5 Improving stability for low-amplitude configurations

Next, we consider the influence of the average inclination of the interface $\overline{\theta}$, see Fig. 6.5a, on the structural response of TIS with wave-faced blocks. Specifically, we focus on how $\overline{\theta} > 0°$ can contribute to ameliorating the load-drop instabilities associated with small amplitudes for $\overline{\theta} = 0°$ observed in Fig. 6.3b for $\mathcal{A} = 0.025$ mm. Specifically, we observe that the $F_y - \delta$ response undergoes a series of fluctuations characterized by multiple local maxima where each local maximum is successively smaller in magnitude compared to the previous one. This behavior is due to the 'pushing-downward' of the central block from the top interface crest to the next one through a sliding mechanism (see Fig. 6.3e). Reconsidering the cases with $\mathcal{A} = 0.025$ mm (see Fig. A.5), but this time with $\overline{\theta} = 5°$, we see that, for all the examined number of oscillations n, with $\overline{\theta} = 5°$ the load-drops are smaller, the ultimate deflections increase by roughly 25%, and, as a result, the work-to-failure roughly doubles Fig. 6.5b. This speaks to the great contribution of the average angle of inclination to the stability of TIS with non-planar blocks.

To gain a deeper understanding of how the average inclination contributes to the stability of the structure, we consider its effect on the internal force transmission by comparing the distribution of the minimum principal stress with $\overline{\theta} = 0°$ and $\overline{\theta} = 5°$ (Fig. 6.5c) and the contact forces of the loaded block (Fig. 6.5d). With $\overline{\theta} = 0°$, the stress and contact force distribution are symmetrical, meaning that the load is transferred equally in yz and xy planes. In contrast, with $\overline{\theta} = 5°$, they are asymmetric, with more load being transmitted in the yz plane compared with the xy plane as reflected by the larger compressive stresses indicated by blue. This bias indicates that larger $\overline{\theta}$ make one direction (in this case yz) stiffer than the perpendicular one, and it suggests that having a stiffer load path contributes to the overall resilience of the structure.
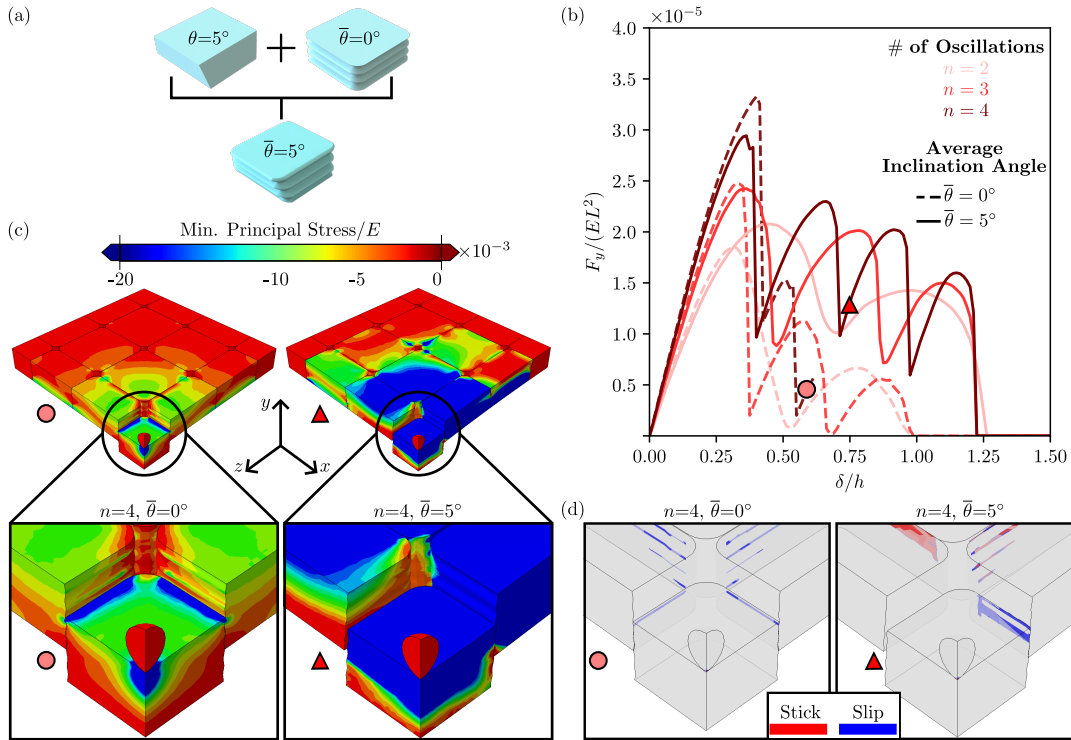
Figure 6.5: (a) Schematic representation of a wave-faced block with average inclination angle $\overline{\theta} = 5°$ as it results from the combination of a planar-faced block with inclination angle $\theta = 5°$ and a wave-faced block with average inclination angle $\overline{\theta} = 0°$. (b) Normalized load $F_y/(E \cdot h^4/L)$ against the normalized prescribed displacement δ/h for structures with different oscillations n, and for amplitude $\mathcal{A} = 0.025$mm. The dashed curves correspond to an average inclination angle $\overline{\theta} = 0°$ and the solid curves to an average inclination angle $\overline{\theta} = 5°$. (c) Snapshots of minimum principal stress distribution normalized with Young's modulus E of the structure at specific δ/h (left) for $n = 4$ and $\overline{\theta} = 0°$ and (right) for $n = 4$ and $\overline{\theta} = 5°$. (d) Snapshots of the stick-slip behavior at the interfaces of the central block for structures (left) with $\mathcal{A} = 0.025$, $n = 4$, and $\overline{\theta} = 0°$ and (right) $\mathcal{A} = 0.025$, $n = 4$, and $\overline{\theta} = 5°$).

6.4 Conclusion

This study examined how, through the use of blocks with non-planar surface morphologies, the hitherto untapped work-to-failure potential of slab-like topologically interlocked structures (TIS) can be better exploited. For this purpose, we considered blocks with wave-like sinusoidal surface morphologies defined by the number of oscillations n, the amplitude $\mathcal{A}$, and the average interface inclination angle $\overline{\theta}$. The effects of these parameters on the mechanical response of the structure were investigated and compared to TIS with planar-faced blocks, shedding new light on their influence in achieving improved structural performance. The main conclusions of our study are:

- Unlike TIS with planar blocks, in slab-like TIS with non-planar blocks, the structural response parameters saturate with a relatively low and realistic value of the friction coefficient.

- With non-planar blocks, the failure mode is more ductile compared to planar ones. This allows to develop much larger work-to-failure, and results in a sub-linear scaling of the work-to-failure as a function of the peak load.

- The key non-dimensional parameter governing non-planar blocks with wave-like surface morphologies, leading to the improved work-to-failure and ultimate deflection, is the local angle of inclination at the hinging contact regions of the structure.

In summary, we have shown that introducing local enhanced interlocking to the structure, promotes the system's stability, work-to-failure, and ultimate deflection. This study can be further expanded by considering multi-layer TIS [59] with architected surface patterns and structures with curved geometries (*i.e.*, arches) [56, 132]. Exploring such configurations could help further improve structural stability, allowing us to obtain the peak load and ultimate deflection simultaneously.

7

Summary and Conclusion

> If we learn to build with local materials, we
> have a future.
>
> Francis Kere

During the last two decades, scientists have been captivated by the potential of topologically interlocked structures (TIS), sparking curiosity across many scientific sectors such as structural engineering, material science, architecture and mathematics. Building upon existing knowledge, this thesis focuses on the fundamental understanding of the main mechanisms that govern the mechanical response of topologically interlocked systems. These are the interface mechanisms (*i.e.*, stick and slip behavior at the interface of the blocks), as well as block rotation, deformation, and separation. Furthermore, this study delved deeper into the geometrical aspect of TIS' blocks, by exploring the effects of block geometry and surface morphology on the mechanical response. This section summarizes the main findings of the study and outlines its main conclusions.

The parameters responsible for TIS's response capacities (*i.e.*, structural stiffness, peak load, work-to-failure, and ultimate deflection) are the Young's modulus, the size of the blocks (*i.e.*, height, length, and overall geometry), the friction coefficient, and the block's surface morphology. These parameters have been exploited for developing a structurally-based systematic approach to identify the theoretical design space envelope of TIS[1]. Such a parametric study can aid scientists and engineers to highlight the importance of each parameter in a topologically interlocked model.

Though this systematic approach, we considered both beam-like and slab-like configurations. The former can be considered as the simplest model that can be utilized for a fundamental research. The latter, is one of the most commonly used configuration and it could not be omitted from the study as it allows generalizing the observations. In fact, the comparison between

---

[1]The term "theoretical design space envelope" refers to the theoretical space of a load-deflection curve, controlled by a range of design parameters (*i.e.*, material, geometrical, and interfacial).

slab-like TIS with planar-faced and the agreement with previous numerical methods [36] adds credibility to the results. We found that the response capacities saturate at a certain friction coefficient (μ_{sat}) both for beam-like and slab-like TIS. Beyond this point, further increase of the friction coefficient does not improve the structural response (we frequently refer to it as saturated response capacity). In addition, the saturation level depends on material, geometrical and interface properties of the structure.

The saturated response capacity for TIS (both beam-like and slab-like) with planar-faced blocks, requires unrealistically high friction coefficient values. This might not be feasible, given that common engineering materials do not exhibit such high friction coefficient values. This raised a question whether the saturated response could be approached using non-planar-faced blocks and realistic friction coefficient. As a result, we proposed structures with non-planar-faced blocks (*i.e.*, in this case blocks with wave-like patterns characterized by two parameters; the number of oscillations and amplitude). We show that the peak load of these structures approaches the theoretical limit, but this time with lower and more realistic friction coefficient. This discovery opens up new avenues, as it widens the range of available engineering materials that can be utilized, regardless of interface properties (*i.e.*, friction coefficient).

Focused on beam-like TIS, with non-planar-faced blocks, we revealed that the surface modifications lead to three different response regimes; structures that approach the theoretical upper limit, structures with instabilities noted by sharp load drops, and structures that never reach the theoretical limit. All three regimes occur for low values of friction coefficient. This suggests that the friction coefficient itself cannot fully describe this observation. As a result, we introduced the effective friction coefficient, which is a combination of the actual friction coefficient and the geometrical friction coefficient (*i.e.*, $\mu_{\text{eff}} = \mu + \mu_{\text{geo}}$). Hence, the geometrical friction coefficient (*i.e.*, a frictional resistance characteristic that arise from the surface morphology of a block), is of decisive importance in determining the effective friction coefficient and ultimately for describing the different regimes of load-deflection curves.

To characterize the geometrical friction coefficient in beam-like TIS with non-planar-faced blocks, we proposed a surface measure that combines surface curvature and surface gradient of the wave-like pattern. This surface measure takes into consideration the full range of surface morphologies. It allows identifying the geometrical friction coefficient, which, in turn, helps in interpreting the influence of surface morphology on the overall mechanical response. The proposed surface measure can be adopted in other non-planar-faced block configurations and compared with the current results. A different surface measure was proposed for slab-like TIS with non-planar-faced blocks and particularly the local angle of inclination at the hinging points. That is, the inclination based on the amplitude and wavelength of the wave-like pattern. Similarly to the proposed surface measure for beam-like TIS, this measure also leads to collapse of the data points irrespective of surface morphology. As a result, the local angle of inclination at the hinging points is considered as the key characteristic for enhancing work-to-failure and ultimate deflection.

Interestingly, we observed that the work-to-failure continued to increase even after the peak-load reached saturation (non-linear scaling). The use of non-planar-faced blocks introduced a pseudo-ductile behavior, allowing the structures to withstand larger deformation before failure compared to slab-like TIS with planar-faced blocks. The observation that wave-like patterns can lead to sustained deflection at a saturated peak load before structural failure without actual ductile deformation indicates potential applications for slab-like TIS in scenarios where limited ductility is required to mitigate catastrophic failure. Furthermore, the combination of inclined interfaces with surface morphology increased the system's stability, improving the work-to-failure and ultimate deflection. These findings highlighted the importance of all parameters that describe a surface morphology (*i.e.*, average inclination angle, number of oscillations, and amplitude) for obtaining the desired response capacities.

Overall, this thesis provides some insights on the mechanics of TIS and points to practically

actionable strategies for enhancing the response capacities of the structure. By systematically exploring the effects of interface mechanisms and surface morphology of TIS's blocks, it could allow for designing efficient structures. The findings on saturated response capacities, pseudo-ductility, stability enhancement through inclined interfaces, and the non-linear scaling behavior for slab-like TIS with non-planar-faced blocks, provide a good starting point for future research and analysis. Notably, the pseudo-ductile behavior allows for higher and noticeable deflection in the structure, which can act as an early warning sign of potential overloading. Furthermore, the advantage of pseudo-ductility imposes that the TIS can deform temporarily but return to its original shape once the load is removed without permanent plastic deformation. The finding of the saturation to the peak load has been observed in TIS configurations, including both basic and more complex design patterns. This approach serves as an effort to generalize the key characteristics that lead to the saturated response. Addressing the aforementioned findings, as well as potential practical implications, would further strengthen the significance of the research results.

As we conclude this study, the future of TIS, opens up new avenues in engineering, architecture, and beyond. The fact that our focus was mainly theoretical and numerical, reminded us once again that fundamental research serves as the stepping stone to pushing the boundaries of knowledge. TIS could potentially provide new ideas in industries, contribute to sustainable practices by carefully selecting the material of the blocks, and foster innovation. This work might offer a glimpse of inspiration, urging us to continue exploring, innovating, and providing new solutions for generations to come.

<div style="text-align: right; font-size: 6em; color: #bbb;">8</div>

Outlook

> Everything is theoretically impossible until
> it is done.
>
> Robert Anson Heinlein

8.1 Transition from research to real-world applications

Even though topologically interlocked structures (TIS) have great potential in various fields, their practical application is not yet fully realized due to manufacturing and mass production challenges, lack of standardized design and testing methods, and many potential obstacles that must be considered for ensuring their effective utilization. Some relevant aspects are:

Design considerations: TIS require precise design and analysis to ensure load resilience. Failure to account for the interlocking features, interface mechanisms and various load scenarios can lead to structural collapse. As a result, both numerical simulations and experiments are of equal importance to test TIS's performance under various loading conditions. Furthermore, to overcome design obstacles and prevent catastrophic failure, physical prototypes of TIS that replicate real-world loading scenarios should be utilized.

Manufacturing challenges: The fabrication of TIS can be challenging due to the complex geometry and detailed specifications for the interlocking features. Even small deviations (*i.e.*, $\approx 1\%$) in manufacturing tolerances can affect the fitting and functionality of the components. Digital fabrication and high-precision manufacturing combined with quality control, can ensure the components are manufactured to the desired specifications. It is plausible that current industry techniques may fall short of TIS development needs, requiring further research for identifying novel manufacturing methodologies.

Installation and maintenance: The installation of TIS requires specialized training, planning that complies with manufacturing protocols, and proper machinery to ensure the accurate assembly of the interlocking blocks. Each structure should be treated differently during the

assembling and maintenance processes, as each block's shape and interlocking pattern can vary significantly. Maintenance schedules should be set, and skilled personnel should carry out routine inspections. Errors during the installation process or failure to meet maintenance obligations might result in misalignment, incorrectly connected components or even block fracture, compromising the system's structural integrity. To properly install and maintain TIS, further research is required to determine appropriate installation guidelines and document safety protocols.

Environmental risks: TIS may be susceptible to environmental conditions such as temperature, humidity, and corrosion. These factors can impact the performance of the interface mechanisms and the geometry and surface morphology of the blocks, resulting in early stage failure or reduced performance. Engineers should thus consider these parameters when selecting materials and coatings for prolonging the lifetime of a structure based on the intended environmental exposure.

8.2 Future prospects

This thesis has provided a groundwork for future research in TIS that can be expanded theoretically, numerically, and experimentally. The following selected topics of interest are grouped below in an effort to offer a little glimpse of the vast area of research that awaits to be explored in the field.

From static to dynamic frameworks

An interesting direction for future work involves the extension of the current study from static numerical simulations to quasi-static and dynamic ones. This will enable both impact resistance investigations and vibration analysis. Dynamic models can help to assess the structural integrity and safety of TIS under different loading and time-depended scenarios. This approach could be implemented using either dynamic explicit or dynamic implicit solvers. While most studies in the literature employ dynamic explicit solvers with mass scaling technique [6, 62, 73], the influence of mass scaling on the mechanical response of the structure remains unclear. In addition, a theoretical saturation to the response capacities has not been observed in impact simulations.

The numerical models can be combined with experimental methods for an interdisciplinary research and a comprehensive understanding, ensuring that the proposed TIS models can withstand dynamic forces, such as vibrations, shocks and impacts. Experimental data can provide additional insights in the response capacity of the structures and constitute benchmarks for numerical studies. As an example, conducting durability tests under vibration modes using different materials could help identify the structural integrity and fatigue response of TIS over time.

The initiation of fracture and beyond

The current study assumed that failure occurs when the central block is completely pushed-out of the structure, neglecting potential fracture of the blocks. In real-world applications, fracture initiation and propagation can significantly impact the mechanical response and failure behavior of TIS.

It still leaves an open question regarding the exact moment where the onset of fracture initiates and its impact on the load-deflection curve. Moreover, fracture propagation, which depends on surface morphology and interface mechanisms, could alter the mechanical response. For instance, local fracture within a block might not lead to structural failure; instead, it could introduce new smaller bodies in the systems entangling TIS's response. Lastly, it remains unknown whether the theoretical response capacity could be obtained when fracture is considered.

Future studies could introduce fracture mechanics (*i.e.*, by incorporating the extended finite element method, cohesive elements or phase field models) in the numerical framework to shed light on crack initiation and propagation, stress redistribution, and their effect on the overall integrity of the structure. In addition, as the crack propagates and block segments become fully fractured, new interfaces are formed, potentially necessitating the implementation of frictional contact interactions. Such a thorough investigation can be challenging it terms of complexity, computational burden and computation time. However, fracture mechanics is a critical aspect in TIS for material selection, design of block geometry, and structural optimization.

Interlocking patterns from a design perspective

TIS can be distinguished in three main categories; beam-like, slab-like (also referred to as plate-like) and curved-like (*i.e.*, arches) [56, 132] with planar-faced or non-planar-faced blocks in single layer or multi-layer [59] configurations. Future studies could adopt blocks with novel geometrical patterns that combine both topologically and geometrically interlocked characteristics [40]. Such models could offer self-interlocked structures without the need of external constraints. An interesting avenue for exploration involves examining the mechanical response of self-interlocked configurations in comparison to externally constraint TIS. Such an approach can be implemented both numerically and experimentally, offering new insights that could potentially bolster the transition of TIS from a concept to reality.

A particularly interesting finding in this study is the non-linear scaling relation between the peak load and work-to-failure in slab-like TIS with non-planar-faced blocks. This observation demonstrates the complex nature of TIS and their unique functionalities. The scalability effect was demonstrated using blocks with linear elastic constitute law. This raises new fundamental questions regarding the effects on the response capacities and the scalability between the peak load and work-to-failure with different types of constitutive laws (elastoplastic or viscoelastic) as well as with hybrid structures.

TIS in architecture and civil engineering

TIS offer a promising potential in architecture. In the event of earthquakes, hurricanes, and other natural disasters, TIS could potentially absorb and distribute energy more effectively than traditional structures, reducing the risk of damage or collapse. In addition to their practical advantages, TIS offer a range of aesthetic benefits. The interlocking patterns and geometrical shapes create visually striking architectural forms, both functional and beautiful. As a result, TIS have great potential in the field of architecture for creating innovative, resilient, and visually stunning structures that could withstand the "test of time". Moreover, TIS could reduce material consumption and waste production in construction and engineering projects promoting sustainable waste management.

Merely grasping the fundamentals of TIS is just the beginning. What is needed now is a collaborative effort between engineers and architects to adopt methodologies that involve extensive experimentation and modeling of interlocked structures at large-scales and various environmental conditions. Such endeavors will enhance our theoretical and practical under-standing of the mechanical response of TIS, bringing us one step closer to realizing practical applications. The main challenge in the numerical modelling of large-scale TIS, involving high number of blocks, is computational cost. A potential way of keeping computational cost at acceptable levels is though hybrid modeling, such as the Level-Set-DEM approach [36, 133].

TIS for outer-space applications

The development of conventional structures in space faces many challenges, mainly because of gravity conditions, space radiation, high-velocity micrometeoroid impact collisions. In addition, the lubrication of mechanical components is a critical process because of the extreme

conditions that can affect the performance and longevity of components. In the absence of gravity and a natural atmosphere, traditional lubrication methods, such as liquid or grease-based lubricants, cannot be used effectively.

An alternative solution would be the use of TIS, as they rely on topological and geometrical interlocking principles, dry-stacking, and frictional sliding to hold the building blocks in place. As a result, TIS can potentially find a place in various forms and sectors of space engineering and extraterrestrial applications [124], including prefabricated panels, dry-stone walls, adjustable radiation shielding assemblies, bullet-proof armors, and mechanical components for dry lubrication.

To assess their relevance for space applications, theoretical and numerical studies are necessary for investigating the response of TIS during microgravity scenarios and extreme space environments. This could be combined with experimental tests in microgravity platforms and space-like conditions such as thermal vacuum chambers to observe their mechanical response and durability. Finally, following on numerical and experimental results, the next step could be to identify the range of suitable materials for fabrication in space or transportation from Earth.

A

Appendix

A.1 On the failure of beam-like topologically interlocked structures

A.1.1 Validation of frictional contact

Since the behavior and failure of TIS completely depends on friction resistance and stick and slip mechanisms, the accuracy of the results depend entirely on the validity of the contact formulation. As further validation of the frictional contact, the Cattaneo and Mindlin's problem is considered. This benchmark involves two elastic cylinders that are pressed together. The bottom half-cylinder has its base constrained in the vertical and horizontal direction while the top surface of the top half cylinder is displaced by δ_x and δ_y (Fig. A.1a). The normal T_n and tangential T_t tractions along the contact surface are computed and plotted together with the analytical solution. For computing the analytical solution, the normal F_n and tangential F_t reaction forces are calculated from the surface where the prescribed displacement is applied. Using the analytical solution [134] T_n and T_t are computed as:

$$T_n(x) = \frac{2F_n\sqrt{\alpha^2 - x^2}}{\pi \alpha^2} \tag{A.1.1}$$

$$T_t(x) = \frac{2\mu_s F_n}{\pi \alpha^2}\left[\sqrt{a^2 - x^2} - H(c^2 - x^2)\sqrt{c^2 - x^2}\right], \quad -\alpha < x < \alpha \tag{A.1.2}$$

where,

$$\alpha = \left[\frac{4F_n R_0 R_1}{\pi(R_0 + R_1)}\left(\frac{1 - \nu_0^2}{E_0} + \frac{1 - \nu_1^2}{E_1}\right)\right]^{\frac{1}{2}} \quad \text{and} \quad c = \alpha\left(1 - \frac{F_t}{\mu_s F_n}\right)^{\frac{1}{2}} \tag{A.1.3}$$

Here, $H(\cdot)$ denotes the Heaviside function. A friction coefficient $\mu_s = 0.5$ is used and penalty parameters $\varepsilon_n = \varepsilon_t = 10^{12}\ N/m^3$. The numerical results of T_t (Fig. A.1b) and T_n (Fig. A.1c) are in good agreement with the results from the analytical solution.
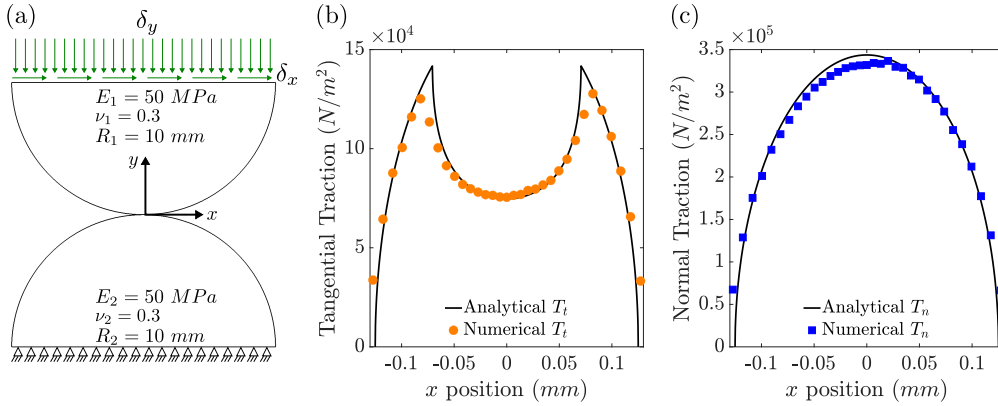
Figure A.1: Benchmark with the Cattaneo and Mindlin's problem. (a) Schematic setup showing the geometry of the half-cylinders, the boundary conditions applied and the material properties used in the simulation. Distribution of (b) T_t and (c) T_n as computed numerically (circles and squares respectively) and in comparison with the analytical solution (solid black lines) for friction coefficient $\mu_s = 0.5$.

A.1.2   Convergence analysis

For the mesh density analysis, a five-block structure is used, with $\theta = 5^o$, $E = 30$ GPa, $h = l = 2$ mm and $\mu = 0.2$ and 1.2. We chose two different μ to ensure that the interface behavior (slip or stick) does not influence the chosen mesh density. The particular mesh design is purely chosen based on computational efficiency. Having a similar fine mesh density everywhere in the domain increases the computational time of the simulation. We ran simulations with same mesh density everywhere and compared the $F_y - \delta$ curves for the case where densities are different (Fig. A.2). As can be observed the behavior difference in mesh densities around an interface does not affect the global response behavior. Fig. A.2a shows the chosen mesh density for the planar-faced interfaces and Fig. A.2c shows the chosen mesh densities for the curved and kinked interfaces.
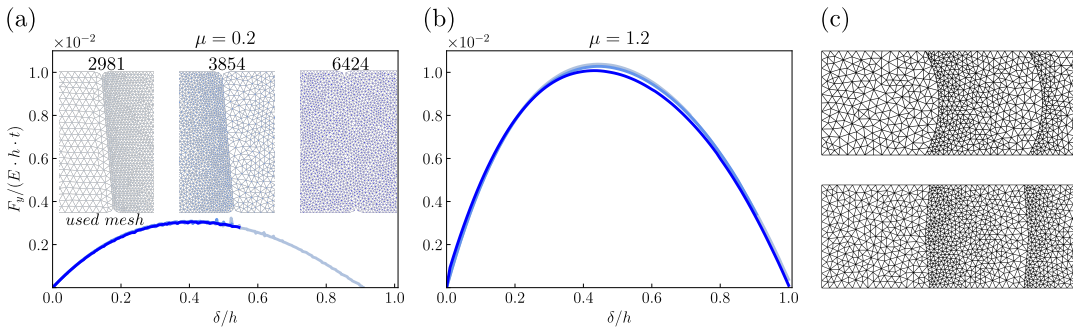
Figure A.2: Mesh density convergence analysis. Load-carrying capacity $F_y/(E \cdot h \cdot t)$ against the prescribed displacement δ/h for (a) $\mu = 0.2$ and (b) $\mu = 1.2$. The number of nodes is shown for each examined mesh density. (c) Mesh density for the curved (top) and kinked (bottom) configurations.

In addition, the chosen mesh from the mesh density analysis (Fig. A.2) is used for the convergence analysis. A five-block structure is used, with $\theta = 5^o$, $E = 1$ GPa, $h = l = 2$ mm and $\mu = 0.6$. The $F_y - \delta$ response is examined for different mesh refinements (Fig. A.3a). The mesh size along the fine and coarse interfaces is chosen based on the ratio between the element size $\mathscr{E}$ and the height h of the structure. The rest of the structure has mesh density equal to the coarse mesh. The results from the $F_y - \delta$ curves are very similar and independent of the chosen mesh refinements. The chosen mesh is based on the fact that a sufficient number of nodes at the interface is needed to properly capture stick and slip mechanisms, but also to

ensure reasonable computational cost. The chosen mesh is then tested for different penalty parameters ε_n and ε_t (Fig. A.3b). The chosen penalty parameters do not affect the $F_y - \delta$ response. Moreover, we tested that the penetration ξ of a slave node is small enough such that $\xi/h < 1\%$ (Fig. A.3c). Finally, ε_n and ε_t are kept constant at a given surface.
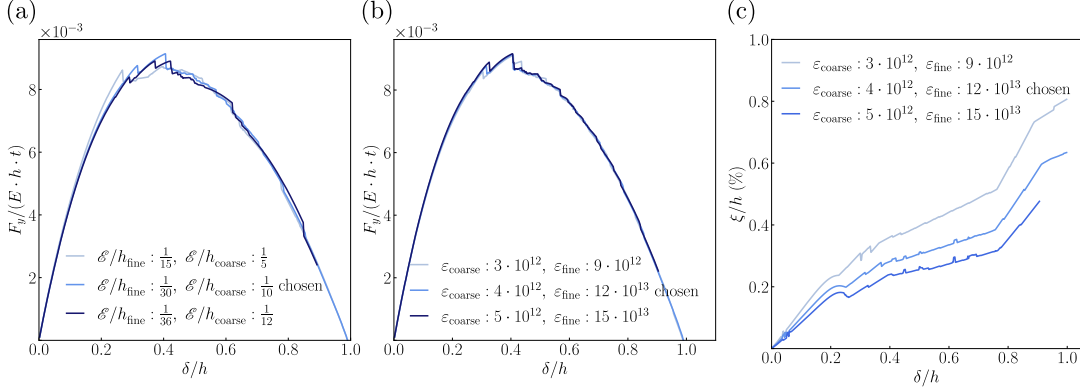
Figure A.3: Convergence analysis. Load-carrying capacity $F_y/(E \cdot h \cdot t)$ against the prescribed displacement δ/h. The curves correspond to (a) different mesh densities (where the mesh density is chosen based on the ratio between the element size $\mathscr{E}$ and h of the structure) and (b) different penalty parameters. (c) The chosen penalty parameters are tested to ensure that the ratio between the penetration ξ and h (*i.e.*, ξ/h) $< 1\%$.

A.1.3   Derivation of analytical expression for stick-slip threshold

The results are compared with an analytical line derived from the truss model (Eq. 4.1.1) marking the boundary between the stick- and slip-governed regions. We derive a theoretical boundary that marks the global transition from sticking to a slipping regime by employing the truss model for TIS, as discussed in [34] and Coulomb's friction law ($T = \mu N$). The tangential force T and the normal force N along an interface of TIS are computed by resolving F_v and F_h into F_a along a respective direction (β) as follows:

$$N = -\left(\Big(sin(\beta)sin(\theta) + cos(\beta)cos(\theta) \Big) F_a \right) \tag{A.1.4}$$

$$T = -\left(\Big(sin(\beta)cos(\theta) - cos(\beta)sin(\theta) \Big) F_a \right) \tag{A.1.5}$$

Angle β is controlled by h_{eff} and l_{eff} (Fig. 4.2). The expressions from (A.1.4) and (A.1.5) are substituted into the Coulomb friction model for computing μ_{sat} that controls the transition from sliding to global sticking:

$$T = \mu_{\text{sat}} N \implies \mu_{\text{sat}} = \frac{sin(\beta)cos(\theta) - cos(\beta)sin(\theta)}{sin(\beta)sin(\theta) + cos(\beta)cos(\theta)} \tag{A.1.6}$$

A.2 Beam-like topologically interlocked structures with hierarchical interlocking
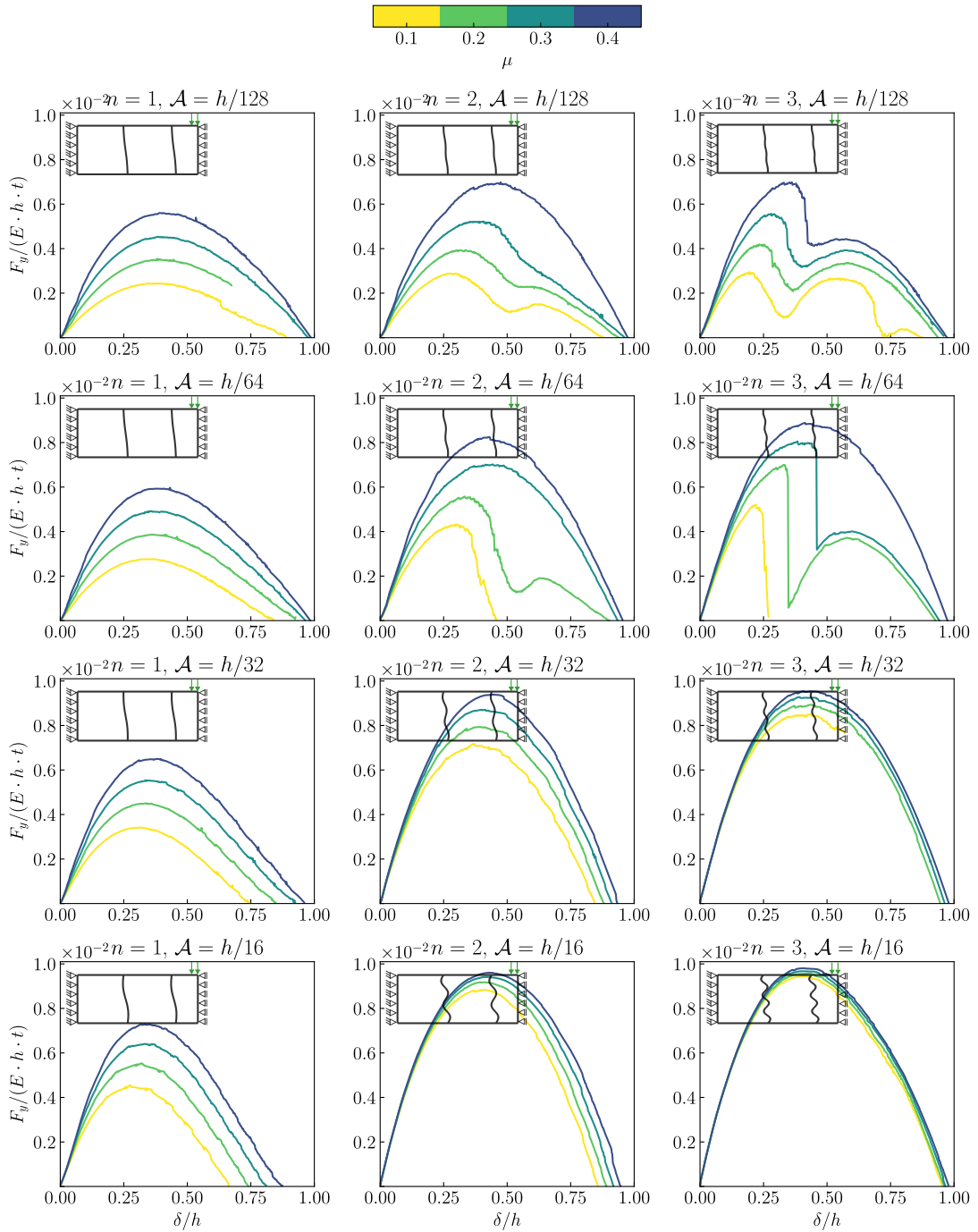
Figure A.4: Normalized load-carrying capacity $F_y/(E \cdot h \cdot t)$ against the normalized prescribed displacement δ/h. The curves correspond to structures with different friction coefficients μ, oscillations n, and amplitude $\mathcal{A}$. The symmetric model of the examined structure is shown in the top left corner of each sub-figure.

A.3 The key to the enhanced performance of slab-like topologically interlocked structures with non-planar blocks

A.3.1 Load-deflection for all amplitudes and oscillations examined
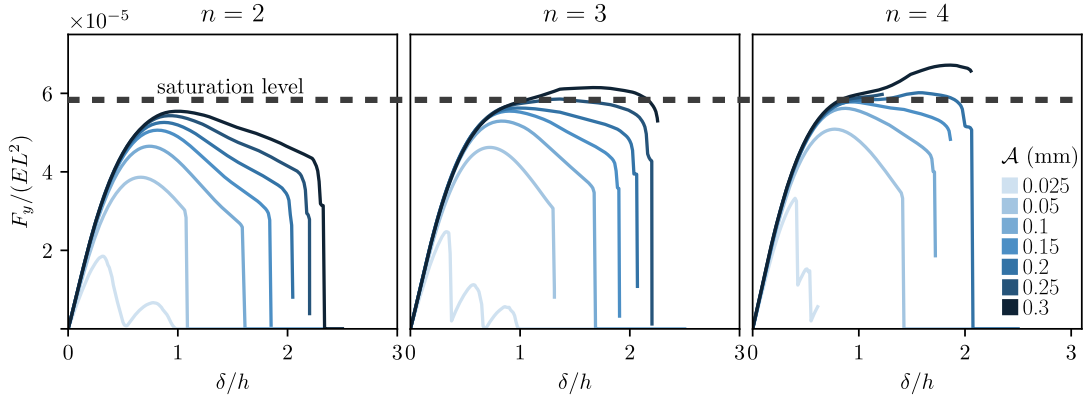
Figure A.5: Normalized load-deflection curves for structures with (a) 2, (b) 3 and (c) 4 oscillations n, and different amplitudes $\mathcal{A}$. The dashed horizontal line indicates the saturation to the peak load $F_{\max}$.

Fig. A.5 shows that the $F_y - \delta$ response saturates to $F_{\max}$ for all n, while further increase of $\mathcal{A}$ promotes pseudo-ductile behavior causing increase in ultimate deflection and work-to-failure. After reaching the saturated response for $F_{\max}$, we have observed significant deformation in the elements, which impacts the accuracy of the $F_y - \delta$ curves (see curves that surpass the saturation level in Fig. A.5b and c). This occurrence arises from significantly reducing the number of contact points within the mesh at the interface between the central block and its neighboring ones. The reduced contact points result from high block rotations, resulting in numerical artifacts and recorded load value inaccuracies.

Bibliography

[1]   A. V. Dyskin et al. "A new concept in design of materials and structures: Assemblies of interlocked tetrahedron-shaped elements". In: *Scripta Materialia* 44.12 (June 2001), pp. 2689–2694. ISSN: 13596462. DOI: 10.1016/S1359-6462(01)00968-X.

[2]   Marc André Meyers et al. "Biological materials: Structure and mechanical properties". In: *Progress in Materials Science* 53.1 (2008), pp. 1–206. ISSN: 00796425. DOI: 10.1016/j.pmatsci.2007.05.002.

[3]   Mohammad Mirkhalaf, Tao Zhou, and Francois Barthelat. "Simultaneous improvements of strength and toughness in topologically interlocked ceramics". In: *Proceedings of the National Academy of Sciences of the United States of America* 115.37 (2018), pp. 9128–9133. ISSN: 10916490. DOI: 10.1073/pnas.1807272115.

[4]   Mohammad Mirkhalaf et al. "Toughness by segmentation: Fabrication, testing and micromechanics of architectured ceramic panels for impact applications". In: *International Journal of Solids and Structures* 158 (Feb. 2019), pp. 52–65. ISSN: 00207683. DOI: 10.1016/j.ijsolstr.2018.08.025.

[5]   Arcady V. Dyskin et al. "Fracture resistant structures based on topological interlocking with non-planar contacts". In: *Advanced Engineering Materials* 5.3 (Mar. 2003), pp. 116–119. ISSN: 14381656. DOI: 10.1002/adem.200390016.

[6]   Lee Djumas et al. "Deformation mechanics of non-planar topologically interlocked assemblies with structural hierarchy and varying geometry". In: *Scientific Reports* 7.1 (Dec. 2017), p. 11844. ISSN: 20452322. DOI: 10.1038/s41598-017-12147-3.

[7]   Bharat Bhushan. "Biomimetics: Lessons from Nature - an overview". In: *Philosophical Transactions of the Royal Society A: Mathematical, Physical and Engineering Sciences* 367.1893 (2009), pp. 1445–1486. ISSN: 1364503X. DOI: 10.1098/rsta.2009.0011.

[8]   Ulrike G.K. Wegst et al. "Bioinspired structural materials". In: *Nature Materials* 14.1 (Jan. 2015), pp. 23–36. ISSN: 14764660. DOI: 10.1038/nmat4089.

[9]   Shinya Inoue and Shigeru Kondo. "Suture pattern formation in ammonites and the unknown rear mantle structure". In: *Scientific Reports* 6.September (2016), pp. 1–7. ISSN: 20452322. DOI: 10.1038/srep33689.

[10] Jessica C. Huss et al. "Topological Interlocking and Geometric Stiffening as Complementary Strategies for Strong Plant Shells". In: *Advanced Materials* 32.48 (2020), pp. 1–7. ISSN: 15214095. DOI: 10.1002/adma.202004519.

[11] Stefanie Krauss et al. "Mechanical function of a complex three-dimensional suture joining the bony elements in the shell of the red-eared slider turtle". In: *Advanced Materials* 21.4 (2009), pp. 407–412. ISSN: 09359648. DOI: 10.1002/adma.200801256.

[12] B. Alheit, S. Bargmann, and B. D. Reddy. "Computationally modelling the mechanical behaviour of turtle shell sutures—A natural interlocking structure". In: *Journal of the Mechanical Behavior of Biomedical Materials* 110 (2020), p. 103973. ISSN: 18780180. DOI: 10.1016/j.jmbbm.2020.103973.

[13]   B. Alheit, S. Bargmann, and B. D. Reddy. "Dynamic mechanical behaviour of suture interfaces as inspiration for architectured hierarchical interlocking composites". In: *Journal of the Mechanics and Physics of Solids* 157.August (Dec. 2021), p. 104620. ISSN: 00225096. DOI: 10.1016/j.jmps.2021.104620.

[14]   Marion Frey et al. "Tunable Wood by Reversible Interlocking and Bioinspired Mechanical Gradients". In: *Advanced Science* 6.10 (2019). ISSN: 21983844. DOI: 10.1002/advs.201802190.

[15]   Takashi Miura et al. "Mechanism of skull suture maintenance and interdigitation". In: *Journal of Anatomy* 215.6 (2009), pp. 642–655. ISSN: 00218782. DOI: 10.1111/j.1469-7580.2009.01148.x.

[16]   Asmaa Maloul, Jeffrey Fialkov, and Cari M. Whyne. "Characterization of the bending strength of craniofacial sutures". In: *Journal of Biomechanics* 46.5 (2013), pp. 912–917. ISSN: 00219290. DOI: 10.1016/j.jbiomech.2012.12.016.

[17]   Robert O. Ritchie. "The conflicts between strength and toughness". In: *Nature Materials* 10.11 (2011), pp. 817–822. ISSN: 14764660. DOI: 10.1038/nmat3115.

[18]   Florian Bouville et al. "Strong, tough and stiff bioinspired ceramics from brittle constituents". In: *Nature Materials* 13.5 (2014), pp. 508–514. ISSN: 14764660. DOI: 10.1038/nmat3915. arXiv: 1506.08979.

[19]   M. Mirkhalaf, A. Khayer Dastjerdi, and F. Barthelat. "Overcoming the brittleness of glass through bio-inspiration and micro-architecture". In: *Nature Communications* 5.1 (May 2014), p. 3166. ISSN: 20411723. DOI: 10.1038/ncomms4166.

[20]   E. Munch et al. "Tough, bio-inspired hybrid materials". In: *Science* 322.5907 (Dec. 2008), pp. 1516–1520. ISSN: 00368075. DOI: 10.1126/science.1164865.

[21]   F. Barthelat et al. "On the mechanics of mother-of-pearl: A key feature in the material hierarchical structure". In: *Journal of the Mechanics and Physics of Solids* 55.2 (Feb. 2007), pp. 306–337. ISSN: 00225096. DOI: 10.1016/j.jmps.2006.07.007.

[22]   Jiyu Sun and Bharat Bhushan. "Hierarchical structure and mechanical properties of nacre: A review". In: *RSC Advances* 2.20 (2012), pp. 7617–7632. ISSN: 20462069. DOI: 10.1039/c2ra20218b.

[23]   Yaning Li, Christine Ortiz, and Mary C. Boyce. "Bioinspired, mechanical, deterministic fractal model for hierarchical suture joints". In: *Physical Review E - Statistical, Nonlinear, and Soft Matter Physics* 85.3 (Mar. 2012), p. 031901. ISSN: 15393755. DOI: 10.1103/PhysRevE.85.031901.

[24]   Erica Lin et al. "Tunability and enhancement of mechanical behavior with additively manufactured bio-inspired hierarchical suture interfaces". In: *Journal of Materials Research* 29.17 (Sept. 2014), pp. 1867–1875. ISSN: 20445326. DOI: 10.1557/jmr.2014.175.

[25]   Jean-Gaffin (1706-1775) Éditeur scientifique Gallon. *Machines et inventions approuvées par l'Académie royale des sciences depuis son établissemen : Tome 6*. Ed. by Hippolyte-Louis Guerin Gabriel Martin, Jean-Baptiste Coignard. Vol. 6. Académie des Sciences, Paris, 1735.

[26]   Michael Glickman. "G-Block System of Vertically Interlocking Paving." In: *Second International Conference on Concrete Block Paving*. Delft, 1984, pp. 345–348.

[27]   R. E. Goodman. "Block theory and its application". In: *Geotechnique* 45.3 (Sept. 1995), pp. 383–423. ISSN: 17517656. DOI: 10.1680/geot.1995.45.3.383.

[28]   Reymond Akpanya, Tom Goertzen, and Sebastian Wiesenhuetter. "Topological Interlocking , Truchet Tiles and Self-Assemblies : A Construction-Kit for Civil Engineering Design". In: July (2023).

[29]   Sébastien Truchet. "Mémoire sur les combinaisons". In: *Mémoires de l'Académie royale des sciences* 1704 (1704), pp. 363–372.

[30] A. V. Dyskin et al. "Topological interlocking of platonic solids: A way to new materials and structures". In: *Philosophical Magazine Letters* 83.3 (2003), pp. 197–203. ISSN: 09500839. DOI: 10.1080/0950083031000065226.

[31] Reymond Akpanya, Tom Goertzen, and Alice C Niemeyer. "A Group-Theoretic Approach for Constructing Spherical- Interlocking Assemblies". In: July (2023).

[32] Reymond Akpanya and Tom Goertzen. "Surfaces with given Automorphism Group". In: 1 (July 2023), pp. 1–30. arXiv: 2307.12681.

[33] S. Khandelwal et al. "Transverse loading of cellular topologically interlocked materials". In: *International Journal of Solids and Structures* 49.18 (Sept. 2012), pp. 2394–2403. ISSN: 00207683. DOI: 10.1016/j.ijsolstr.2012.04.035.

[34] S. Khandelwal et al. "Scaling of the elastic behavior of two-dimensional topologically interlocked materials under transverse loading". In: *Journal of Applied Mechanics, Transactions ASME* 81.3 (2014), pp. 1–9. ISSN: 00218936. DOI: 10.1115/1.4024907.

[35] S. Khandelwal et al. "Adaptive mechanical properties of topologically interlocking material systems". In: *Smart Materials and Structures* 24.4 (Apr. 2015), p. 045037. ISSN: 1361665X. DOI: 10.1088/0964-1726/24/4/045037.

[36] Shai Feldfogel et al. "Scaling, saturation, and upper bounds in the failure of topologically interlocked structures". In: *International Journal of Solids and Structures* 269.December 2022 (May 2023), p. 112228. ISSN: 00207683. DOI: 10.1016/j.ijsolstr.2023.112228. arXiv: 2212.11554.

[37] Y. Estrin, A. V. Dyskin, and E. Pasternak. "Topological interlocking as a material design concept". In: *Materials Science and Engineering C* 31.6 (2011), pp. 1189–1194. ISSN: 09284931. DOI: 10.1016/j.msec.2010.11.011.

[38] Maciej Piekarski. "Floor slabs made from topologically interlocking prefabs of small size". In: *Buildings* 10.4 (Apr. 2020), p. 76. ISSN: 20755309. DOI: 10.3390/buildings10040076.

[39] Francesca Lecci et al. "Design of Flat Vaults with Topological Interlocking Solids". In: *Nexus Network Journal* 23.3 (2021), pp. 607–627. ISSN: 15224600. DOI: 10.1007/s00004-020-00541-w.

[40] Yuri Estrin, Vinayak R. Krishnamurthy, and Ergun Akleman. "Design of architectured materials based on topological and geometrical interlocking". In: *Journal of Materials Research and Technology* 15 (Nov. 2021), pp. 1165–1178. ISSN: 22387854. DOI: 10.1016/j.jmrt.2021.08.064.

[41] Andrew Williams and Thomas Siegmund. "Mechanics of topologically interlocked material systems under point load: Archimedean and Laves tiling". In: *International Journal of Mechanical Sciences* 190.August 2020 (2021), p. 106016. ISSN: 00207403. DOI: 10.1016/j.ijmecsci.2020.106016. arXiv: 2004.07115.

[42] Michael Weizmann, Oded Amir, and Yasha Jacob Grobman. "Topological interlocking in buildings: A case for the design and construction of floors". In: *Automation in Construction* 72 (2016), pp. 18–25. ISSN: 09265805. DOI: 10.1016/j.autcon.2016.05.014.

[43] Michael Weizmann, Oded Amir, and Yasha Jacob Grobman. "Topological interlocking in architecture: A new design method and computational tool for designing building floors". In: *International Journal of Architectural Computing* 15.2 (2017), pp. 107–118. ISSN: 20483988. DOI: 10.1177/1478077117714913.

[44] S. Saari, B. H.Abu Bakar, and N. A. Surip. "Factors of non-uniform properties of interlocking compressed earth brick units". In: *Developments in the Built Environment* 5.December 2020 (Mar. 2021), p. 100042. ISSN: 26661659. DOI: 10.1016/j.dibe.2021.100042.

[45] Ziqi Wang et al. "Design and structural optimization of topological interlocking assemblies". In: *ACM Transactions on Graphics* 38.6 (Dec. 2019), pp. 1–13. ISSN: 15577368. DOI: 10.1145/3355089.3356489.

[46] Yi Bao and Victor C. Li. "Feasibility study of lego-inspired construction with bendable concrete". In: *Automation in Construction* 113.September 2019 (2020), p. 103161. ISSN: 09265805. DOI: 10.1016/j.autcon.2020.103161.

[47] Rojyar Barhemat et al. "Lego-inspired reconfigurable modular blocks for automated construction of engineering structures". In: *Automation in Construction* 139.April (2022), p. 104323. ISSN: 09265805. DOI: 10.1016/j.autcon.2022.104323.

[48] Yu Zhang et al. "A template design and automated parametric model for sustainable corbel dwellings with interlocking blocks". In: *Developments in the Built Environment* 14.January (2023), p. 100148. ISSN: 26661659. DOI: 10.1016/j.dibe.2023.100148.

[49] M. Brocato and L. Mondardini. "A new type of stone dome based on Abeille's bond". In: *International Journal of Solids and Structures* 49.13 (2012), pp. 1786–1801. ISSN: 00207683. DOI: 10.1016/j.ijsolstr.2012.03.036.

[50] C. Casapulla, E. Mousavian, and M. Zarghani. "A digital tool to design structurally feasible semi-circular masonry arches composed of interlocking blocks". In: *Computers and Structures* 221 (Sept. 2019), pp. 111–126. ISSN: 00457949. DOI: 10.1016/j.compstruc.2019.05.001.

[51] Faidra Oikonomopoulou et al. "Interlocking cast glass components, Exploring a demountable dry-assembly structural glass system". In: *Heron* 63.1-2 (2018), pp. 103–137. ISSN: 15744078.

[52] A. Snijder et al. "Design and engineering of a dry assembled glass block pedestrian bridge". In: *Challenging Glass Conference Proceedings - Challenging Glass 5: Conference on Architectural and Structural Applications of Glass, CGC 2016* June (2016), pp. 547–556.

[53] Stijn Brancart et al. "UNDULATUS: design and fabrication of a self-interlocking modular shell structure based on curved-line folding Rapidly assembled systems with flexible components View project Enhancing the Adaptable Capacity of Urban Fragments View project UNDULATUS: desig". In: (2015).

[54] Christopher Robeller and Yves Weinand. "Interlocking folded plate - Integral mechanical attachment for structural wood panels". In: *International Journal of Space Structures* 30.2 (2015), pp. 111–122. ISSN: 20598033. DOI: 10.1260/0266-3511.30.2.111.

[55] Irina Miodragovic Vella and Toni Kotnik. "Geometric Versatility of Abeille Vault A Stereotomic Topological Interlocking Assembly". In: *Proceedings of the International Conference on Education and Research in Computer Aided Architectural Design in Europe*. Vol. 2. 2016, pp. 391–397. ISBN: 9789491207112. DOI: 10.52842/conf.ecaade.2016.2.391.

[56] Urvi Sheth and Aysha Fida. "Funicular structures using topological assemblies". In: *RE: Anthropocene, Design in the Age of Humans - Proceedings of the 25th International Conference on Computer-Aided Architectural Design Research in Asia, CAADRIA 2020* 1 (2020), pp. 75–84. DOI: 10.52842/conf.caadria.2020.1.075.

[57] P. Y. Chen et al. "Structure and mechanical properties of selected biological materials". In: *Journal of the Mechanical Behavior of Biomedical Materials* 1.3 (2008), pp. 208–226. ISSN: 17516161. DOI: 10.1016/j.jmbbm.2008.02.003.

[58] Z Yin, F Hannard, and F Barthelat. "Impact-resistant nacre-like transparent materials". In: 1263.June (2019), pp. 1260–1263.

[59] H. Yazdani Sarvestani et al. "Multilayered architectured ceramic panels with weak interfaces: energy absorption and multi-hit capabilities". In: *Materials and Design* 167 (2019). ISSN: 18734197. DOI: 10.1016/j.matdes.2019.107627.

[60] M. Mirkhalaf, J. Tanguay, and F. Barthelat. "Carving 3D architectures within glass: Exploring new strategies to transform the mechanics and performance of materials". In: *Extreme Mechanics Letters* 7 (June 2016), pp. 104–113. ISSN: 23524316. DOI: 10.1016/j.eml.2016.02.016.

[61] Andrey Molotnikov et al. "Sandwich panels with a core segmented into topologically interlocked elements". In: *Advanced Engineering Materials* 15.8 (2013), pp. 728–731. ISSN: 14381656. DOI: 10.1002/adem.201300002.

[62] Lee Djumas et al. "Enhanced Mechanical Performance of Bio-Inspired Hybrid Structures Utilising Topological Interlocking Geometry". In: *Scientific Reports* 6.1 (July 2016), p. 26706. ISSN: 20452322. DOI: 10.1038/srep26706.

[63] Anooshe Rezaee Javan et al. "Mechanical behaviour of composite structures made of topologically interlocking concrete bricks with soft interfaces". In: *Materials and Design* 186 (Jan. 2020), p. 108347. ISSN: 18734197. DOI: 10.1016/j.matdes.2019.108347.

[64] Yaning Li, Christine Ortiz, and Mary C. Boyce. "Stiffness and strength of suture joints in nature". In: *Physical Review E - Statistical, Nonlinear, and Soft Matter Physics* 84.6 (Dec. 2011), p. 062904. ISSN: 15393755. DOI: 10.1103/PhysRevE.84.062904.

[65] M. Monsef Khoshhesab and Yaning Li. "Mechanical behavior of 3D printed biomimetic Koch fractal contact and interlocking". In: *Extreme Mechanics Letters* 24 (Oct. 2018), pp. 58–65. ISSN: 23524316. DOI: 10.1016/j.eml.2018.09.003.

[66] Wenzhi Wang et al. "Tensile behavior of bio-inspired hierarchical suture joint with uniform fractal interlocking design". In: *Journal of the Mechanical Behavior of Biomedical Materials* 113.March 2020 (Jan. 2021), p. 104137. ISSN: 18780180. DOI: 10.1016/j.jmbbm.2020.104137.

[67] Idris A. Malik and Francois Barthelat. "Toughening of thin ceramic plates using bioinspired surface patterns". In: *International Journal of Solids and Structures* 97-98 (Oct. 2016), pp. 389–399. ISSN: 00207683. DOI: 10.1016/j.ijsolstr.2016.07.010.

[68] Idris A. Malik and Francois Barthelat. "Bioinspired sutured materials for strength and toughness: Pullout mechanisms and geometric enrichments". In: *International Journal of Solids and Structures* 138 (May 2018), pp. 118–133. ISSN: 00207683. DOI: 10.1016/j.ijsolstr.2018.01.004.

[69] I. A. Malik, M. Mirkhalaf, and F. Barthelat. "Bio-inspired "jigsaw"-like interlocking sutures: Modeling, optimization, 3D printing and testing". In: *Journal of the Mechanics and Physics of Solids* 102 (May 2017), pp. 224–238. ISSN: 00225096. DOI: 10.1016/j.jmps.2017.03.003.

[70] Steven Laudage, Ethan Guenther, and Thomas Siegmund. "Design and analysis of a lightweight beam-type topologically interlocked material system". In: *Structures* 51.December 2022 (2023), pp. 1402–1413. ISSN: 23520124. DOI: 10.1016/j.istruc.2023.03.126.

[71] T. Krause et al. "Mechanical properties of topologically interlocked structures with elements produced by freeze gelation of ceramic slurries". In: *Advanced Engineering Materials* 14.5 (2012), pp. 335–341. ISSN: 14381656. DOI: 10.1002/adem.201100244.

[72] A. Molotnikov et al. "Design of responsive materials using topologically interlocked elements". In: *Smart Materials and Structures* 24.2 (Feb. 2015), p. 025034. ISSN: 1361665X. DOI: 10.1088/0964-1726/24/2/025034.

[73] S. Schaare et al. "Point loading of assemblies of interlocked cube-shaped elements". In: *International Journal of Engineering Science* 46.12 (Dec. 2008), pp. 1228–1238. ISSN: 00207225. DOI: 10.1016/j.ijengsci.2008.06.012.

[74] Majid Ali, Romain Briet, and Nawawi Chouw. "Dynamic response of mortar-free interlocking structures". In: *Construction and Building Materials* 42 (May 2013), pp. 168–189. ISSN: 09500618. DOI: 10.1016/j.conbuildmat.2013.01.010.

[75] Y. Estrin et al. "Negative stiffness of a layer with topologically interlocked elements". In: *Scripta Materialia* 50.2 (Jan. 2004), pp. 291–294. ISSN: 13596462. DOI: 10.1016/j.scriptamat.2003.09.053.

[76] Antoine Autruffe et al. "Indentation behaviour of interlocked structures made of ice: Influence of the friction coefficient". In: *Advanced Engineering Materials* 9.8 (Aug. 2007), pp. 664–666. ISSN: 14381656. DOI: 10.1002/adem.200700111.

[77] Ahmed S. Dalaq and Francois Barthelat. "Strength and stability in architectured spine-like segmented structures". In: *International Journal of Solids and Structures* 171 (2019), pp. 146–157. ISSN: 00207683. DOI: 10.1016/j.ijsolstr.2019.04.012.

[78] Ahmed S. Dalaq and Francois Barthelat. "Manipulating the geometry of architectured beams for maximum toughness and strength". In: *Materials and Design* 194 (Sept. 2020), p. 108889. ISSN: 18734197. DOI: 10.1016/j.matdes.2020.108889.

[79] Chenchen Zhou et al. "Microfluidic Assembly of Microblocks into Interlocked Structures for Enhanced Strength and Toughness". In: *ACS Applied Materials and Interfaces* 14.5 (2022), pp. 7261–7269. ISSN: 19448252. DOI: 10.1021/acsami.1c21408.

[80] Aram Bahmani, J. William Pro, and Francois Barthelat. "Vibration-induced assembly of topologically interlocked materials". In: *Applied Materials Today* 29.July (Dec. 2022), p. 101601. ISSN: 23529407. DOI: 10.1016/j.apmt.2022.101601.

[81] Aram Bahmani et al. "Vibration-driven fabrication of dense architectured panels". In: *Matter* 5.3 (Mar. 2022), pp. 899–910. ISSN: 25902385. DOI: 10.1016/j.matt.2022.01.002.

[82] Thomas Siegmund et al. "Manufacture and Mechanics of Topologically Interlocked Material Assemblies". In: *Applied Mechanics Reviews* 68.4 (2016), pp. 1–15. ISSN: 00036900. DOI: 10.1115/1.4033967.

[83] Seyed Nabaei and Yves Weinand. "Geometrical description and structural analysis of a modular timber structure". In: *International Journal of Space Structures* 26.4 (Dec. 2011), pp. 321–330. ISSN: 20598033. DOI: 10.1260/0266-3511.26.4.321.

[84] Klaus-Jürgen -J Bathe, Ekkehard Ramm, and Edward L. Wilson. "Finite element formulations for large deformation dynamic analysis". In: *International Journal for Numerical Methods in Engineering* 9.2 (1975), pp. 353–386. ISSN: 10970207. DOI: 10.1002/nme.1620090207.

[85] Klaus-Jürgen -J Bathe and Saïd Bolourchi. "Large displacement analysis of three-dimensional beam structures". In: *International Journal for Numerical Methods in Engineering* 14.7 (1979), pp. 961–986. ISSN: 10970207. DOI: 10.1002/nme.1620140703.

[86] Heinrich Hertz. *Über die Berührung fester elastischer Körper*. Vol. 171. 92. 1882, pp. 156–171.

[87] K. L. Johnson. *Contact Mechanics*. Cambridge University Press, May 1985. ISBN: 9780521255769. DOI: 10.1017/CBO9781139171731.

[88] Stephen Timoshenko and J. N. Goodier. *Theory of elasticity*. 3rd ed. McGraw-Hill, New York, 1970.

[89] Yih-O Tu and D. C. Gazis. "The Contact Problem of a Plate Pressed Between Two Spheres". In: *Journal of Applied Mechanics* 31.4 (Dec. 1964), pp. 659–666. ISSN: 0021-8936. DOI: 10.1115/1.3629728.

[90] Yih-O Tu. "A Numerical Solution for an Axially Symmetric Contact Problem". In: *Journal of Applied Mechanics* 34.2 (June 1967), pp. 283–286. ISSN: 0021-8936. DOI: 10.1115/1.3607680.

[91] T. F. Conry and A. Seireg. "A Mathematical Programming Method for Design of Elastic Bodies in Contact". In: *Journal of Applied Mechanics* 38.2 (June 1971), pp. 387–392. ISSN: 0021-8936. DOI: 10.1115/1.3408787.

[92] Thomas J.R. Hughes et al. "A finite element method for a class of contact-impact problems". In: *Computer Methods in Applied Mechanics and Engineering* 8.3 (July 1976), pp. 249–276. ISSN: 00457825. DOI: 10.1016/0045-7825(76)90018-9.

[93] P. Wriggers, W. Wagner, and E. Stein. "Algorithms for non-linear contact constraints with application to stability problems of rods and shells". In: *Computational Mechanics* 2.3 (1987), pp. 215–230. ISSN: 01787675. DOI: 10.1007/BF00571026.

[94] E. A. Wilson and B. Parsons. "Finite element analysis of elastic contact problems using differential displacements". In: *International Journal for Numerical Methods in Engineering* 2.3 (July 1970), pp. 387–395. ISSN: 0029-5981. DOI: 10.1002/nme.1620020307.

[95] S.K. Chan and I.S. Tuba. "A finite element method for contact problems of solid bodies—Part I. Theory and validation". In: *International Journal of Mechanical Sciences* 13.7 (July 1971), pp. 615–625. ISSN: 00207403. DOI: 10.1016/0020-7403(71)90032-4.

[96] Tod A. Laursen. *Computational Contact and Impact Mechanics*. Berlin, Heidelberg: Springer Berlin Heidelberg, 2003. ISBN: 978-3-642-07685-5. DOI: 10.1007/978-3-662-04864-1.

[97] P. Wriggers. *Computational contact mechanics, 2nd ed., Springer*. 2006. ISBN: 9783540326083.

[98] Alexander Konyukhov and Karl Schweizerhof. *Computational Contact Mechanics*. Vol. 67. Lecture Notes in Applied and Computational Mechanics. Berlin, Heidelberg: Springer Berlin Heidelberg, 2013. ISBN: 978-3-642-31530-5. DOI: 10.1007/978-3-642-31531-2.

[99] A. Konyukhov and K. Schweizerhof. "Covariant description for frictional contact problems". In: *Computational Mechanics* 35.3 (Feb. 2005), pp. 190–213. ISSN: 01787675. DOI: 10.1007/s00466-004-0616-7.

[100] P. Wriggers, L. Krstulovic-Opara, and J. Korelc. "Smooth C1-interpolations for two-dimensional frictional contact problems". In: *International Journal for Numerical Methods in Engineering* 51.12 (2001), pp. 1469–1495. ISSN: 00295981. DOI: 10.1002/nme.227.

[101] P. Wriggers. "Finite element algorithms for contact problems". In: *Archives of Computational Methods in Engineering* 2.4 (Dec. 1995), pp. 1–49. ISSN: 1134-3060. DOI: 10.1007/BF02736195.

[102] Nagi El-Abbasi and Klaus Jürgen Bathe. "Stability and patch test performance of contact discretizations and a new solution algorithm". In: *Computers and Structures* 79.16 (2001), pp. 1473–1486. ISSN: 00457949. DOI: 10.1016/S0045-7949(01)00048-7.

[103] Giorgio Zavarise and Laura de Lorenzis. "A modified node-to-segment algorithm passing the contact patch test". In: *International Journal for Numerical Methods in Engineering* 79.4 (July 2009), pp. 379–416. ISSN: 00295981. DOI: 10.1002/nme.2559.

[104] Ioannis Koureas et al. "On the failure of beam-like topologically interlocked structures". In: *International Journal of Solids and Structures* 259 (Dec. 2022), p. 112029. ISSN: 00207683. DOI: 10.1016/j.ijsolstr.2022.112029. arXiv: 2207.01688.

[105] A. V. Dyskin et al. "Toughening by Fragmentation—How Topology Helps". In: *Advanced Engineering Materials* 3.11 (Nov. 2001), p. 885. ISSN: 14381656. DOI: 10.1002/1527-2648(200111)3:11<885::AID-ADEM885>3.0.CO;2-P.

[106] Kyle Mahoney and Thomas Siegmund. "Mechanics of tubes composed of interlocking building blocks". In: *International Journal of Engineering Science* 174.February (Apr. 2022), p. 103654. ISSN: 00207225. DOI: 10.1016/j.ijengsci.2022.103654.

[107] Milad Zakeri et al. "Numerical analysis of linear and nonlinear buckling instability of plates made of topologically interlocked materials". In: *Mechanics Based Design of Structures and Machines* 51.6 (June 2023), pp. 3260–3272. ISSN: 15397742. DOI: 10.1080/15397734.2021.1921596.

[108] A. Konyukhov and K. Schweizerhof. "Contact formulation via a velocity description allowing efficiency improvements in frictionless contact analysis". In: *Computational Mechanics* 33.3 (Feb. 2004), pp. 165–173. ISSN: 01787675. DOI: 10.1007/s00466-003-0515-3.

[109] Peter Wriggers and Tod A. Laursen. "Computational Contact Mechanics: CISM Courses and Lectures." In: 498 (2007), p. 248.

[110] Vladislav A Yastrebov. *Numerical Methods in Contact Mechanics*. Ed. by Vladislav A. Yastrebov and Piotr Breitkopf. London, SW UK: ISTE Ltd, Feb. 2013. ISBN: 9781848215191. DOI: 10.1002/9781118647974.

[111] Giorgio Zavarise and Laura De Lorenzis. "The node-to-segment algorithm for 2D frictionless contact: Classical formulation and special cases". In: *Computer Methods in Applied Mechanics and Engineering* 198.41-44 (Sept. 2009), pp. 3428–3451. ISSN: 00457825. DOI: 10.1016/j.cma.2009.06.022.

[112] Ioannis Koureas et al. "Beam-Like Topologically Interlocked Structures With Hierarchical Interlocking". In: *Journal of Applied Mechanics* 90.8 (Aug. 2023), pp. 1–7. ISSN: 0021-8936. DOI: 10.1115/1.4062348. arXiv: 2212.06454.

[113] Itay Odessa and Igor Shufrin. "Nonlinear mechanics of fragmented beams". In: *European Journal of Mechanics, A/Solids* 93.January (2022), p. 104488. ISSN: 09977538. DOI: 10.1016/j.euromechsol.2021.104488.

[114] P. Ranganath Nayak. "Random process model of rough surfaces". In: *Journal of Tribology* 93.3 (1971), pp. 398–407. ISSN: 15288897. DOI: 10.1115/1.3451608.

[115] Vladislav A. Yastrebov, Guillaume Anciaux, and Jean François Molinari. "Contact between representative rough surfaces". In: *Physical Review E - Statistical, Nonlinear, and Soft Matter Physics* 86.3 (2012), pp. 1–4. ISSN: 15393755. DOI: 10.1103/PhysRevE.86.035601. arXiv: 1207.5364.

[116] Ioannis Koureas et al. "The key to the enhanced performance of slab-like topologically interlocked structures with non-planar blocks". In: *International Journal of Solids and Structures* 285.August (Dec. 2023), p. 112523. ISSN: 00207683. DOI: 10.1016/j.ijsolstr.2023.112523.

[117] Yuezhong Feng et al. "Impact mechanics of topologically interlocked material assemblies". In: *International Journal of Impact Engineering* 75 (2015), pp. 140–149. ISSN: 0734743X. DOI: 10.1016/j.ijimpeng.2014.08.003.

[118] A. Rezaee Javan et al. "The impact behaviour of plate-like assemblies made of new interlocking bricks: An experimental study". In: *Materials and Design* 134.August (2017), pp. 361–373. ISSN: 18734197. DOI: 10.1016/j.matdes.2017.08.056.

[119] Arcady Dyskin, Elena Pasternak, and Yuri Estrin. "Topological interlocking as a design principle for hybrid materials". In: *8th Pacific Rim International Congress on Advanced Materials and Processing 2013, PRICM 8* 2 (2013), pp. 1525–1534. DOI: 10.1002/9781118792148.ch192.

[120] Arcady V. Dyskin, Elena Pasternak, and Yuri Estrin. "Mortarless structures based on topological interlocking". In: *Frontiers of Structural and Civil Engineering* 6.2 (2012), pp. 188–197. ISSN: 20952430. DOI: 10.1007/s11709-012-0156-8.

[121] Milad Zakeri, Majid Safarabadi, and Mojtaba Haghighi-Yazdi. "A comprehensive investigation of compressive behavior of architectured materials based on topologically interlocking structures: Experimental and numerical approaches". In: *Mechanics Research Communications* 130.5 (2023), p. 104132. ISSN: 00936413. DOI: 10.1016/j.mechrescom.2023.104132.

[122] Silvan Ullmann, David S. Kammer, and Shai Feldfogel. "The Deflection Limit of Slab-Like Topologically Interlocked Structures". In: *Journal of Applied Mechanics* 91.2 (Oct. 2023), pp. 1–14. ISSN: 0021-8936. DOI: 10.1115/1.4063345. arXiv: 2307.00918.

[123] Y. Estrin et al. "Topological interlocking of protective tiles for the space shuttle". In: *Philosophical Magazine Letters* 83.6 (June 2003), pp. 351–355. ISSN: 09500839. DOI: 10.1080/0950083031000120873.

[124] A. V. Dyskin et al. "The principle of topological interlocking in extraterrestrial construction". In: *Acta Astronautica* 57.1 (2005), pp. 10–21. ISSN: 00945765. DOI: 10.1016/j.actaastro.2004.12.005.

[125] A. Molotnikov et al. "Percolation mechanism of failure of a planar assembly of interlocked osteomorphic elements". In: *Engineering Fracture Mechanics* 74.8 (May 2007), pp. 1222–1232. ISSN: 00137944. DOI: 10.1016/j.engfracmech.2006.07.012.

[126] Oliver Tessmann. "Topological Interlocking Assemblies". In: *Proceedings of the International Conference on Education and Research in Computer Aided Architectural Design in Europe*. Vol. 2. Lynn 2009. 2012, pp. 211–219. ISBN: 9789491207037. DOI: 10.52842/conf.ecaade.2012.2.211.

[127] Anooshe Rezaee et al. "Design of a new type of interlocking brick and evaluation of its dynamic performance". In: *Proceeding of the IASS Annual Symposium 2016* January 2019 (2016), pp. 2–9.

[128] A. Rezaee Javan et al. "Impact behaviour of plate-like assemblies made of new and existing interlocking bricks: A comparative study". In: *International Journal of Impact Engineering* 116.February (2018), pp. 79–93. ISSN: 0734743X. DOI: 10.1016/j.ijimpeng.2018.02.008.

[129] Wenzheng Xu, Xiaoshan Lin, and Yi Min Xie. "A novel non-planar interlocking element for tubular structures". In: *Tunnelling and Underground Space Technology* 103.June (Sept. 2020), p. 103503. ISSN: 08867798. DOI: 10.1016/j.tust.2020.103503.

[130] Dassault Systemes. *Abaqus*. 2019.

[131] M. Short and T. Siegmund. "Scaling, Growth, and Size Effects on the Mechanical Behavior of a Topologically Interlocking Material Based on Tetrahedra Elements". In: *Journal of Applied Mechanics* 86.11 (Nov. 2019). ISSN: 0021-8936. DOI: 10.1115/1.4044025.

[132] Ergun Akleman et al. "Generalized abeille tiles: Topologically interlocked space-filling shapes generated based on fabric symmetries". In: *Computers and Graphics (Pergamon)* 89 (June 2020), pp. 156–166. ISSN: 00978493. DOI: 10.1016/j.cag.2020.05.016.

[133] Shai Feldfogel et al. "Failure of topologically interlocked structures — a Level-Set-DEM approach". In: *European Journal of Mechanics - A/Solids* 103 (Jan. 2024), p. 105156. ISSN: 09977538. DOI: 10.1016/j.euromechsol.2023.105156. arXiv: 2210.14155.

[134] J. R. Barber. *Elasticity*. Vol. 172. Solid Mechanics and Its Applications. Dordrecht: Springer Netherlands, 2010. ISBN: 978-90-481-3821-0. DOI: 10.1007/978-90-481-3809-8.

Curriculum Vitae

Ioannis Koureas

Location	Laura-Hezner-Weg 7
	8093 Zurich, Switzerland
Email	ikoureas@ethz.ch
Phone	+41 44 633 35 65

Education

May 2019 – present	**ETH Zurich, Switzerland** PhD in Computational Mechanics
Oct 2017 – Oct 2018	**University of Southampton, UK** MSc in Computational Engineering and Design
Sept 2013 – Sept 2017	**Cyprus University of Technology, Cyprus** BEng in Mechanical Engineering & Materials Science
Sept 2014 – Sept 2015	**ERASMUS at Aristotle University of Thessaloniki, Greece** BEng Mechanical Engineering

Research Experience

May 2019 – present	**ETH Zurich, Switzerland** – Scientific Assistant – **CMBM** Studied the effect of interface mechanisms, block geometry and surface morphology on the failure mode of topologically interlocked structures using numerical frameworks and performing finite element simulations
Jan 2018 – Sep 2018	**University of Southampton , UK** – Master Student Researcher – **MINATHER** Numerical and experimental investigation of the flow distribution of microbubbles in the human microvasculature using microfluidic devices
Sep 2016 – May 2017	**Cyprus University of Technology, Cyprus** – Bachelor Student Researcher – **MEP** Experimental analysis and fabrication of organic photovoltaic systems based on state-of-the-art techniques

Research Interests

- studying the failure of topologically interlocked structures
- modeling the mechanics of structures and materials
- developing finite element algorithms
- designing novel structures based on interlocking principles
- fabricating complex elements using additive manufacturing

Publications

Articles in peer-reviewed journals

Ioannis Koureas, Mohit Pundir, Shai Feldfogel, and David S. Kammer. On the failure of beam-like topologically interlocked structures. International Journal of Solids and Structures, page 112029, Nov 2022.

Ioannis Koureas, Mohit Pundir, Shai Feldfogel, and David S. Kammer. Beam-like topologically interlocked structures with hierarchical interlocking. Journal of Applied Mechanics, pages 1–7, May 2023.

Ioannis Koureas, Mohit Pundir, Shai Feldfogel, and David S. Kammer. The key to the enhanced performance of slab-like topologically interlocked structures with non-planar blocks. International Journal of Solids and Structures, page 112523, Dec 2023.